Crystallization of Inorganic Compounds – Scaling in Seawater Desalination

Eingereicht am Zentrum für Ingenieurwissenschaften
Martin-Luther-Universität Halle-Wittenberg

zur Erlangung des akademischen Grades
Doktor-Ingenieur (Dr.-Ing.)
genehmigte

Dissertation

von

M.Sc. Chem. Eng. Ali Mousa Al-Atia
geboren 6. Mai 1977 in Bagdad, Irak

Gutachter:
1. Prof. Dr.-Ing. habil. J. Ulrich
2. Prof. Dr. Schulte

Halle (Saale), 08. December 2008

<u>Dedication</u>

I dedicate this work to my father, who passed away while I am far away from him busy with this work, may God bless his soul, and to my mother who is proud of me as I am proud of her.

Dad... You are always in my thoughts!

Acknowledgment

Halle (Saale), August 2008

1. <u>Introduction</u>

There is a big effort in developing techniques to improve the seawater desalinisation. That means to reduce the costs of fresh water and to reduce the impacts on environment.

One of the most important factors that contribute to high production costs of fresh water from seawater in desalination is scale formation (encrustation). Scale formation e.g. $CaCO_3$ in seawater desalination is a crystallization phenomenon. This phenomenon can be defined as crystallization of inorganic compounds in a multi-component solution (seawater). This type of crystallization is considered to be complicated, since the crystallization process is influenced by the compounds which exist in seawater and the complex plant operational conditions.

Most known techniques that are used to reduce the encrustation in seawater desalination are not based on crystallization processes as will be shown in the next chapters. On this account, the motivation of this work is to find alternative technologies to reduce the encrustation by applying the principles of crystallization.

It would be desirable therefore first to study the effect of inorganic compounds on the nucleation step of crystallization in inorganic solutions. In order to fill the gap in the literature in terms of finding an interpretation to the effect of additives concerning suppression, enhancement or non of both of these effects on the metastable zone width of inorganic solutions. This study will indeed be helpful in a better understanding of crystallization processes.

Reducing the scale formation in seawater desalination can be achieved by a pre-treatment process where a precipitation and a separation of $CaCO_3$ is taking place. A spontaneous precipitation of $CaCO_3$ in seawater can not occur without modifying the degree of supersaturation of $CaCO_3$ in seawater as it will be presented.

The aspects of using a pre-treatment process as alternative method by means of an environmental friendly and economical solution will be discussed.

2. <u>State of the Art</u>

2.1   Electrolyte solutions

Compounds that exist as ions, as cations and anions, when dissolved in water are called electrolytes and thus, the mixture of cations, anions and water molecules is called an electrolyte solution. This electrolyte solution can be formed pure or as mixture according to the number of dissolved substances (solute) in water (solvent). Further, the electrolyte solutions are divided into week and strong solution, this is due to the ionization process of electrolytes that dissolve in water. There are references which are dealing with types, properties, structures and the thermodynamics of electrolyte solutions [MUR84], [ZEM86], [LOB89].

In solution and under special conditions (supersaturation), a solid phase can form from the dissolved compounds. This phase separation process is called crystallization. Generally speaking, crystallization from solutions can be achieved by two steps, nucleation and crystal growth. Both steps are controlling the crystalline products in terms of crystal shape, size distribution, purity and morphology. Furthermore, they could strongly affect the product yield.

Decades ago, many researchers started to investigate and interpret the effect of additives on nucleation and crystal growth processes. The methodology of their research was so far concentrated on the conditions accompanied to the solid phase formation (crystals in bulk solutions) [DAV74], [KUB97], [HEN98], [SAN04]. The liquid phase structure changes of the bulk solutions [ONO68], [KUB95] and [NYV98] were hardly be considered. Especially, when they studied the effect of impurities on the nucleation process.

Thereby, the present study will show how the change in the structure of solutions can play a big role in interpreting the effect of impurities on the nucleation process.

2.2   Thermodynamics of ion solvation

Solvation is defined as the attraction and association of molecules of a solvent with molecules or ions of a solute [DOG85]. As salts dissolve in a solvent they spread out and become surrounded by solvent molecules. There are different types of intermolecular interactions: ion-ion, ion-dipole and dipole-dipole attractions or van der Waals forces which occur only in polar solvents. Figure 2-1 shows the sequence of thermodynamic steps for a general case of salt dissolution in water.

2
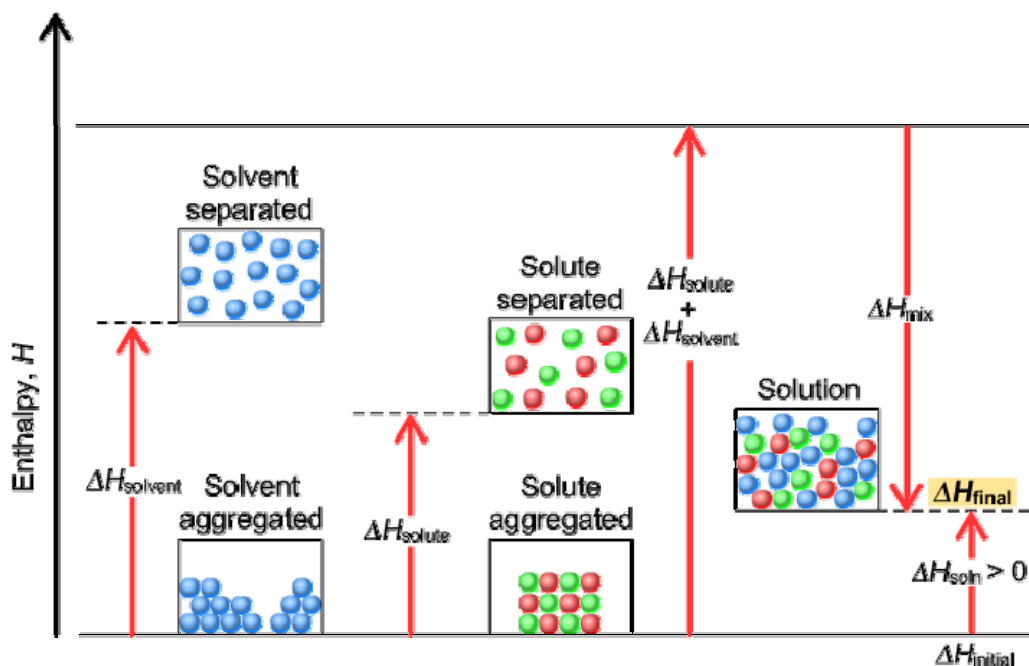
Figure 2-1: The enthalpy change of ion-dipole formation during the dissolution process according to Norton [CTS08]

The dissolution process can be thermodynamically summarized as follows:

1. Breaking of solute ionic bonds, i.e. lattice enthalpy.
2. The spherical symmetrical field of individual ions may tear water dipoles out the liquid structure (Breaking of hydrogen bonds in solvent, i.e. enthalpy of solvent).
3. A certain number of water molecules in the immediate vicinity of the ion are trapped. And water dipole charged ends are oriented towards the center of ions to form a hydration shell (primary solvation shell) of **ion-dipole**. It can have a positive or a negative charge as shown in e.g. figure 2-2. The energy required to form the shell of hydration is called the enthalpy of hydration. This energy represents the **ion-dipole intermolecular force interaction**, which is the value which depends on the ionic radius and charge [BUR88]. Further, it depends on the temperature, pressure and number of water molecules in the hydration shell.

The enthalpy of hydration values for different inorganic compounds in terms of cations and anions have been calculated through thermodynamic models as can be found by Marcus [MAR87]. These values will be the factor of setting up a new rule to study and interpret the effect of inorganic additives on the nucleation of inorganic compounds, as will be described later.
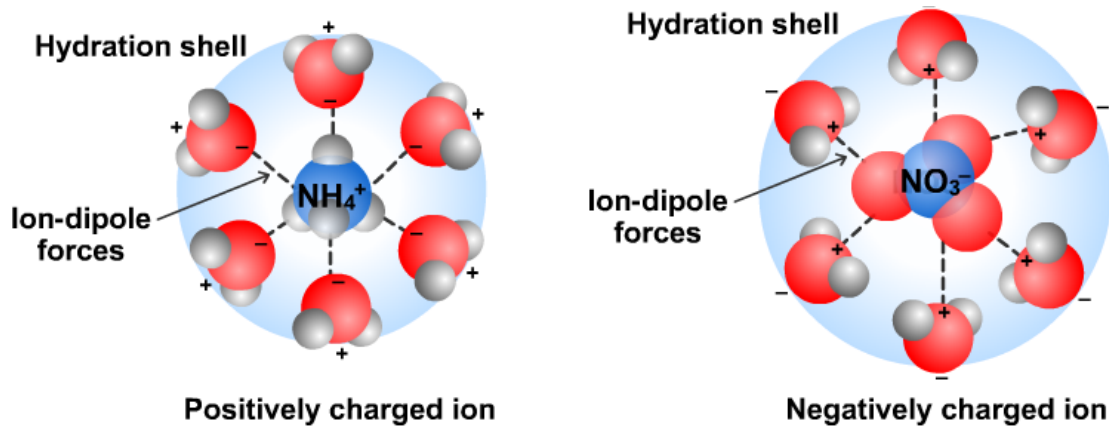
Figure 2-2: Hydration shell represented by ammonium nitrate dissolved in water [CTS08]

Accordingly, **ion-ion intermolecular forces** can be understood through the following concepts:

1.   Each solvated ion, i.e. ion-dipole may be assumed to undergo random motion in solution.

2.   The positive and negative charges of solvated ions may be trapped in the columbic field of each other, the electrostatic force (F) between these ions can be represented by the following equation [SAN07]:

$$F = \frac{z_1 \cdot z_2 \cdot e^2}{\varepsilon \cdot r^2}$$
(2-1)

With: z_i valence of ion (-)

e   elementary charge ($1.6022 \ast 10^{-19}$ c)

r   distance between the ions (nm)

ε dielectric constant of the solvent ($\varepsilon = \varepsilon_r \varepsilon_o$)

ε_r relative dielectric constant (relative permittivity) of solvent (water [DAV95])

ε_o vacuum permittivity ($8.854187 \ast 10^{-12}$ $c^2/N.m^2$)

In concentrated electrolyte solutions, the electrostatic force is very strong between the positive and negative ion-dipole in the bulk water.

From all of above, the intermolecular forces namely **ion-ion** and **ion-dipole** interaction are the key factors to study the effect of additives on nucleation.

2.3   Solubility and nucleation

One of the basic requirements in crystallization process design is to find the phase diagram of solute-solvent equilibrium. Generally speaking, the phase diagram

can be defined as those equilibrium states ($\Delta G=0$) between gas, liquid and solid phases.

In crystallization based on liquid solution, liquid-solid phase equilibrium is the case concerned. The term solubility represents the state of equilibrium between dissolution and growth of solute (solid) in pure solution (liquid). The dissolution or growth process is zero at that specific temperature and pressure. Figure 2-3 is an experimental example to show the zones of K_2SO_4 stability.
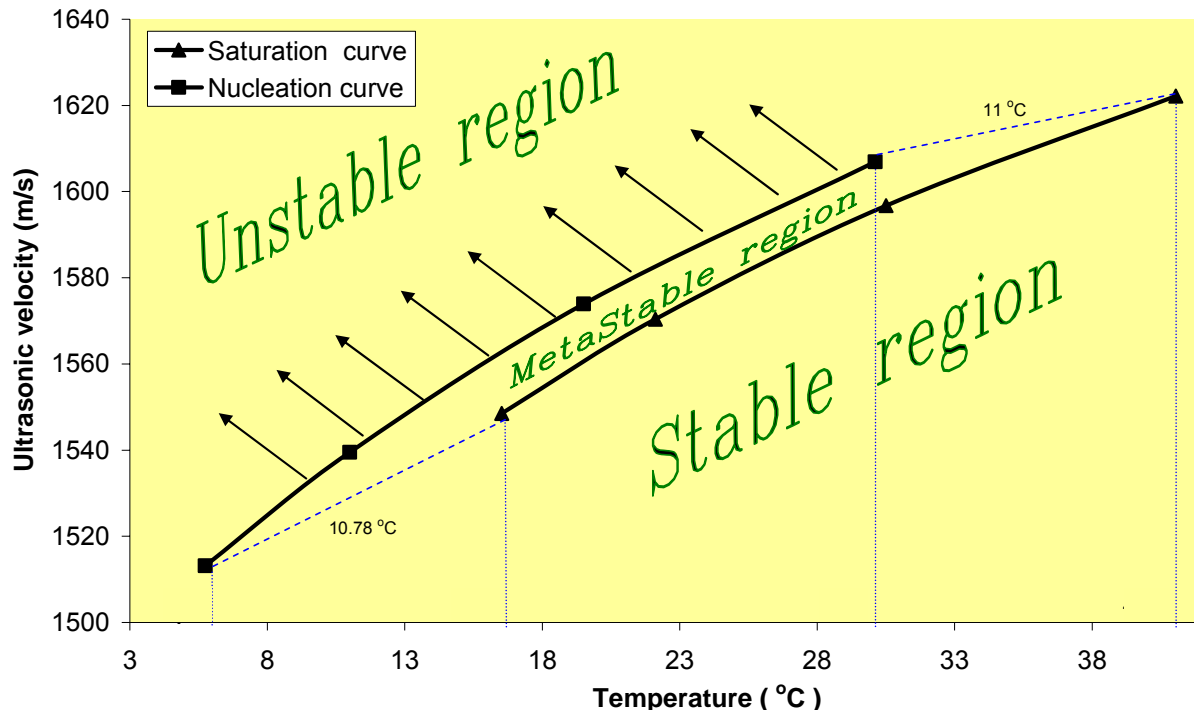
Figure 2-3: Three zones that describe the stability states of K_2SO_4 are shown. Here the ultrasonic velocity is taken as a measure for the concentration [OMA99]. The upper limit of the metastable zone (Nucleation) is found by measurement with a cooling rate of in this case 5 K/h. 1) The stable (undersaturated) zone: a crystal dissolution process can occur here. 2) The metastable (supersaturated) zone: a crystal growth process can only occur here. 3) The unstable (supersaturated) zone: instant nucleation happens here.

Normally one of methods to create a supersaturated state is for most compounds to diminish the temperature of the solution. While for some other it is an elevating in temperature that can change the system to the state of instability. Consequently, the unstable region has been divided into two main areas, metastable and unstable, by a nucleation curve (upper limit of the metastable zone) which referred to first visible nuclei, of e.g. K_2SO_4 as appeared in figure 2-3. This kind of nucleation is classified as homogeneous nucleation. Nucleation has been classified, e.g. by **Mullin** [MUL93] as shown below:

5

Nucleation

Primary

Secondary

(induced by crystalline
material of the same kind)

Homogenous

(spontaneous)

Heterogeneous

(induced e.g. by foreign particles)
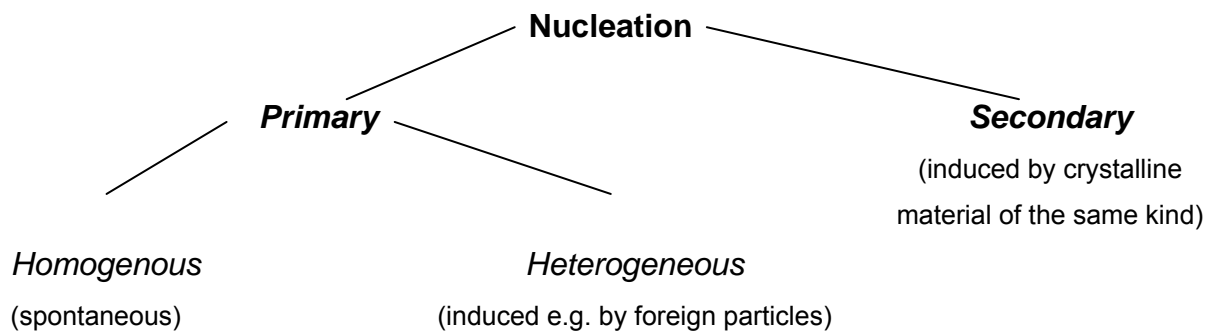
It is worth while to mention that the changes in free energy which associated with homogenous nucleation processes are illustrated below [MUL93]. The changes in free energy leads to a formation of a new phase in the bulk solution and are represented by equation 2-2:

$$\Delta G$$

$$\parallel$$

$$\Delta Gs + \Delta G_V \qquad\qquad\qquad\text{(2-2)}$$

$$\Delta Gs = 4\pi\gamma\, r^2$$

$$\Delta G_V = \frac{4\pi}{3} r^3 \Delta G_v$$

Change in free energy leads to formation
of surface

Change in free energy leads to formation
of volume

Hence, to form a new nucleus in a supersaturated solution, work should be done on the system to change it from equilibrium state ($\Delta G = 0$) to unstable state at which the $\Delta G > 0$. The maximum value of ΔG that is required to create a cluster of a new crystal can be found by minimizing the equation 2-2 as shown below:

$$\because \frac{d\Delta G}{dr} = 8\pi\gamma\, r + 4\pi\, r^2 \,\Delta G_v = 0 \qquad\qquad\text{(2-3)}$$

$$\therefore r_c = \frac{-2\gamma}{\Delta G_v} \qquad\qquad\text{(2-4)}$$

By substitution equation 2-4 in equation 2-2, this lead to:

$$\Delta G_{crit} = \frac{16\pi\gamma^3}{3(\Delta G_v)^2} = \frac{4\pi \cdot \gamma \cdot r_c^2}{3} \qquad\qquad\text{(2-5)}$$

With:

ΔG_{crit}	Minimum value of free energy required for nucleation
γ	Interfacial tension
ΔG_v	Free energy change of the transformation per unit volume
r_c	Critical size of nucleus

In figure 2-4, the critical free energy can be seen with the corresponding critical radius of a nucleus.
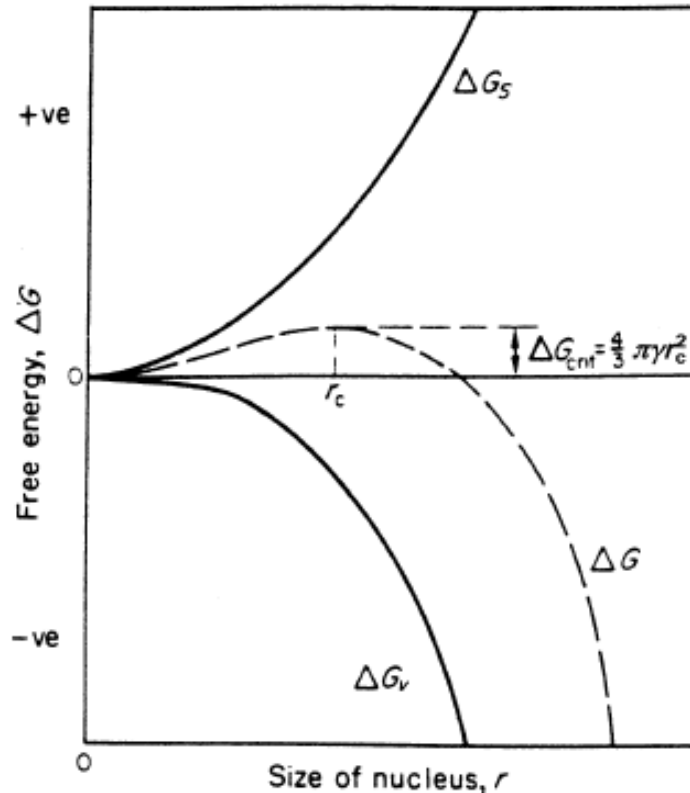
Figure 2-4: Free energy diagram to illustrate the nucleation in terms of critical radius of the nucleus [MUL93]

As shown in figure 2-4 the value of ΔG_{crit} is always positive which gives an indication of a non spontaneous process. Further ΔG_{crit} (nucleation) is effected by different conditions, e.g. temperature level and pressure level.

In contrast to the nucleation process (a kinetic process), the solubility is defined purely by thermodynamics. It may be considered here the pure salt (M) making a strong electrolyte solution of the constituent ions (A) and (B) saturated with respect to that salt as illustrated in following equations [ZEM86]:

$$M = aA + bB \tag{2-6}$$

$$\mu_i(T) = \mu_i^o(T) + RT \ln(\gamma_i m_i) \tag{2-7}$$

Using the chemical potential thermodynamic concept equation 2-7 represent equation 2-6 leads to:

$$\because \quad \mu_M(T) = a \cdot \mu_A(T) + b \cdot \mu_B(T) \tag{2-8}$$

$$\therefore \quad \mu_M^o(T) + RT \ln(\gamma_M m_M) = a \, [\mu_A^o(T) + RT \ln(\gamma_A m_A)] + b \, [\mu_B^o(T) + RT \ln(\gamma_B m_B)]$$

$$(\mu_M^o (T) - [a \ \mu_A^o (T) + b \ \mu_B^o (T)]) = RT \ \ln \left(\frac{(\gamma_A m_A)^a \cdot (\gamma_B m_B)^b}{(\gamma_M m_M)} \right) \tag{2-9}$$

It is known, that the $\mu_i^o (T)$ is a reference chemical potential or the standard chemical potential and the partial molar Gibbs free energy is also known as a chemical potential. Thus, the left side of equation 2-9 can be substituted by the quantity of $\bar{G}_i^o (T)$. These quantities are given in form of $\Delta G_{f_i}^o$:

$$\exp \left(-\frac{([a\Delta G_A^o (T) + b\Delta G_B^o (T)] - \Delta G_M^o (T))}{RT} \right) = \left(\frac{(\gamma_A m_A)^a \cdot (\gamma_B m_B)^b}{(\gamma_M m_M)} \right) \tag{2-10}$$

or

$$K_{sp} = \frac{(\gamma_A m_A)^a \cdot (\gamma_B m_B)^b}{(\gamma_M m_M)} \tag{2-11}$$

Where K_{sp} is the solubility product of a single compound (M) dissolved in pure water at a certain temperature and one atmosphere total pressure. Solubility of any substance can be calculated by using the solubility product and the activity coefficient (γ_i) of the component which is normally be effected by the purity of the solution. Hence, in the case of multi-component electrolyte solutions, many models may be found to calculate the activity coefficients of solution such as the Guggenheim, Bromley, Meissner and Pitzer model [ZEM86]. Thereby, the solubility can be calculated.

2.4 Metastable zone width and influence of the additive

The design of crystallizers requires to respect a set of different conditions for their design. One of these important conditions is the width of metastable zone (MSZ). The MSZ width is important to achieve a desired product property in terms of crystal shape, purity and size distribution. In industrial crystallization, the optimum operation conditions for a crystallizer is in the middle of the width of the MSZ, in the range of 0.1 < $\triangle T_{opt}$ /$\triangle T_{MSZ}$ < 0.5 [MER98]. This level of supersaturated (MSZ) is affected by many other conditions. One of these conditions is the level of impurities existing in the solution. The impurity level might reduce or increase the width of metastable zone. However, some additives are not effecting the MSZ width. This depends on the type and amount of impurities in solution.

As it is well known, the metastable zone width is limited by the solubility and nucleation curves as appeared in e.g. figure 2-3. The effect of impurities on the MSZ

width can occur either by changing the nucleation or the solubility curves or just one of them. The effect of impurities on the solubility curve is predictable through such models as the *Pitzer model.* This needs to calculate the activity coefficient for multi-component systems as mentioned in section 2.3. Therefore, the big challenge in studying the effect of impurities on the MSZ width lies in the prediction and the explanation of the effect of impurities on the nucleation curve which is unknown till now. This can be seen quite clearly in many studies (e.g. [SAY01, TIT02, GIN93]). In those studies experimentally found influences of additives on the width of the metastable zone are shown *without giving any interpretation to describe the found effects.*

2.5 Induction time

The induction time of precipitation can be defined as the time elapsed between the establishing of a supersaturation and the first change in the systems physical properties. This change is due to the formation a new solid phase in the bulk solution. Experimentally, induction time is determined either visually, by turbidity, or by measuring the change in concentration decreases through methods such as conductivity, pH, or ultrasonic velocity of the solution. When the induction time is determined visually, the measured time is a summation of the time required to form a critical nucleus (t_i) and the time for the growth of this nucleus to a visible size (t_g), (t_{ind}= t_i+ t_g). However, the induction time is related to supersaturation as shown in equation 2-12 [SOH92]:

$$\log(t_{ind}) = \frac{B}{T^3 \cdot (\log S)^2} - A \qquad\qquad (2\text{-}12)$$

Where

A = empirical constant

$$B = \frac{\alpha \cdot N_A \cdot \sigma^3 \cdot V_m^{\ 2} \cdot f(\Theta)}{(2.3 \cdot R)^3}$$

$\alpha =$ geometric shape factor (equal to $16\pi/3$ of the spherical nucleus)

$N_A = 6.0221415 * 10^{23}$ mol^{-1}
$V_m = molar$ volume cm$^3/mol$
$R = 8.314$ J/mol.K
$f(\Theta) = correction$ factor, if homogeneous equal 1, if heterogenous equal 0.01
$\sigma = \mathrm{int}\,erfacial\ energy$ J/m^2

Basically, the measurement of the induction time is one of the essential steps in the study of precipitation processes. Especially, to study scaling processes for those insoluble substances such as $CaCO_3$, $CaSO_4$ and $Mg(OH)_2$ in e.g. seawater

desalination processes. Where the process of precipitation takes relatively long time, certainly, this depends on the level of the instant supersaturation. However, in many industrial processes where scaling problems can occur a great effort has been spent to prolong the induction time through employing different methods such as suppression of calcium carbonate scale by antiscalants [HAS98], magnetic treatment [HAS85] and surface coating techniques [WAN07] etc., to control the scaling problem and achieve fresh water at low costs.

Seawater desalination (reverse osmosis or thermal process) is one of these important industry processes, at which $CaCO_3$ represented the main scaling problem. In several studies [RED71], [SOH82], [KOU84], [GOM96], [ELF04] the induction time of $CaCO_3$ in **aqueous solution** was investigated at different conditions. However, it is well known that the induction time is affected by different parameters such as the level of supersaturation, presence the impurities, state of agitation, viscosity, etc [MUL93].

It is rare to find a study in literature of direct measurement of the induction time for $CaCO_3$ in the **bulk of a seawater** solution! It can be useful, however, in many applications to reduce the impact of $CaCO_3$ scaling.

2.6 Seawater composition and saturation state

Seawater is defined as multi-component electrolyte solution, wherein the solutes are primarily sodium and chloride ions, with lesser amounts of other inorganic ions as can be seen in table 2-1. The total amount of dissolved solid content in seawater is called salinity and usually expressed in part per thousand by weight. The salinity of normal seawater is approximately 35 g/kg [BUT82].

Table 2-1: Composition of the natural and artificial seawater [DAN67]

Ion	Atomic weight	Artificial seawater (g/kg)	Natural seawater (g/kg)
Cl^-	35.453	19.353	19.353
Na^+	22.9898	10.764	10.76
SO_4^{2-}	96.06	2.701	2.712
Mg^{2+}	24.312	1.297	1.294
Ca^{2+}	40.08	0.408	0.413
K^+	39.102	0.387	0.387
HCO_3^-	61.01	0.142	0.142
Br^-	79.91	0.066	0.067
Sr^{2+}	87.62	0.014	0.008
H_3BO_3	61.83	0.026	0.026
F^-	19.00	0.001	0.001

Normally, for research study, artificial seawater is used in order to minimize the biological effects and to provide a reproducible solution of known composition. The preparation methods of artificial seawater can be found in many references such as [MIL00] and [DAN67]. Table 2-2 shows the requirement amounts of inorganic salts to prepare artificial seawater with 35.17 g/kg salinity. Further, ASW with different values of salinities can also be obtained through the use of the same composition that is listed in table 2-2 but after multiplying by a conversion factor.

Table 2-2: Preparation of artificial seawater, here 35 g/kg salinity

Salt	Unit mass (g/kg)
NaCl	23.926
Na$_2$SO$_4$	4.008
KCl	0.677
NaHCO$_3$	0.196
KBr	0.098
H$_3$BO$_3$	0.026
NaF	0.003
MgCl$_2$	5.072
CaCl$_2$	1.147
SrCl$_2$	0.014
Total dissolved salts	**35.17**

Chemically, seawater as a complicated electrolyte solution can form sparingly soluble compounds such as $CaCO_3$, $CaSO_4$ and $Mg(OH)_2$ which can be deposited on the outer surface of heat transfer units in desalination systems.

It is worthwhile to mention that $CaCO_3$ is in saturation state in seawater, where the **supersaturation** of $CaCO_3$ in surface seawater was first noted in the central Atlantic by Wattenberg and Timmerman in 1936. Also it appears that most surface waters of the world's oceans are supersaturated with respect to $CaCO_3$. This non equilibrium state of the $CaCO_3$ system in surface seawater has generally been attributed to some non-specific inorganic reaction kinetic control [CHA70]. In contrast the $CaCO_3$ state in deep seawater is **undersaturated** because its solubility increases strongly with pressure and salinity. Also to a lesser extent an effect comes from the slight decreases in solubility with decreasing temperature. Hence, this decrease of saturation with depth is not due to a change in total carbonate or alkalinity [CHA70]. Table 2-3 shows the degree of supersaturation of $CaCO_3$ in the surface and deep seawater as calculated by BUTLER [BUT82].

It has been investigated that when S~7, the deposition rate of $CaCO_3$ is quite small, this value is considered a critical value of supersaturation. The larger this value is the more the deposition rate will increase and remain roughly constant for a fixed condition [GLA01]. The degree of supersaturation of the $CaCO_3$ value in the surface of seawater is **_considered to be very small_**. Hence, the surface of seawater is generally supersaturated with $CaCO_3$ but it will not precipitate from natural seawater in a convenient experimental time [CHA70].

Table 2-3: Degree of supersaturation of $CaCO_3$ in natural seawater (T = 25 °C, salinity = 35 g/kg) [CHA70]

Parameter	Surface	Depth
	0 m	6730 m
Pressure	1 atm	667 atm
pH	8.25	8.10
$[CO_3^{2-}]$	0.00023	0.00007
$[Ca^{2+}][CO_3^{2-}]$	0.00239	0.0000006
$S = \dfrac{[Ca^{2+}][CO_3^{2-}]}{K_{so}}$	**5.2481**	**0.3802**

Here it is very necessary to mention that the $CaCO_3$ activity coefficient in seawater was calculated and included with solubility product (K_{so}) in the calculation of the degree of supersaturation.

2.7 Chemical definition of scales

Scaling can be defined as the non wanted deposit of inorganic compounds on surfaces as an example on a heat exchanger. The most negative effect of scaling is in decreasing the efficiency of the heat transfer rate affecting the yield of the process. The biggest problem that faces the seawater desalination industry other than corrosion is the scale formation. Many intensive studies showed the most important conditions, which are accompanying the scale formation in seawater desalination. Scales can be divided into two main classes in the seawater desalination [GLA 01]:
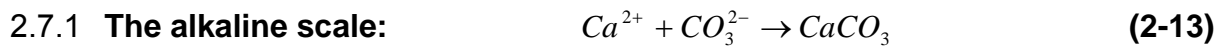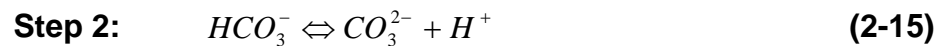
2.7.1 The alkaline scale: $\qquad Ca^{2+} + CO_3^{2-} \rightarrow CaCO_3$ **(2-13)**

Reaction mechanism I (acidic mechanism):

$\qquad\qquad$ **Step 1:** $\qquad CO_2 + H_2O \Leftrightarrow HCO_3^- + H^+$ **(2-14)**

$\qquad\qquad$ **Step 2:** $\qquad HCO_3^- \Leftrightarrow CO_3^{2-} + H^+$ **(2-15)**

Reaction mechanism II (alkaline mechanism):

$\qquad\qquad$ **Step 1:** $\qquad CO_2 + OH^- \Leftrightarrow HCO_3^-$ **(2-16)**

$\qquad\qquad$ **Step 2:** $\qquad HCO_3^- + OH^- \Leftrightarrow CO_3^{2-} + H_2O$ **(2-17)**

The overall reaction: $\qquad 2HCO_3^- \Leftrightarrow CO_2 + CO_3^{2-} + H_2O$ **(2-18)**

Normally the CO_3^{2-} ions are the limiting reactants in seawater, which is, however, not enough to reach the required degree of supersaturation for a precipitation. But when changes in the conditions of:

- Temperature and pressure
- Concentration of HCO_3^-
- Concentration of CO_2 gas dissolved

occur, equation 2-18 can shift to the right side and this will lead to an increase in the concentration of CO_3^{2-} in the bulk solution of seawater. This is essential to form the major scales of $CaCO_3$ in seawater desalination.

2.7.2 The non alkaline scale: $\qquad Ca^{2+} + SO_4^{2-} \rightarrow CaSO_4$ **(2-19)**
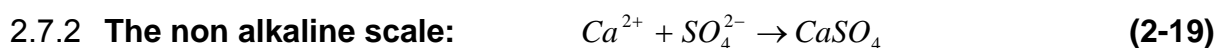
This kind of scales has a different chemical mechanism which is not the case here.

2.8   Desalination methods

Desalination can be defined as any process that removes salts from water. Desalination processes may be used in municipal, industrial, or commercial applications. With improvements in technology, desalination processes are becoming cost-competitive with other methods of producing usable water.

There are two major types of technologies that are used around the world for desalination. They can be broadly classified as either **thermal** or **membrane**. Both technologies need energy to operate and produce fresh water. Within those two broad types, there are sub-categories (processes) using different techniques. The major desalination processes are identified in table 2-4:

Table 2-4: Desalination Technologies and processes

Thermal Technology	Membrane Technology
Multi-Stage Flash Distillation (MSF) [WAN07]	Electrodialysis (ED)
Multi-Effect Distillation (MED)	Electrodialysis reversal (EDR)
Vapor Compression Distillation (VCD)	Reverse Osmosis (RO)

Thermal technologies, as the name implies, involve the heating of saline water and collecting the condensed vapour (distillate) to produce pure water. Thermal technologies have rarely been used for brackish water desalination, because of the high costs involved. They have, however, been used for seawater desalination and can be sub-divided into three groups: Multi-Stage Flash Distillation (MSF), Multi-Effect Distillation (MED), and Vapour Compression Distillation (VCD).

Membrane technologies can be subdivided into two broad categories as can be seen in table 2-4, *Electrodialysis (ED)* is a voltage-driven membrane process. An electrical potential is used to move salts through a membrane, leaving fresh water behind as product water. The *Electrodialysis Reversal (EDR)* unit operates on the same general principle as an ED unit, except that both the product and concentrate channels are identical in construction.

In relation to thermal processes, *Reverse Osmosis (RO)* is a relatively new process that was commercialized in the 1970s. Currently, the RO processes use pressure as the driving force to push saline water through a semi-permeable membrane into a product water stream and a concentrated brine stream [HAR08].

2.9   Problems caused by scaling

One of biggest challenges that face the seawater desalination industry is scales formation. Scales formation occurs due to the elevating the degree of supersaturation of scales (sparingly soluble inorganic compounds). Scales causes reduction in the performance of desalination process, this reduction can be seen in different ways according to the types of technology as following:

2.9.1   **Thermal technologies**

The effect of scaling in this technology can be summarized in two main types:

- Formation of an insulating film on the tube surface, which leads to additional resistances to heat transfer, hence, resulting in a reduction of plant thermal efficiency.
- Narrowing the passage way of seawater. This leads to higher pumping costs.

Both effects are involved in the increase of the saline water production cost [GLA01].

2.9.2   **Membrane technologies**

Reverse osmosis plants have at their heart a membrane that if damaged reduces output, increases costs and gives poor water quality. It is therefore important to keep it clean.

When the sparingly solubility compounds are exposed along the membrane surface due to an increase in their concentrations, a precipitation process starts onto the membrane surface that results in a scale formation. The amount of scales will be increased with time leading to a reduced output and increased product water conductivity.

The worst of these solids being calcium carbonate and calcium sulphate and so the prevention of their precipitation is vital if the membrane is to function efficiently [ACC08].

2.10   Methods of scale reduction; disadvantages

A lot of efforts have been carried out to find methods in order to prevent the scaling phenomena from taking place in industrial applications. Chemical and mechanical treatments are widely used in industry. Dosing traces of amounts of chemicals that are inhibiting crystal growth of the scaling materials is called chemical treatment [HAS98]. This treatment is effective but it has a disadvantage in terms of not being friendly to environment and it is costly. Another kind of chemical treatment is known as acid cleaning [HAN03]. Even though, acid treatment is a very effective

method, it contributes to increase corrosion in case of an excess acid addition. Large quantities of acid; leads to increasing costs.

The mechanical treatment has different mechanisms. One of these mechanisms is a mechanical cleaning; this can be achieved through circulating sponge balls injected inside the tubes of the heat exchanger. By this way the scaling in the heat exchanger can be reduced [ALB93].

In the literature it was further suggested to prevent scale formation by removing minerals from the feed in a prior unit operation [NIS04]. This can be achieved by using equipments in which the precipitation and separation process can take place for the scaling materials.

2.11 Aims of research work

The crystallization industry is still facing many challenges at different levels in terms of e.g. obtaining the desired product and solving industrial problems by using crystallization technology. One of these challenges is to study the width of metastable zone of inorganic compounds. Since the most important influences on the width of the metastable zone is due to the kind and concentration of the impurities existing in solutions. However, the presence of impurities in a solution leads to different disturbances in the yield of a product. So far only an experimental determination for the effects of impurities exists in the relevant literature, however, without any interpretation of these results. Most explanations of nucleation and crystal growth in presents of additives start at the solid phase but do not take into account the change in the structure of the solution when additives are added to a solution.

In the present work, it is investigated if the properties of intermolecular interactions of cations and anions of each additive, solvent and salt in the solution are the key to the interpretation of the influence of additives on the metastable zone width of inorganic compounds.

The polythermal method was used to measure the effect of the additives, e.g. Al^{3+}, Fe^{2+}, Ba^{2+}, Li^+ and K^+ on the MSZ width of $ZnSO_4$. *These additive ions were selected according to a suggested rule which takes the amount of hydration enthalpy values into account as will be illustrated.*

A better understanding for the thermodynamics of crystallization processes of multi-component systems can contribute highly in improving and modifying methods to solve different problems in crystallization applications. One of these applications is the seawater desalination. Since the scale reduction is still a competitive topic in terms of minimizing the process cost and environmental impact due to use of chemical methods.

The other important part in this work is to show the possibility to reduce scale formation e.g. in seawater desalination. The principal idea of the concept is a reduction of the amount of calcium ions, which are causing the main scaling problem in seawater desalination such as $CaCO_3$ and $CaSO_4$ scales. This reduction of calcium ions can be carried out before the feed of the seawater goes into the desalination unit. It can be defined as pre-precipitation and pre-separation unit. In this unit, it is suggested to use the power of ultrasound to accelerate the precipitation of calcium carbonate after modifying the degree of supersaturation in seawater.

Moreover, the crystal growth of natural calcite has been used to see if a reduction of the $CaCO_3$ concentration is possible in seawater?

The induction time of $CaCO_3$ in artificial seawater after modifying the degree of supersaturation was investigated. This is necessary in understanding the kinetics of $CaCO_3$ precipitation in artificial seawater that will be very helpful in selecting a suitable method to achieve the reduction purpose. In addition, this will fill the shortfall in the literatures.

2.12 Present work methodology

2.12.1 Suggested rule to select the additives

On the basis of the dissolution steps as illustrated in the figure 2-1, it is suggested to create a selection rule that takes the amount of hydration enthalpy values into account as shown in table 2-5. Where some inorganic compounds have been classified in terms of their hydration enthalpy values for cations and anions [MUR84]. According to this table different groups (see figure 2-5) can be obtained to study the effect of additives on the MSZ width. In table 2-5, rows and columns refer to the hydration enthalpy values of the cation and anion of the salts, respectively.

Table 2-5: Classification of inorganic compounds in terms of hydration enthalpy value

Hydration enthalpy (kJ/mol)			Additives	
Anion values / Cation values	1500-1000	500-0	Cations	Anions
5000-4000	$Al_2(SO_4)_3$	$AlCl_3$	Al^{3+}	SO_4^{2-} or Cl^-
4000-3000		$ScCl_3$	Sc^{3+}	SO_4^{2-} or Cl^-
2500-2000	$ZnSO_4$ or $CuSO_4$		Cu^{2+}	SO_4^{2-} or Cl^-
2000-1500	$FeSO_4$	$FeCl_2$	Fe^{2+}	SO_4^{2-} or Cl^-
1500-1000		$BaCl_2$ or $MgCl_2$	Ba^{2+} or Mg^{2+}	SO_4^{2-} or Cl^-
1000-500	Li_2SO_4	$LiCl$	Li^+	SO_4^{2-} or Cl^-
500-0	K_2SO_4	KCl	K^+	SO_4^{2-} or Cl^-

The first group can be obtained by selecting as an example $ZnSO_4$ as the compound to study and the other salts {$Al_2(SO_4)_3$, $FeSO_4$, $BaCl_2$, Li_2SO_4 and K_2SO_4} as additives. This is how a selection procedure for additives for the rest of the compounds in the table can be set up. Therefore it can be studied if this rule can be used to explain the effect of additives on the MSZ width with respect to their hydration enthalpy values.

$$ZnSO_4 \quad \begin{matrix} Al_2(SO_4)_3 \\ FeSO_4 \\ BaCl_2 \\ Li_2SO_4 \\ K_2SO_4 \end{matrix} \qquad LiCl \quad \begin{matrix} AlCl_3 \\ FeCl_2 \\ MgCl_2 \\ BaCl_2 \end{matrix} \qquad K_2SO_4 \quad \begin{matrix} CuSO_4 \\ BaCl_2 \\ Li_2SO_4 \end{matrix} \qquad \cdots$$
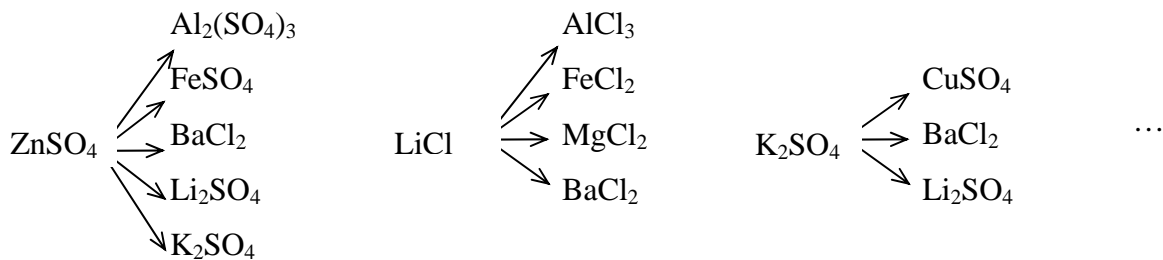
Figure 2-5: Some groups (main compounds and potential additives), which are obtained from table 2-5 in order to study the additive effect

2.12.2 Suggested methods to reduce scaling in seawater desalination

Two principles of crystallization have been suggested to reduce the resource of $CaCO_3$ scaling from artificial seawater:

⬥ **Crystal growth**

The principle of crystal growth can be applied through providing a growth medium for $CaCO_3$ in artificial seawater without chemical addition. A fluidized bed crystallizer was used for this purpose.

⬥ **Precipitation**

The power of ultrasound has been used to accelerate the precipitation of $CaCO_3$ in the bulk solution of seawater. This precipitation cannot occur without modifying the supersaturation of calcium carbonate. Because the degree of supersaturation is considered very low when it is compared with S~7 (see section 2.6), as illustrated in table 2-6. In spite of increasing the temperature and salinity, it shows a small difference in the degree of supersaturation. The calculations have been done according to the degree of supersaturation defined by equation 2-20 [ALR 04].

$$S = \frac{[Ca^{2+}][CO_3^{2-}]}{K_{sp}} \tag{2-20}$$

Table 2-6: Degree of supersaturation (S) of $CaCO_3$ in seawater as a function of salinity and temperature

T (°C)	Salinity (g/kg)	pH	$K_{sp\ calcite}$	$[Ca^{2+}]$	$[CO_3^{2-}]$	$\gamma_{Ca^{2+}}$	$\gamma_{CO_3^{2-}}$	S
25	35	7.82	6.411E-07	0.01027	0.00017	0.2282	0.0228	2.73
25	45	7.9	9.045E-07	0.01320	0.00030	0.2398	0.0154	4.41
25	55	7.91	1.247E-06	0.01614	0.00040	0.2607	0.0103	5.23
25	65	7.91	1.721E-06	0.01907	0.00048	0.2903	0.0066	5.29
25	75	7.9	2.410E-06	0.02201	0.00050	0.3296	0.0042	4.60
25	85	7.91	3.451E-06	0.02494	0.00051	0.3802	0.0025	3.68
80	35	7.68	4.356E-07	0.01027	0.00060	0.1914	0.0123	14.07
80	45	7.67	6.895E-07	0.01320	0.00086	0.2024	0.0074	16.39
80	55	7.72	1.054E-06	0.01614	0.00120	0.2222	0.0044	18.45
80	65	7.76	1.597E-06	0.01907	0.00152	0.2507	0.0026	18.16
80	75	7.77	2.439E-06	0.02201	0.00170	0.2889	0.0015	15.37
80	85	7.71	3.789E-06	0.02494	0.00159	0.3390	0.0008	10.48

It should be observed that the $CaCO_3$ activity coefficient in seawater was calculated and is included together with the solubility product (K_{sp}) in the calculation of the degree of supersaturation in equation 2-20.

Furthermore, the limit of metastable zone of $CaCO_3$ in pure water has been investigated [ELF04]. Table 2-7 shows the conditions for the spontaneous precipitation of calcite at T=30 °C.

Table 2-7: The required degree of supersaturation for spontaneous $CaCO_3$ precipitation

T (°C)	$[Ca^{2+}]$	$[CO_3^{2-}]$	$\gamma_{\pm}^{v}$	t_G (min)	$S=\gamma_{\pm}^{v}[Ca^{2+}][CO_3^{2-}]/K_{sp\ calcite}$
30	0.005	0.000136	0.783183	11	172.3
30	0.004	0.000131	0.786566	16	133.4
30	0.003	0.000123	0.785697	22	94.0
30	0.0025	0.000112	0.820394	32	74.6
30	0.0015	0.000048	0.933858	120	21.8
30	0.001	0.000035	0.930877	1000	10.5

Consequently, the degree of supersaturation can be increased artificially by adding a compound containing calcium ions or compounds which are sources of carbonate ions. In the case of seawater desalination, the carbonate ions are the limiting reactant affected by different conditions of temperature, pressure, bicarbonate ions concentration and the amount of CO_2 gas dissolved in seawater. Moreover, the calcium ions are caused also by another kind of scaling which is known as $CaSO_4$. Therefore, only the addition of CO_3^{2-} ion can achieve the logic of the goal of reducing Ca^{2+} ions, i.e. the scale formation in seawater. This can be done by the addition of e.g. $NaHCO_3$.

3. <u>Experimental Work</u>

The principle work of some experimental methods, tools and equipments that are used in this work have been explained in details in many previous works which will be referred in this chapter as references. Here only the new information should be mentioned to describe the experimental work.

To achieve the aims of this work three different types of experimental methods were carried out:

- Polythermal and isothermal methods to determine:

  - The effect of inorganic impurities on the width of the metastable zone of inorganic compounds.
  - The induction time of calcium carbonate in artificial seawater.

- The fluidized bed crystallizer technique to reduce the calcium ion concentration in artificial seawater by:
  - Seeds of natural calcite.
  - The hot finger technique.

- Ultrasonic irradiation to accelerate the precipitation process of $CaCO_3$ in artificial seawater.

The following analyzing techniques have been used:
1. The atomic absorption spectroscopy to determine the change of the calcium ion concentration in samples.
2. The X-ray diffraction technique to analyze the type of the solid product.
3. The complex metric titration method to determine the total concentration of calcium and magnesium ions in seawater.

3.1   Polythermal and isothermal methods

3.1.1 **The effect of inorganic impurities on the width of the metastable zone**

Principally the determination of the metastable zone width can be achieved by optical detection. The polythermal method is used in this work and is described by Nyvlt [NYV85]. The measurement of metastable zone can also be carried out by means of an ultrasonic device [OMA99] which has the advantage in terms of online measurement, and data recording. Figure 3-1 shows the experimental setup used here. The prepared solution is divided into a number of parts of equal volume.

The number (N) of stages corresponds to the number of additives which are added to every part of the solution separately. The aim of carrying out these measurements in parallel is to reduce the total required time for all experiments. Furthermore, each run was repeated three times to have at the end the average of three points each. The other important factor is the selection of the concentration of additives to start with. It is important to start with addition of a trace of amounts at first in order to observe the expected maximum change in MSZ width which has been shown in the literature.
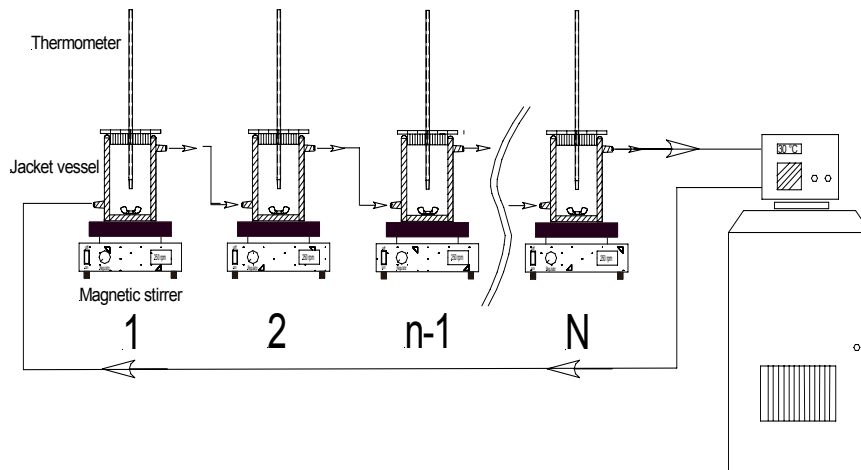
Figure 3-1: Experimental setup for the measurements of the effect of the additives on the metastable zone width

The operation conditions of experiments to determine the effect of impurities on the metastable zone of e.g. zinc sulfate, lithium chloride and potassium sulfate are shown in the tables 3-1, 3-2 and 3-3, respectively.

Table 3-1: Operational conditions of the measurements of the effect of impurities on the metastable zone width of $ZnSO_4$

Impurities	$Al_2(SO_4)_3$, $FeSO_4$, $BaCl_2$, Li_2SO_4 and K_2SO_4
Stirring rate	300 rpm
Volume of solution	300 mL
Cooling rate	10 K/h
Saturation temperature	26 °C

Table 3-2: Operational conditions of the measurements of the effect of impurities on the metastable zone width of LiCl

Impurities	$AlCl_3$, $FeCl_2$, $MgCl_2$ and $BaCl_2$,
Stirring rate	300 rpm
Volume of solution	300 mL
Cooling rate	10 K/h
Saturation temperature	15.5 °C

Table 3-3: Operational conditions of the measurements of the effect of impurities on the metastable zone width of K_2SO_4

Impurities	$CuSO_4$, $BaCl_2$ and Li_2SO_4
Stirring rate	300 rpm
Volume of solution	300 mL
Cooling rate	10 K/h
Saturation temperature	25.5 °C

3.1.2 Induction time of calcium carbonate in artificial seawater

The induction time measurements of precipitation in bulk solution can be carried out in different ways. The most important factor which should be taken it into account in determination the induction time is a fast sensitive method for detection [MUL93].

In the present work, the online pH measurement of the bulk solution was selected as detection method to determine the induction time of $CaCO_3$ in the artificial seawater.

The experimental requirements on a set-up for the determination of the induction time of $CaCO_3$ in ASW are shown in the figure 3-2. The experiments were conducted in 0.5 L thermostat vessel, with a magnetic stirrer, and a condenser to keep the volume of the solution constant during

Figure 3-2: Experimental set-up of the measurements of the induction time of $CaCO_3$ in artificial seawater

each run and to allow the dissolving carbon dioxide in the seawater solution to equilibrate with the atmosphere. A pH meter (AIMEMO 2290-8) was used to record the online change in the concentration of the bulk solution with time.

The operational volume of the artificial seawater [DAN67] of a specific salinity has been fixed 125 mL for each run. The online pH measurements start when the temperature of the artificial seawater is constant with time. A certain amount of $NaHCO_3$ was added as solid phase in order to avoid a change in the ASW concentration, what would be the case by the addition of the $NaHCO_3$ in aqueous solution form.

3.2 Fluidized bed crystallizer

3.2.1 Seeds of natural calcite

A fluidized bed crystallizer is a laboratory equipment used to measure the growth and dissolution rates of crystals in suspension from supersaturated solution. Figure 3-3 shows the equipment as it is built in the laboratory and previously used and described e.g. by [KRU92].
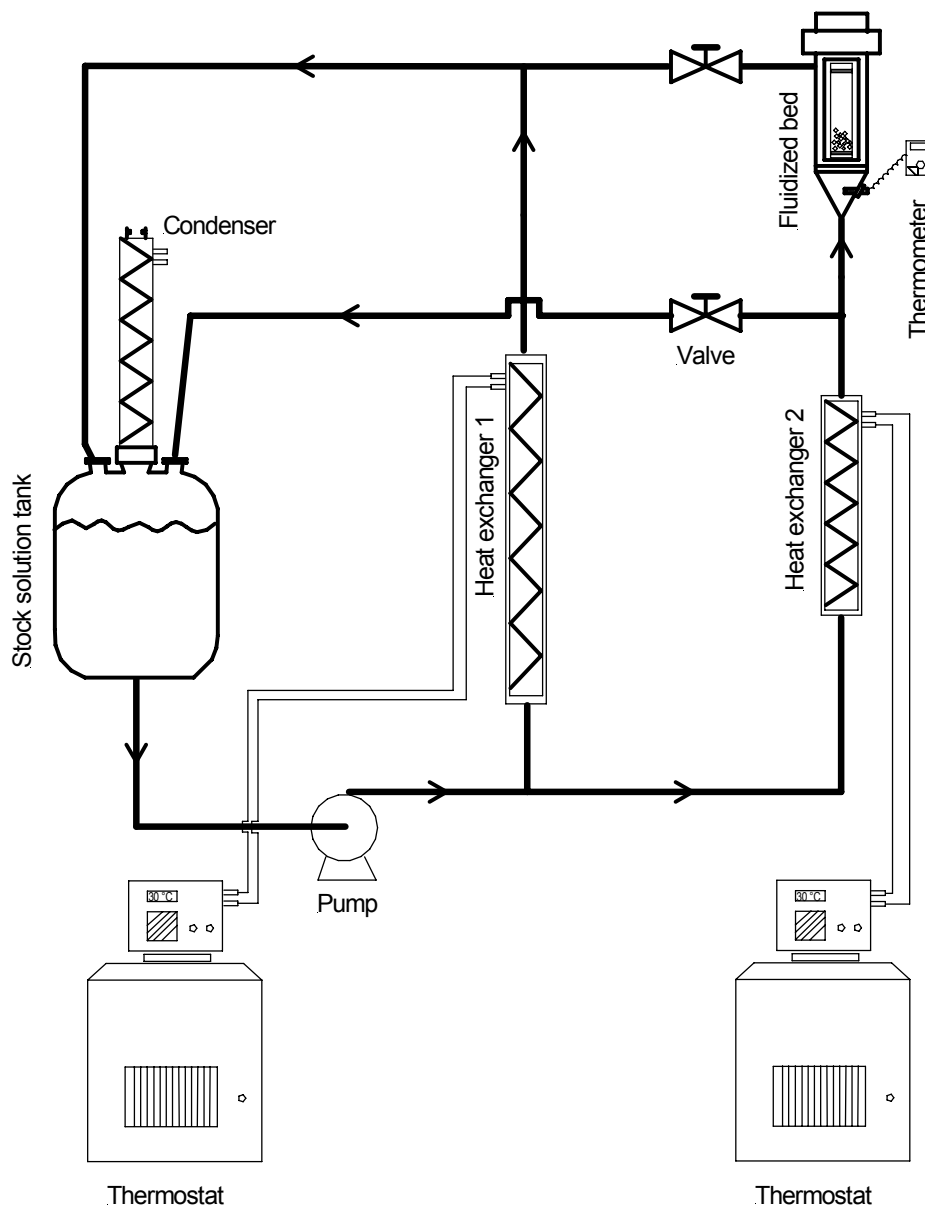
Figure 3-3: Schematic diagram of a fluidized bed crystallizer

Artificial sea water with a specific salinity (see [DAN67]) is prepared to circulate in the closed system. The temperature in the fluidized bed is controlled to obtain the

required level of supersaturation staying within the metastable zone width. No nucleation should occur. Furthermore, the temperature of the stock solution should always be at a certain level in the tank where the solution should always be in an undersaturated condition. To achieve a supersaturation of $CaCO_3$ the saturated solution has to be heated. This is due to the fact that $CaCO_3$ has solubility which diminishes with increasing temperature as can be seen in figure 3-4.
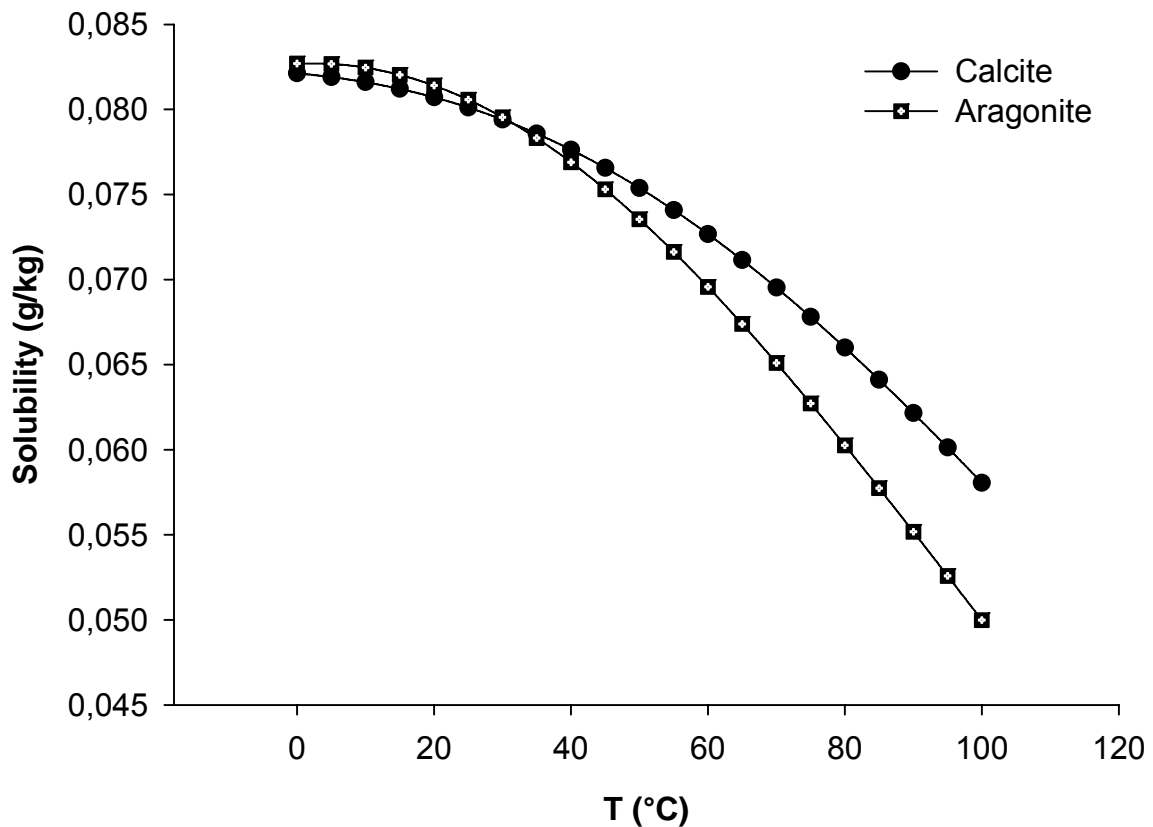
Figure 3-4: Solubility curve of calcite and aragonite in the seawater with 35 g/kg salinity [MUC83]

The fluidized bed crystallizer can serve to see if a reduction of the amount of $CaCO_3$ in seawater due to growth of $CaCO_3$ seeds occurs while fluidized in the seawater.

Usually the available size of seeds of $CaCO_3$ is not larger than 10-20 µm (see commercial products). This size is not appropriated for the operation of fluidized bed crystallizer. Therefore, natural calcite crystals (see figure 3-5) were used where the length of each crystal is about 18 mm. These natural calcite crystals are grinded in a mortar. Then the product has been sieved to get the desired size fractions that are between 500-1000 µm was collected.

24

Figure 3-5: Natural calcite originating from cavities in the lava layers from northwest of Brazil

3.2.2 **The hot finger technique**

The concept of applying the overgrowth process of $CaCO_3$ on a heat transfer surface which is already coated with an initial scale layer of $CaCO_3$ to reduce scaling problem, is a result of study has done by Hasson [HAS67]. The study of mechanism of $CaCO_3$ scale deposition on heat-transfer surfaces showed that the rate of deposition is increased with surface temperature increased. Therefore and to exam the possibility of reducing $CaCO_3$ amount in the seawater, a hot metallic heat exchanger that coated with $CaCO_3$ as shown in figure 3-6 has been used. The coating process can be achieved by immersing the hot finger for several days at 80 °C in the solution of $CaCO_3$ which is over saturated.

The reduction of concentration of the $CaCO_3$ measurements can be carried out by keeping the circulating seawater at a temperature lower than the temperature of the surface of heat exchanger which is connected with a thermostat. This leads to

the most important conditions which accelerate the decomposition process in terms of:

* Diffusion process of reactant Ca^{2+} and HCO_3^- from bulk seawater to the scale surface interface.
* Chemical reaction of producing the CO_3^{2-} and CO_2 at the scale surface interface.
* Crystallization of $CaCO_3$ on the scale surface layer.
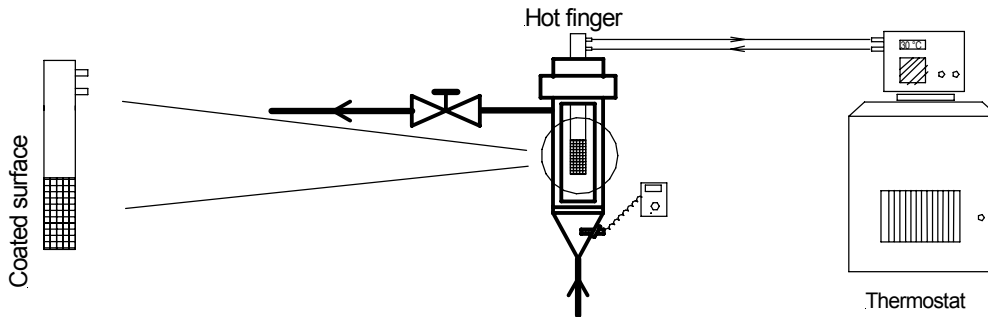
Figure 3-6: Hot finger fixed in the fluidized bed

3.3 Ultrasonic irradiation

The process of $CaCO_3$ precipitation can be achieved using the apparatus shown in figure 3-7. It consists of three main parts: 1) Ultrasound generator and probe to accelerate the precipitation process in terms of creating very high local pressures and temperatures [GUO06]; 2) Condenser to keep the volume of seawater constant during the time of the experiment; 3) water bath and thermostat to control the temperature of seawater in the vessel. The experimental conditions of measuring the reduction of calcium ions are illustrated in table 3-4.

Table 3-4: Operational conditions of experiments

Operational condition	*Values*	*Units*
Temperature	50, 60, 70, 80, 90	°C
Mass of $NaHCO_3$	0, 1, 1.5, 2, 2.5, 3, 3.5, 4	g
Operational time	2, 4, 6	min
Power of ultrasound	20, 40, 60, 80, 100	W
Seawater salinity	35, 59, 80	g/kg H_2O

The temperature of the artificial seawater (ASW) was kept constant using a water bath. Then the degree of supersaturation of $CaCO_3$ has been increased by addition of stoichiometric amounts of sodium bicarbonate as shown in table 3-4. An ultrasonic

power input with a specific intensity leads to very fast precipitation process producing a solid product, which can be obtained after a high pressure filtration with a 0.45 µm pore size filter paper. Two methods were used to determine the changes in the calcium ions content in the seawater. A quality test using X-ray diffraction to analyze the solid product. And atomic absorption spectroscopy (AAS) that has been used to determine the calcium ion concentration change in ASW. Additionally, the complex metric titration method was used to determine the total amount of magnesium and calcium ions in ASW as quantity methods [UOC08]. Other operational conditions studied are related with the CO_2 releasing rate which is accompanying the $CaCO_3$ process.
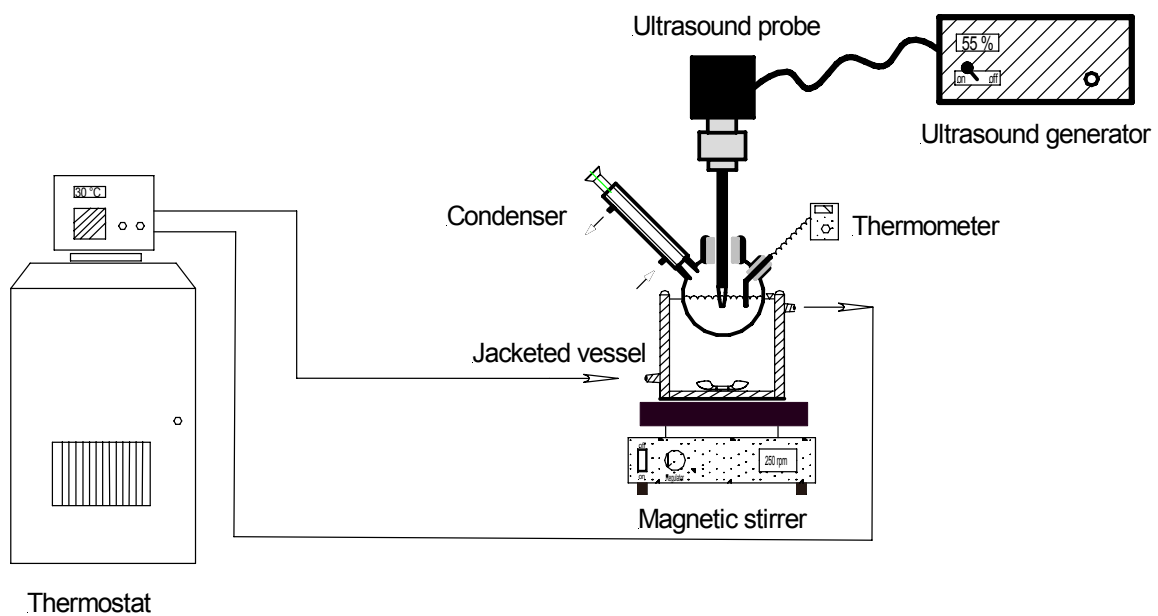
Figure 3-7: Schematic diagram of the experimental apparatus.

4. <u>Results</u>

In this chapter, the results of the experimental work will be shown:

* The effects of inorganic additives on the metastable zone width of inorganic compounds, selected according to the suggested rule (see section 2.12.1).
* Results of the measurements of $CaCO_3$ induction time in artificial seawater at different level of supersaturation, temperature and salinity.
* $CaCO_3$ reduction from artificial seawater by the use of a fluidized bed crystallizer, without modifying the $CaCO_3$ supersaturation.
* $CaCO_3$ reduction from artificial seawater by the use of an ultrasound technique, with modifying the $CaCO_3$ supersaturtion by $NaHCO_3$ addition.
* **Statistical error test results:** every experimental result is subjected to two categories of errors:

1. <u>**Random error:**</u> this kind of error is caused by unknown and unpredictable changes in the experiment. These changes may occur in the measuring instruments or in the environmental conditions. Statistical methods are used normally to analyze the data and to find how the data are precise. For example, the ***mean*** of a number of measurements of the same quantity is the best estimate of that quantity and the ***standard deviation*** of the measurements as well shows the accuracy of the estimate. Moreover, the ***standard error*** (SE) also can be used to obtain more accurate estimation of the true mean. Since, the smaller the value of the standard error is the more accurate is the mean. *For the results*, here vertical error bars are used to represent the standard deviation of data mean for each measurement separately. As well as, standard error (SE) values are also used to analyze the data.

2. <u>**Systematic error**</u>: this kind of error usually results from the measuring instruments and experimenters. The **accuracy** of a measurement is its nearness to the true value of the quantity being measured. Consequently, the measurement of weight, volume and temperature can be considered as the determining factors for systematic errors for this work.

4.1   The effect of selected inorganic additives on the MSZ width of inorganic compounds

4.1.1   **The effects of $Al_2(SO_4)_3$, $FeSO_4$, $BaCl_2$, Li_2SO_4 and K_2SO_4 on the MSZ width of $ZnSO_4$**

The effect of the additives Al^{3+}, Fe^{2+}, Ba^{2+}, K^+, Li^+ and Cl^- on the MSZ width and the pH of $ZnSO_4$ are shown in **figures 4-1 to 4-10**. These results represent the first group of selected ions as additives of table 2-5.

4.1.1.1 The effect of Al$_2$(SO$_4$)$_3$ on the MSZ width of ZnSO$_4$

Figure 4-1 shows the change in the MSZ width of ZnSO$_4$ as a function of Al^{3+} ion addition to ZnSO$_4$ solution. A very small amount (about 5 ppm) of salt was added at the beginning of each experiment to reveal if the maximum change in the MSZ width can be found as it was reported by Titiz-Sargut and Ulrich [TIT02]?

In figure 4-1 it can be seen that there is a change in the MSZ width as a line with a maximum due to Al$_2$(SO$_4$)$_3$ addition in the concentration range between 5 and 30 ppm. By adding more Al^{3+} ions to the solution a decrease in the MSZ width is achieved. In addition, the pH value of ZnSO$_4$ solution is seen to be constant (about pH=4) with the variety of Al^{3+} ion concentration (10 - 50 ppm).

The most important factor in the change in the MSZ width due to additives is the combined change of the saturation and nucleation temperature. Figure 4-2 shows the saturation and nucleation temperature as a function of Al^{3+} ions concentration. It is clear that the change in MSZ width of ZnSO$_4$ is due to the change in both the saturation and the nucleation temperature.
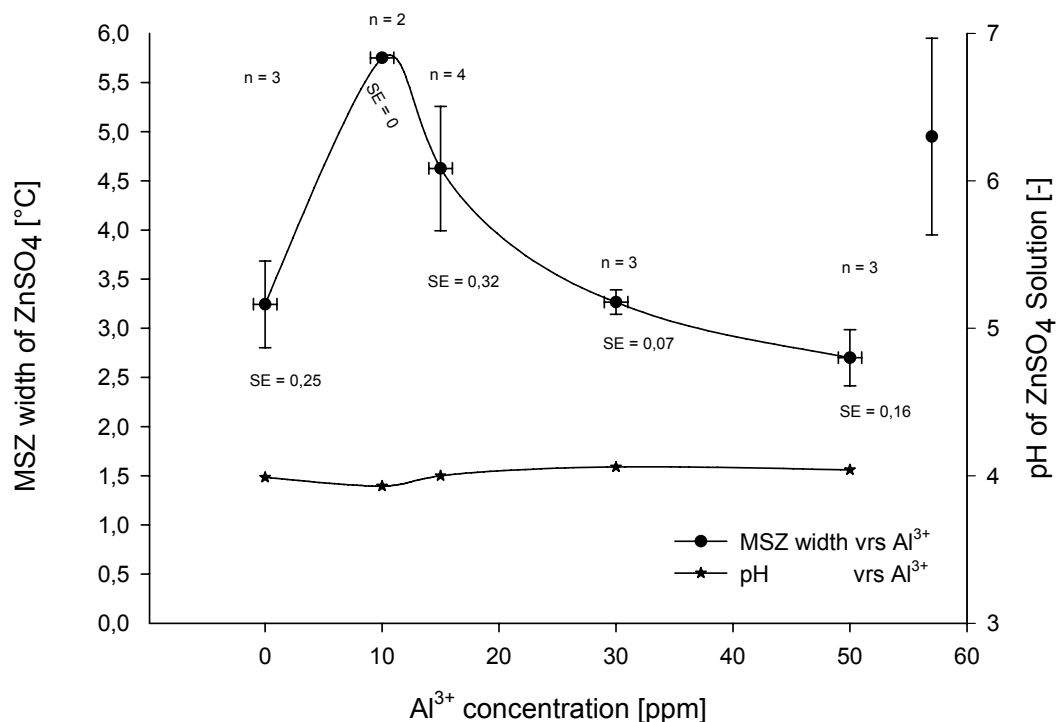
Figure 4-1: Effect of Al^{3+} ions on the MSZ width and pH of ZnSO$_4$ – water solution
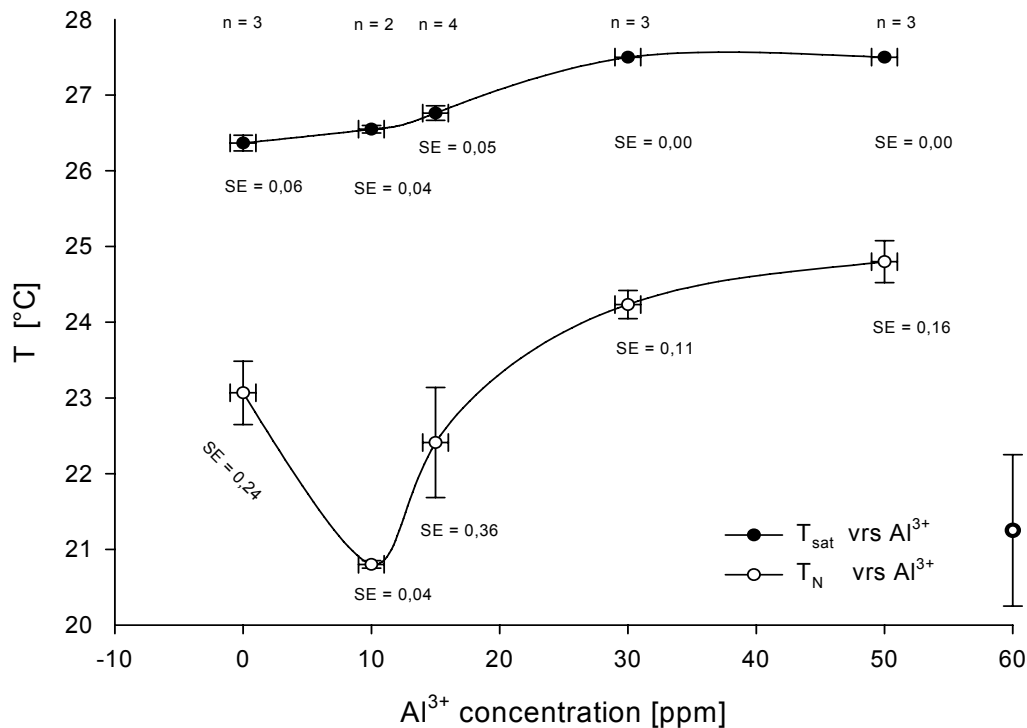
Figure 4-2: Effect of Al^{3+} ions on the saturation and nucleation temperature of $ZnSO_4$ – water solution

The slope of the saturation temperature curve is increased with a small increase of Al^{3+} ions (in the range of 10-30 ppm). Then, there is no further change in the slope when the addition of Al^{3+} increased beyond the value of 30 ppm.

In contrast, the nucleation temperature of $ZnSO_4$ has shifted to the lowest point when 10 ppm of Al^{3+} ions was added as to be seen in figure 4-2. But after this limit and up to 50 ppm, the nucleation temperature was increased.

Here it is very important to mention that the vertical error bars as shown in the figures 4-1 and 4-2 are referring to the standard deviation values. The standard deviation value of each measurement can be recalculated from each figure by dividing the length of certain vertical bars on the length of the reference bar which can be found on the right side in each figure. This is a reference bar application. In addition, it can be used also to give a fast comparison. The value of the reference bar *__for those figures__* is equal to the maximum value of standard deviation which might be reached by any result of each experiment.

The standard error (SE) is an addition of statistical evaluation method that has been used as shown in the figures 4-1 and 4-2. One can see how the value of standard error changed proportionally with length of vertical error bars. Additionally, figures 4-1 and 4-2 show the horizontal error bars that referred to the accuracy percentage of the weight of $Al_2(SO_4)_3$, the volume of $ZnSO_4$ solution and the temperature reading which

totally equals 1% of measured value of mass, volume and temperature, respectively. This value of systematic error is used for the reset results of studying the additive effect on the MSZ width.

4.1.1.2 The effect of FeSO$_4$ on the MSZ width of ZnSO$_4$

In figure 4-3 the Fe^{2+} ion addition in the concentration range between 5-150 ppm shows no effect on the pH value of the solution and no change in the MSZ width of zinc sulphate. Figure 4-4 shows the image of the effect more clear when the saturation temperature of ZnSO$_4$ is constant with an addition of Fe^{2+} ions. In contrast, the slope of the nucleation curve is decreasing very slightly with a Fe^{2+} addition only in the range between 5-50 ppm.

The variation of error bar values in terms of standard deviations is shown in figure 4-3. The values of the error bars can be estimated by comparing each bar length with the length of the reference bar on the lower right side in the figure 4-3.
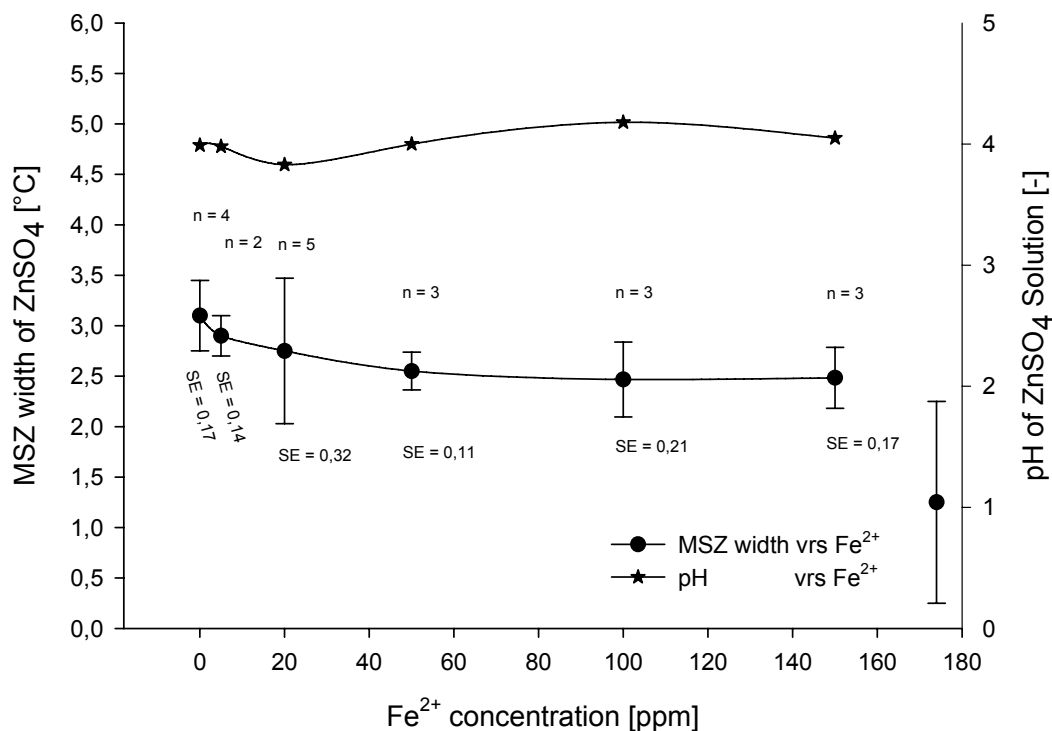
Figure 4-3: Effect of Fe^{2+} ions on the MSZ width and pH of ZnSO$_4$ – water solution

On the other hand, the standard deviation of each saturation temperature point is very low as to be seen in figure 4-4, but on the contrary, in the case of nucleation curve it is seen to be high. Additionally, the standard error of each measurement point of the saturation temperature is seen to be low compared to the nucleation curve.
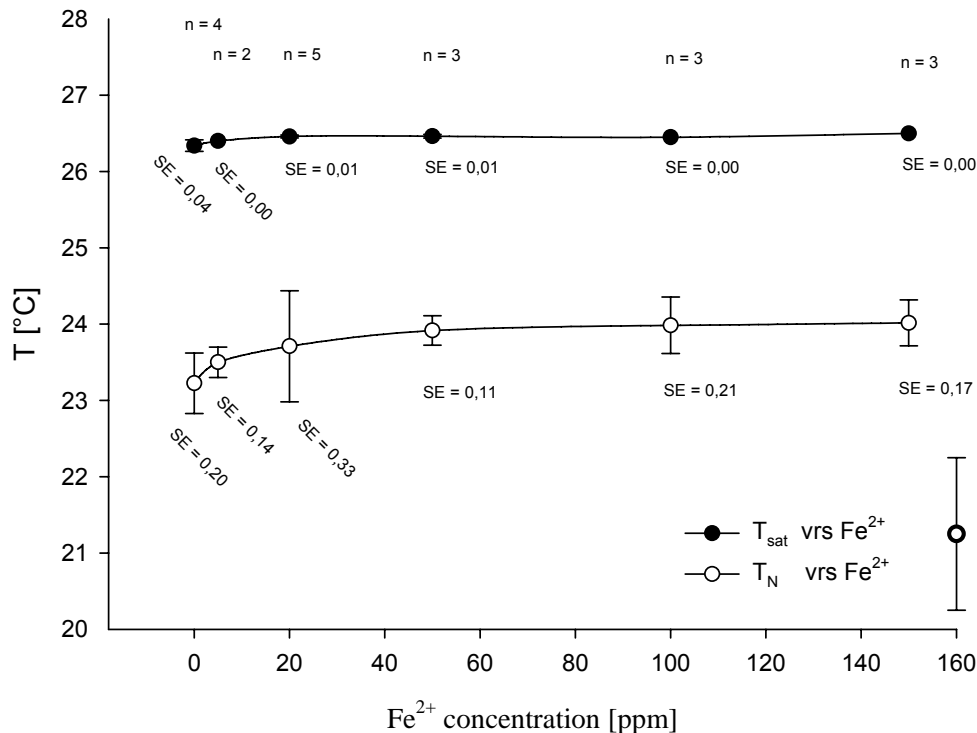
Figure 4-4: Effect of Fe^{2+} ions on the saturation and nucleation temperature of $ZnSO_4$ – water solution

4.1.1.3 The effect of $BaCl_2$ on the MSZ width of $ZnSO_4$

Figure 4-5 shows the same response to an $Al_2(SO_4)_3$ addition to the $ZnSO_4$ solution in terms of reaching a maximum enlargement of MSZ width. This maximum increase happens at a lower addition amount of Al^{3+}=10 ppm, than in the case of Ba^{2+} = 25 ppm. Further, the pH of $ZnSO_4$ solution is seen to be constant with $BaCl_2$ addition in the concentration range between 5-100 ppm.

The maximum enlargement of MSZ width is due to both the change in the saturation and nucleation temperature as to be seen in figure 4-6. In the other words, an addition of 25 ppm of Ba^{2+} ion leads to an increase in the saturation temperature to 27.33 °C above the saturation temperature of the pure solution that is equal to 26.67 °C. At the same time, the nucleation temperature has been shifted from 23.85 °C to 23.10 °C. One may see the change in saturation and nucleation temperature separately is very small but when one sees the combined change for both saturation and nucleation, it is seen to be high (MSZ width =1.41).

The error bars, as shown in figure 4-5, are due to the error that occurred by the nucleation measurements (see figure 4-6).
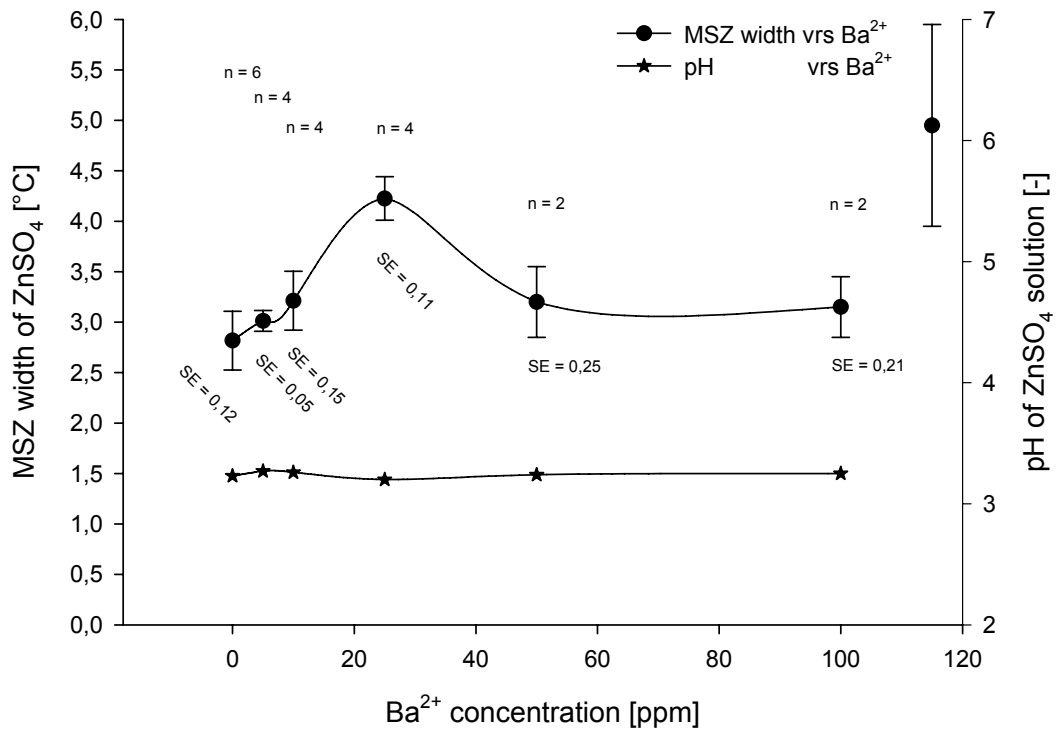
Figure 4-5: Effect of Ba^{2+} ions on the MSZ width and pH of ZnSO$_4$ – water solution
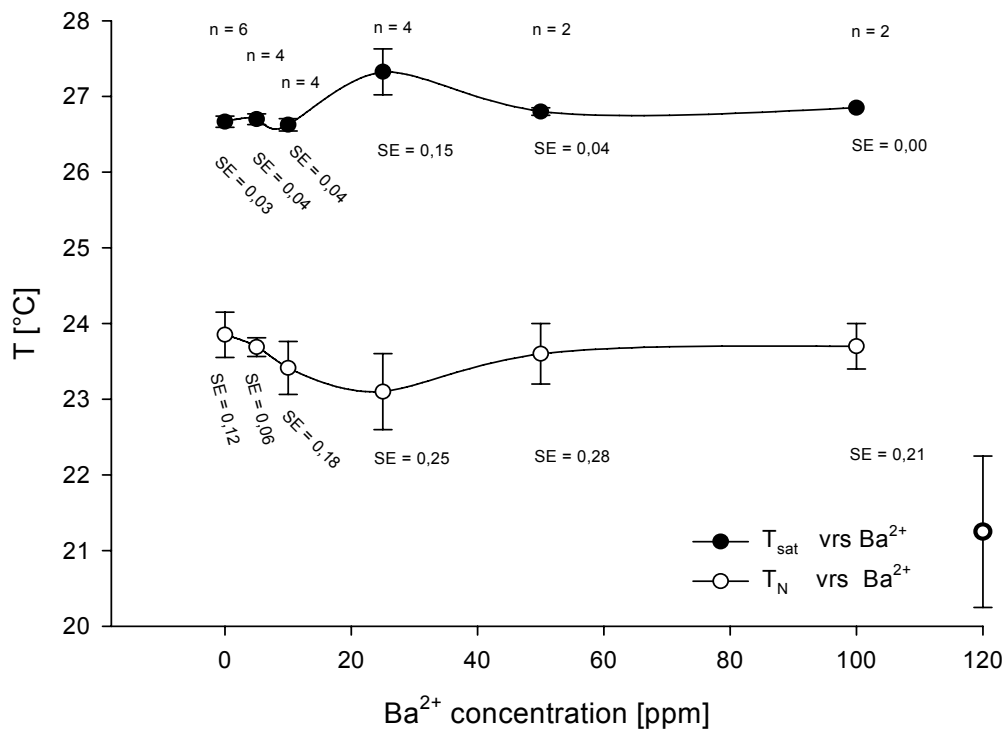
Figure 4-6: Effect of Ba^{2+} ions on the saturation and nucleation temperature of ZnSO$_4$ – water solution

4.1.1.4 The effect of Li$_2$SO$_4$ on the MSZ width of ZnSO$_4$

From the data in the figure 4-7, there can no effect on the MSZ width of ZnSO$_4$ be found due to the Li$^+$ ion addition in the concentration range between 5-150 ppm. But on the other hand, the lithium ion has a very small effect on the saturation and nucleation temperature as to be seen in figure 4-8. This effect can be observed when the Li$^+$ ions are in the concentration range 5 to 10 ppm. By adding more than these limit, the saturation and nucleation temperature show a constant change.

In terms of a statistical indication, the standard deviation value of MSZ width measurements is quite high for point that corresponds to 5 ppm of Li$^+$ on the MSZ width curve (see figure 4-7). This is because of the highest value of the standard deviation of the nucleation temperature measurement for the same additive concentration as plotted in figure 4-8.

The pH value of the ZnSO$_4$ – water solution is plotted as a function Li$^+$ ion concentration as presented in figure 4-7. The pH of the solution is determined constant with Li$^+$ ion addition in the concentration form 5 ppm to 150 ppm.
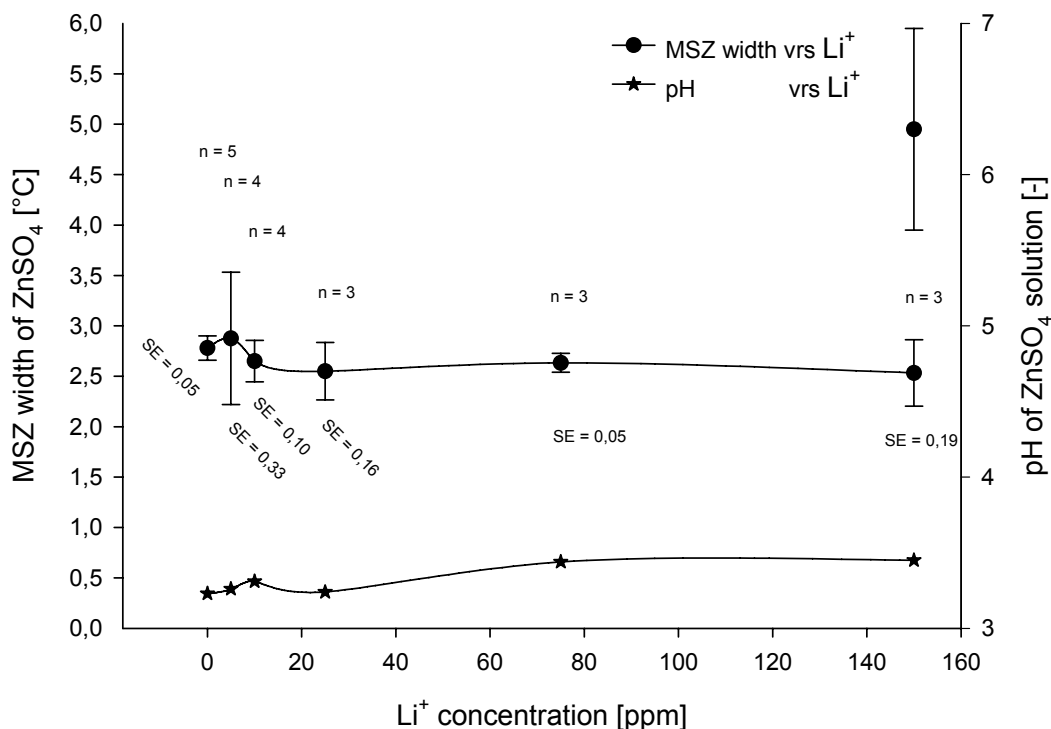
Figure 4-7: Effect of Li$^+$ ions on the MSZ width and pH of ZnSO$_4$ – water solution
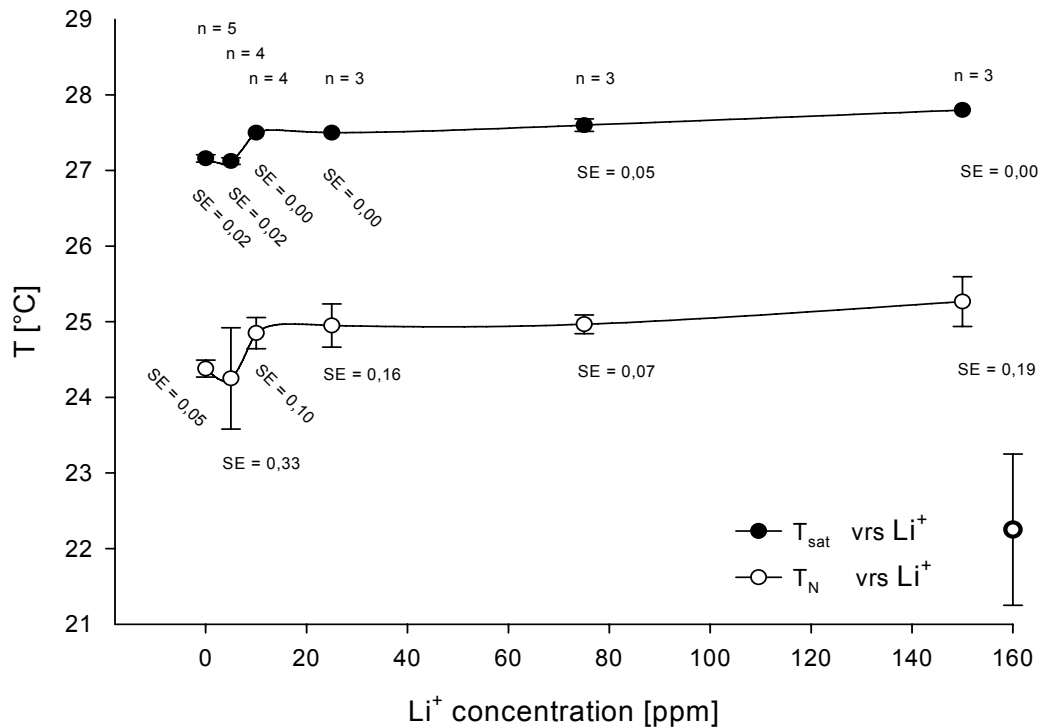
Figure 4-8: Effect of Li$^+$ ions on the saturation and nucleation temperature of ZnSO$_4$ – water solution

4.1.1.5 The effect of K$_2$SO$_4$ on the MSZ width of ZnSO$_4$

The change in the MSZ width appears to have a minimum due to the K$^+$ ion addition as shown figure 4-9. This effect is inversely different compared to both an Al$_2$(SO$_4$)$_3$ and a BaCl$_2$ addition. The minimum suppression of the MSZ width of ZnSO$_4$ happened at the concentration of K$^+$ = 50 ppm. By adding more K$^+$ ions but not more than 150 ppm, the MSZ width of ZnSO$_4$ will be increased to reach its maximum value of pure ZnSO$_4$-water solution. Furthermore, the pH of the solution was not affected by the K$^+$ ions addition in a concentration range of 5 -150 ppm.

Figure 4-10 shows the saturation and nucleation temperature as a function of K$^+$ ions. It can be seen that the saturation temperature was not affected by the addition of K$^+$ ions. On the other side, there is a change in the nucleation temperature of ZnSO$_4$ - water solution. On this basis, the effect of K$^+$ ions on the MSZ width of ZnSO4 that has been shown in figure 4-9 was only the result of the change in the nucleation temperature.

The standard deviation values are relatively high when compared to the length of reference bar especially for the first and second measurements as shown in figure 4-9. These large values of standard deviation result obviously from the nucleation temperature measurements as to be seen in figure 4-10.
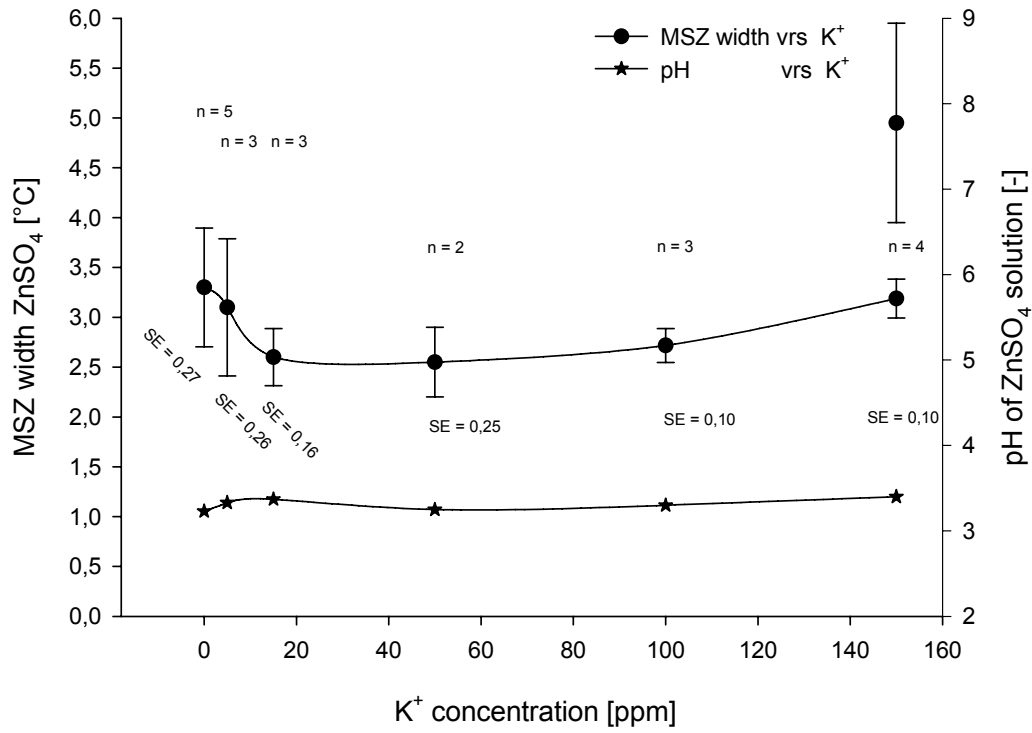
Figure 4-9: Effect of K$^+$ ions on the MSZ width and pH of ZnSO$_4$ – water solution
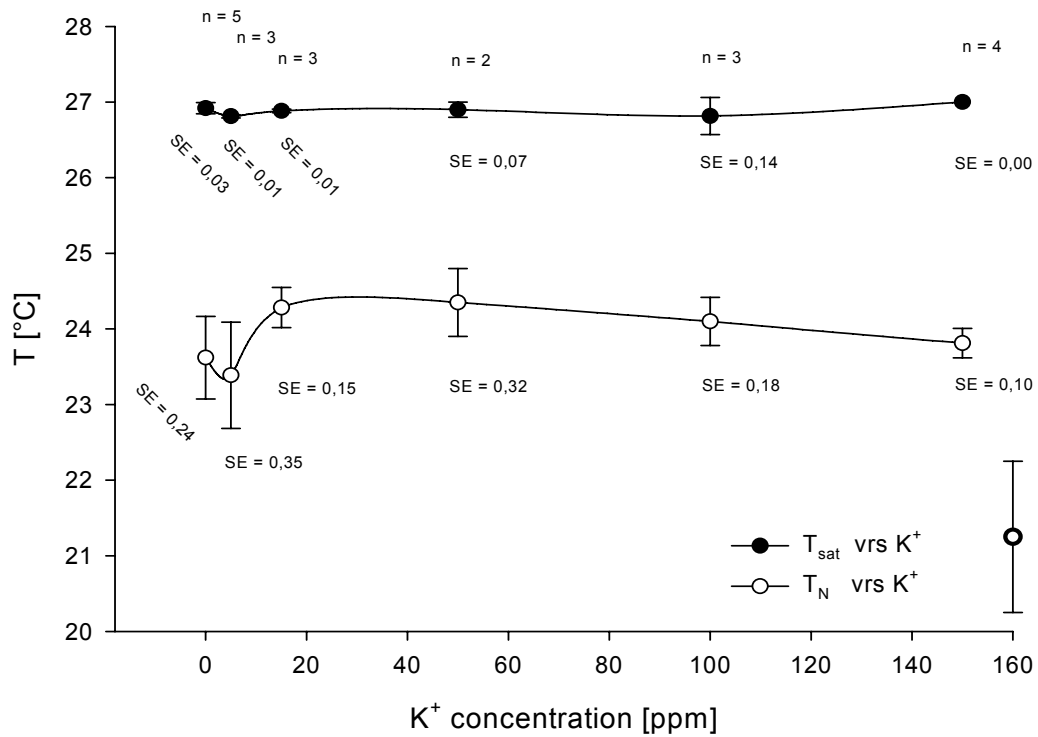
Figure 4-10: Effect of K$^+$ ions on the saturation and nucleation temperature of ZnSO$_4$ – water solution

4.1.2 The effects of AlCl$_3$, FeCl$_2$, MgCl$_2$, and BaCl$_2$ on the MSZ width of LiCl

The effect of the additives Al^{3+}, Fe^{2+}, Mg^{2+} and Ba^{2+} on the MSZ width and the pH of LiCl are shown in the **figures 4-11 to 4-18**. These results represent the second group of selected ions as additives from table 2-5.

4.1.2.1 The effect of AlCl$_3$ on the MSZ width of LiCl

The pH function of LiCl-water solution is decreasing from 2.48 to 0.61 with adding Al^{3+} ions in the concentration range of 5-75 ppm as shown in figure 4-11. On the other side, this addition of AlCl$_3$ to LiCl solutions shows no effect on the MSZ width of LiCl for the same concentration of Al^{3+} ions. However, from the presented data in figure 4-11, the average value of MSZ width of LiCl is 2.71 °C. The shown effect of Al^{3+} ion on the MSZ width of LiCl is seen more clearly in figure 4-12. Both functions of saturation and nucleation temperature are not changed significantly with addition of AlCl$_3$.

The standard deviation values are very low as to be seen in figure 4-11 and figure 4-12, except the measurement point which corresponds to the Al^{3+} ion concentration equal 50 ppm.
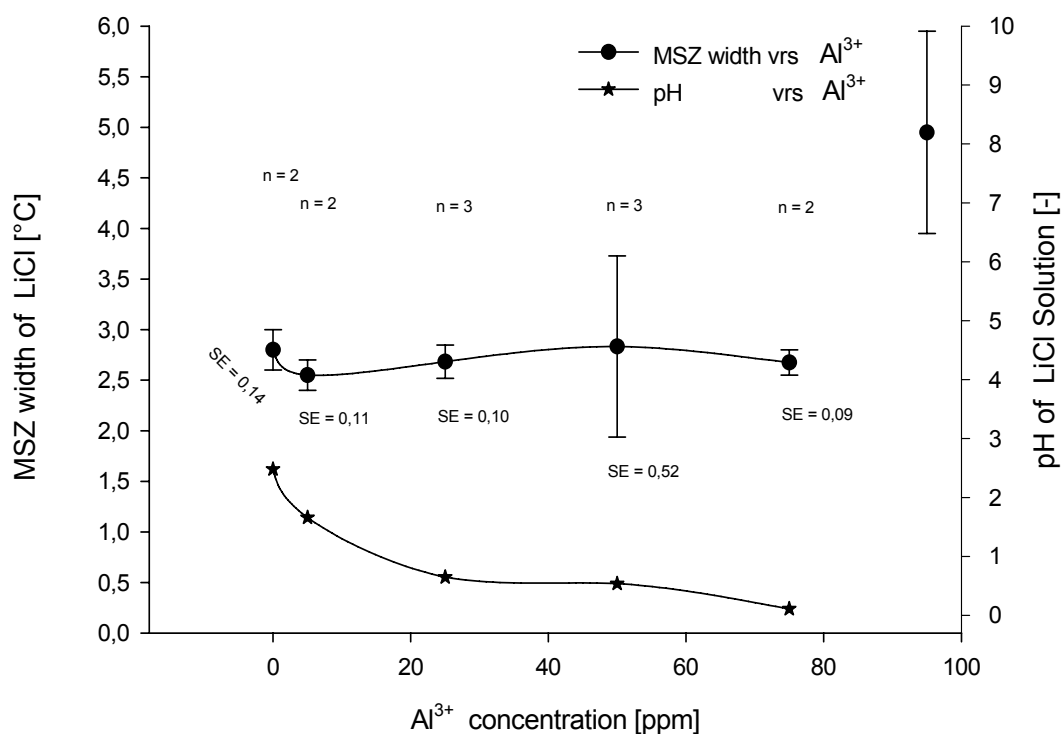
Figure 4-11: Effect of Al^{3+} ions on the MSZ width and pH of LiCl – water solution
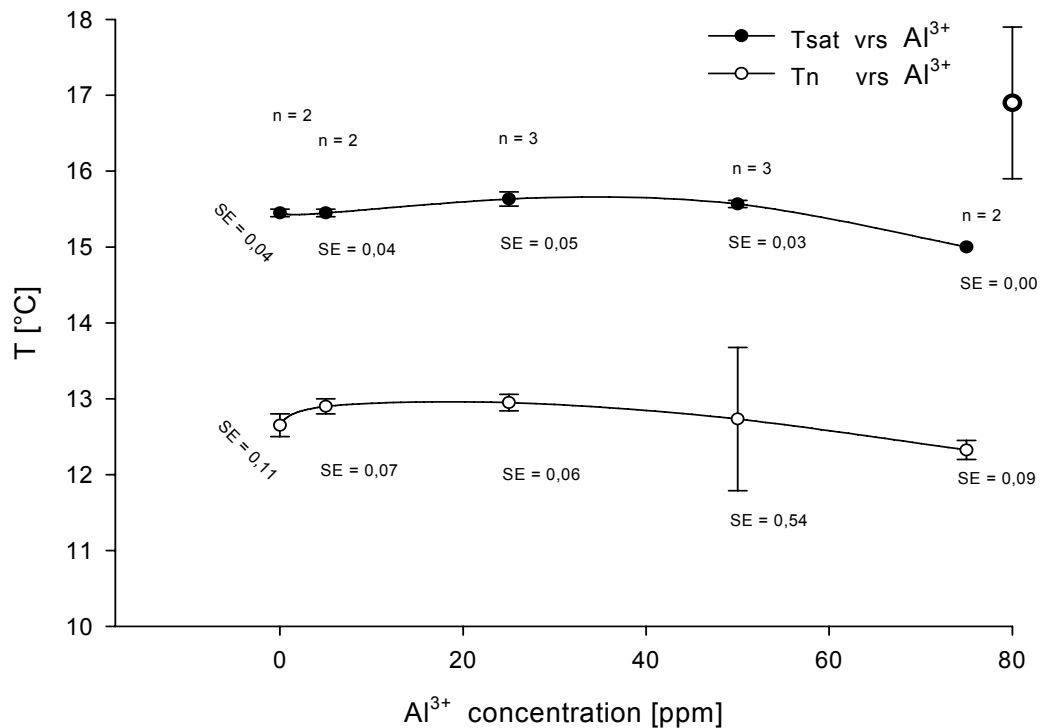
Figure 4-12: Effect of Al^{3+} ions on the saturation and nucleation temperature of LiCl – water solution

4.1.2.2 The effect of FeCl$_2$ on the MSZ width of LiCl

The effect of Fe^{2+} ions on the MSZ width of LiCl is plotted in figure 4-13. The minimum suppression in MSZ width of LiCl happened at the concentration of Fe^{2+} = 35 ppm. By adding more of Fe^{2+} ions, the suppression of LiCl of the MSZ width will be less as can be seen at a Fe^{2+} ion concentration of 75 and 150, respectively. This change in the MSZ width of LiCl is only due to the change in the nucleation temperature as to be seen in figure 4-14. Since the nucleation temperature is raised from about 10.5 to 12 °C in the concentration range of Fe^{2+} ions between 10 to 150 ppm. On the other side there is no effect on the saturation temperature of LiCl solution due to a Fe^{2+} ion addition.

The pH of LiCl solution was not changed by Fe^{2+} ion addition as shown in figure 4-13. Furthermore, the standard deviation values are quite high especially for the last two points of MSZ width measurement. The high values of standard deviation are caused by the nucleation temperature measurement as one may see in figure 4-14.
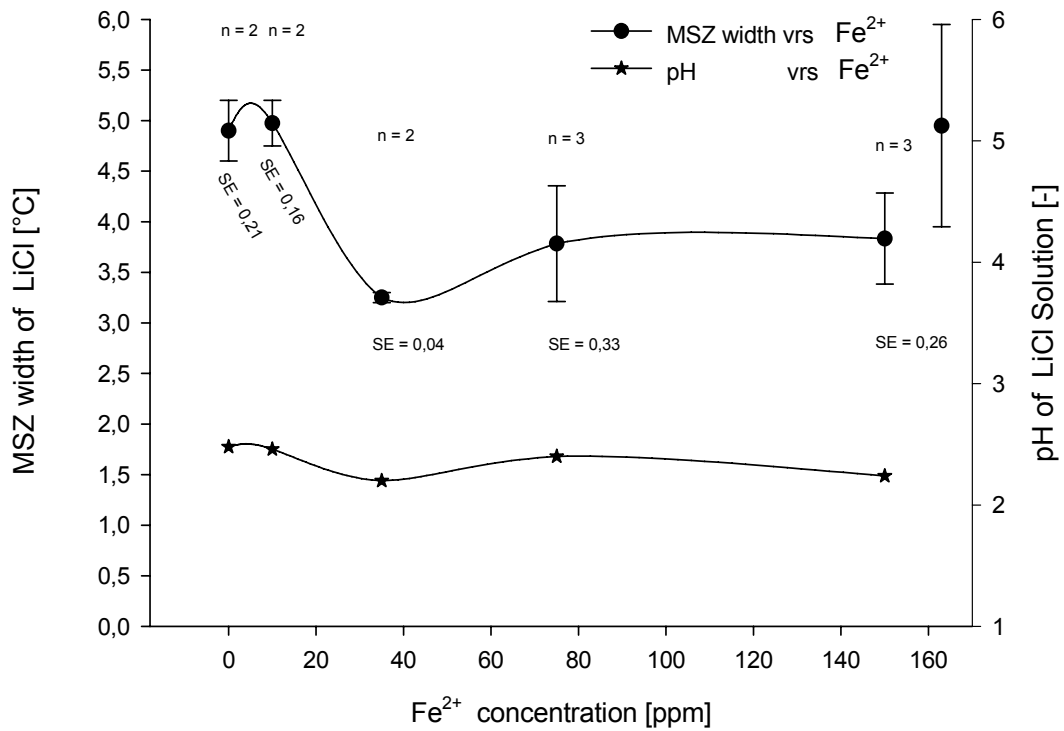
Figure 4-13: Effect of Fe^{2+} ions on the MSZ width and pH of LiCl – water solution
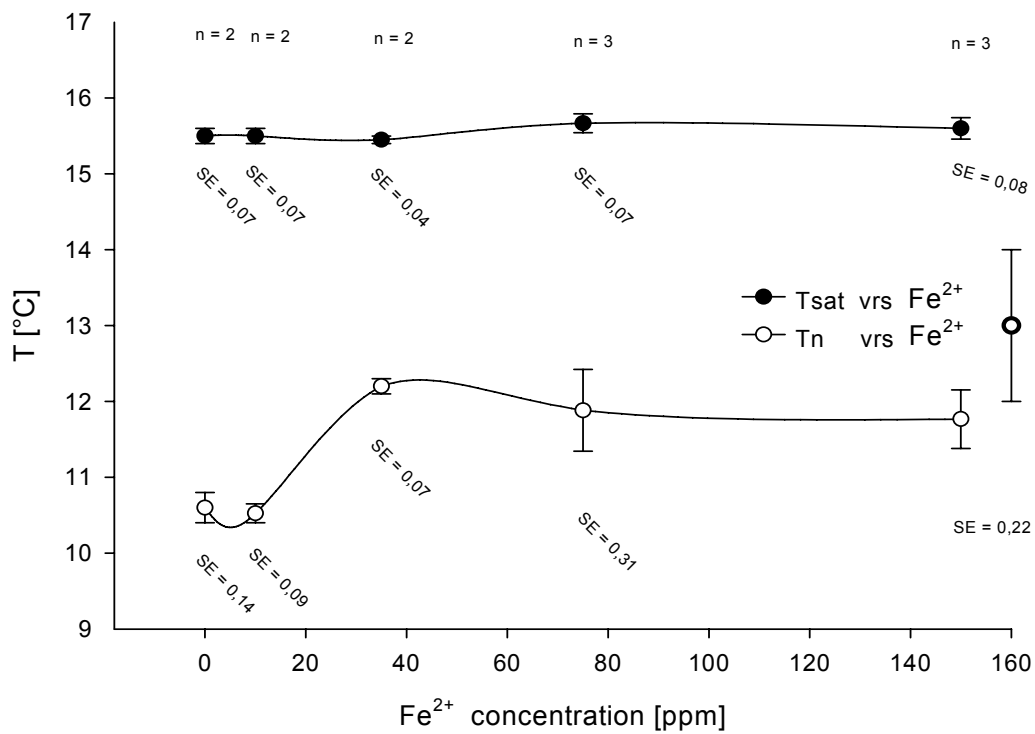
Figure 4-14: Effect of Fe^{2+} ions on the saturation and nucleation temperature of LiCl – water solution

4.1.2.3 The effect of MgCl$_2$ on the MSZ width of LiCl

Figure 4-15 shows the effect of Mg^{2+} ion addition (10-125 ppm) on the MSZ width of LiCl-water solution. The maximum enlargement in the MSZ width of LiCl occurs at 75 ppm of the Mg^{2+} ion concentration. By adding 125 ppm of Mg^{2+} ion, the MSZ width of LiCl will be less than its value without Mg^{2+} ion addition.

Figure 4-16 shows the saturation and nucleation temperature as a function of Mg^{2+} ion addition to the LiCl-water solution. The saturation temperature has decreased very slightly with the Mg^{2+} ion addition. In addition, the nucleation temperature was decreased to a minimum value at the Mg^{2+} ion concentration of 75 ppm. On this basis, the MSZ width of LiCl was changed due to both changes of the saturation and nucleation temperatures, respectively. Moreover, the standard deviation values are low for the first three measurements of the saturation and nucleation temperatures. But it is high for the last two measurements.

The pH value of the LiCl solution is increased with increasing the value of Mg^{2+} ions in the solution as shown in figure 4-15. An adding of 10 ppm of Mg^{2+} ions leads to a sharp increase in the pH but thereafter only to a slight increasing in pH.
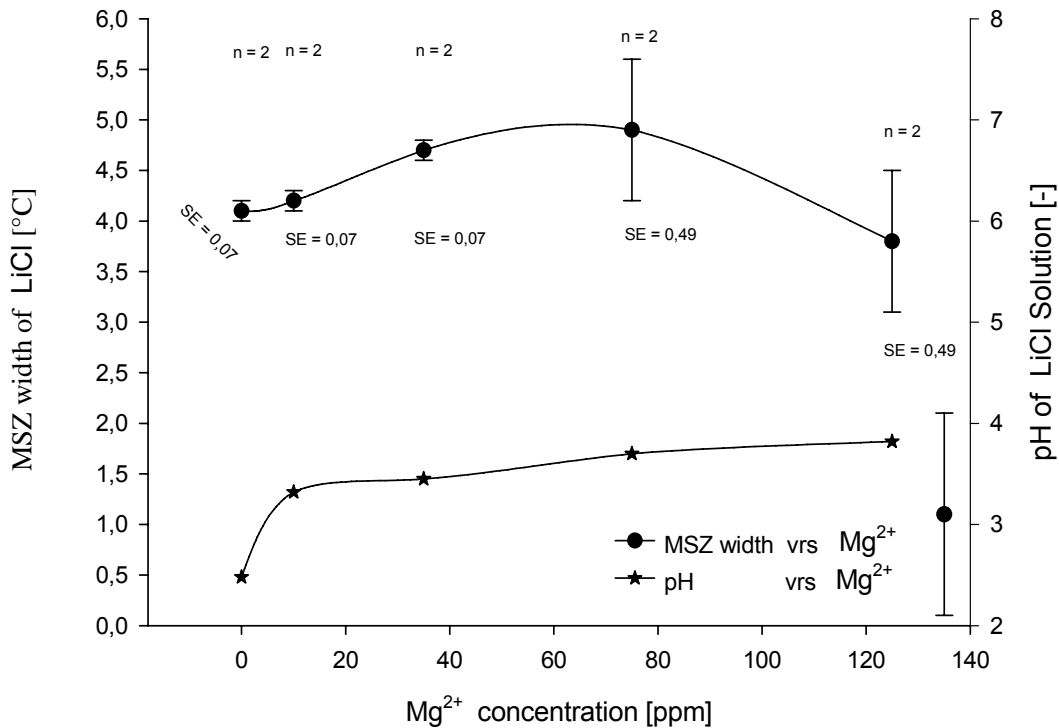
Figure 4-15: Effect of Mg^{2+} ions on the MSZ width and pH of LiCl – water solution
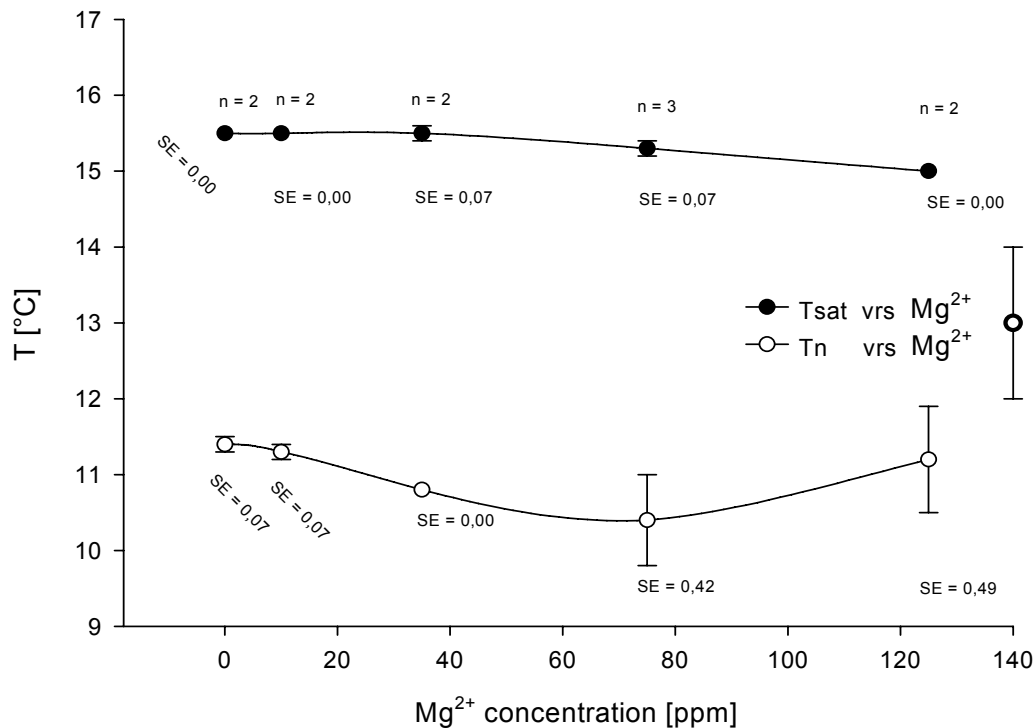
Figure 4-16: Effect of Mg^{2+} ions on the saturation and nucleation temperature of LiCl – water solution

4.1.2.4 The effect of $BaCl_2$ on the MSZ width of LiCl

There is a significant decrease in the MSZ width of LiCl as shown in figure 4-17 due to the Ba^{2+} ion addition (15 ppm < $[Ba^{2+}]$ ≤ 100 ppm). But there is also an increase in the pH value of LiCl-water solution due to that addition.

In figure 4-18, the effect of Ba^{2+} ion addition as $BaCl_2$ on the saturation and nucleation temperature of LiCl is displayed. One may see that the saturation temperature has not been changed with Ba^{2+} ion addition in the concentration range between 15-100 ppm. In contrary, there is an increase in the nucleation temperature from 11 to 11.90 °C due to that addition.

The standard deviation values of MSZ width, saturation temperature and nucleation temperature results as to be seen in figures 4-17 and 4-18 are very low except the third point measurement of MSZ width.
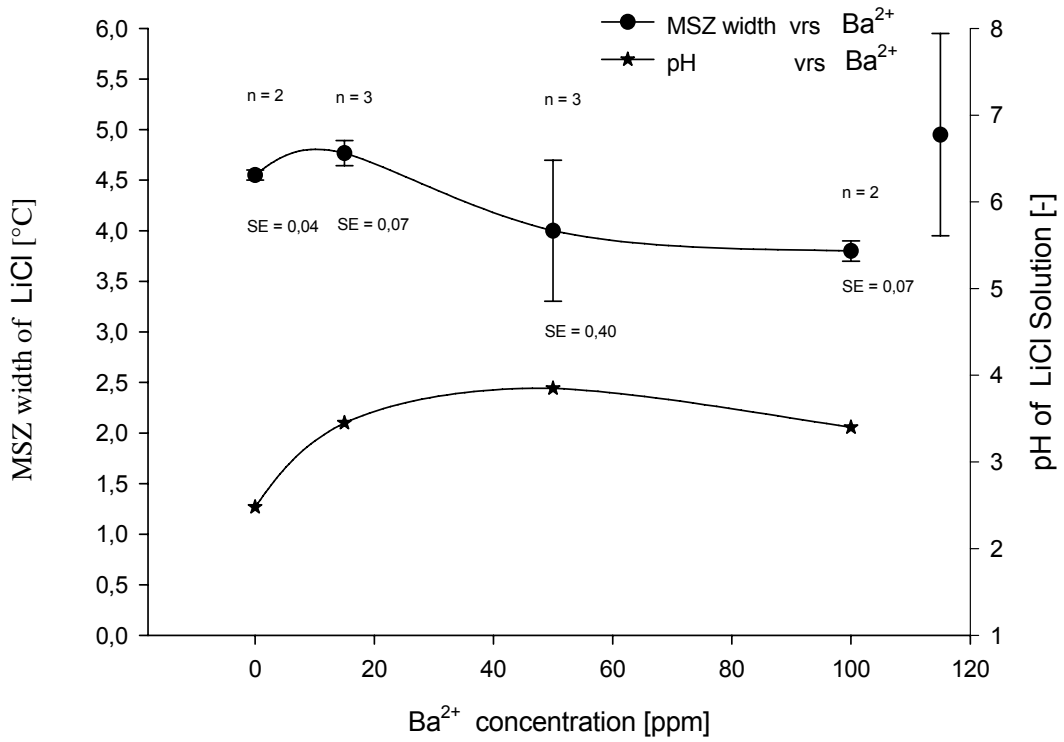
Figure 4-17: Effect of Ba^{2+} ions on the MSZ width and pH of LiCl – water solution
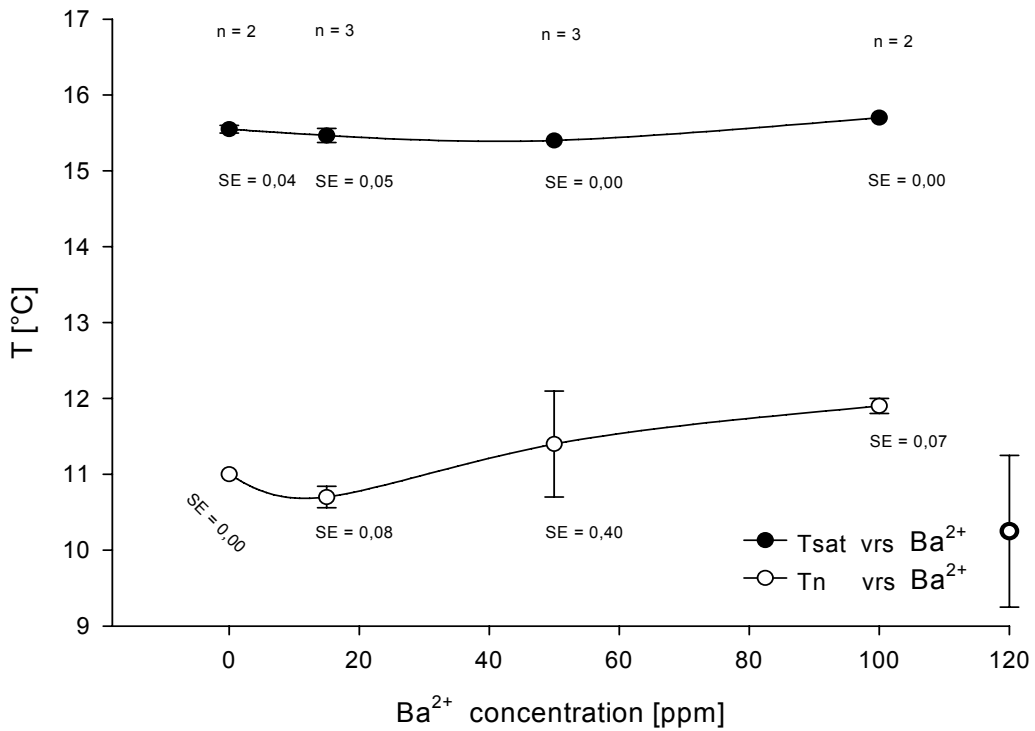
Figure 4-18: Effect of Ba^{2+} ions on the saturation and nucleation temperature of LiCl – water solution

4.1.3 **The effect of CuSO$_4$, BaCl$_2$ and Li$_2$SO$_4$ on the MSZ width of K$_2$SO$_4$**

The effect of the additives Cu^{2+}, Ba^{2+} and Li$^+$ on the MSZ width and the pH of K$_2$SO$_4$ are shown in the **figures 4-19 to 4-24**. These results represent the third group of selected ions as additives from table 2-5.

4.1.3.1 **The effect of CuSO$_4$ on the MSZ width of K$_2$SO$_4$**

Figure 4-19 shows the effect of Cu^{2+} ion addition on the MSZ width of a K$_2$SO$_4$-water solution. The maximum enlargement in the MSZ width of K$_2$SO$_4$ occurs at 50 ppm of Cu^{2+} ion addition. By adding more Cu^{2+} ions, the MSZ width of K$_2$SO$_4$ is reduced again.

Figure 4-20 shows the saturation temperature of K$_2$SO$_4$ - water solution with respect to the Cu^{2+} ion addition. But this addition shows a different effect on the nucleation temperature of K$_2$SO$_4$-water. The minimum suppression in the nucleation was recorded at 50 ppm concentration of Cu^{2+} ions.

The pH function of K$_2$SO$_4$-water solution shows a constant change with Cu^{2+} ion addition as plotted in figure 4-19.
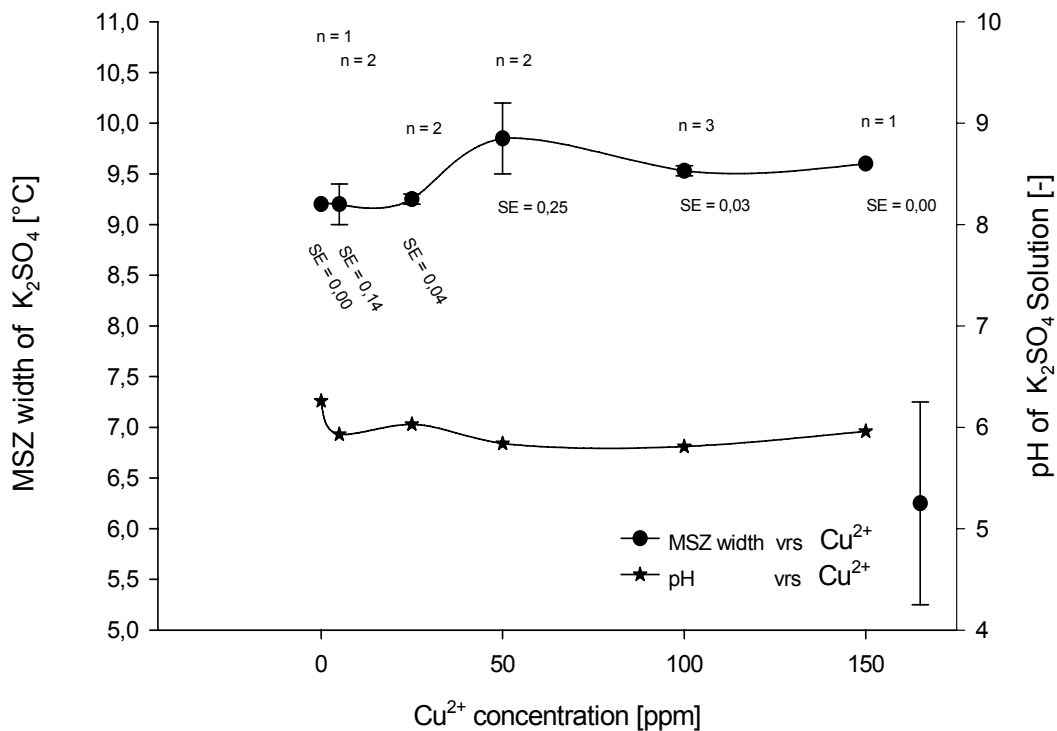
Figure 4-19: Effect of Cu^{2+} ions on the MSZ width and pH of K$_2$SO$_4$ – water solution
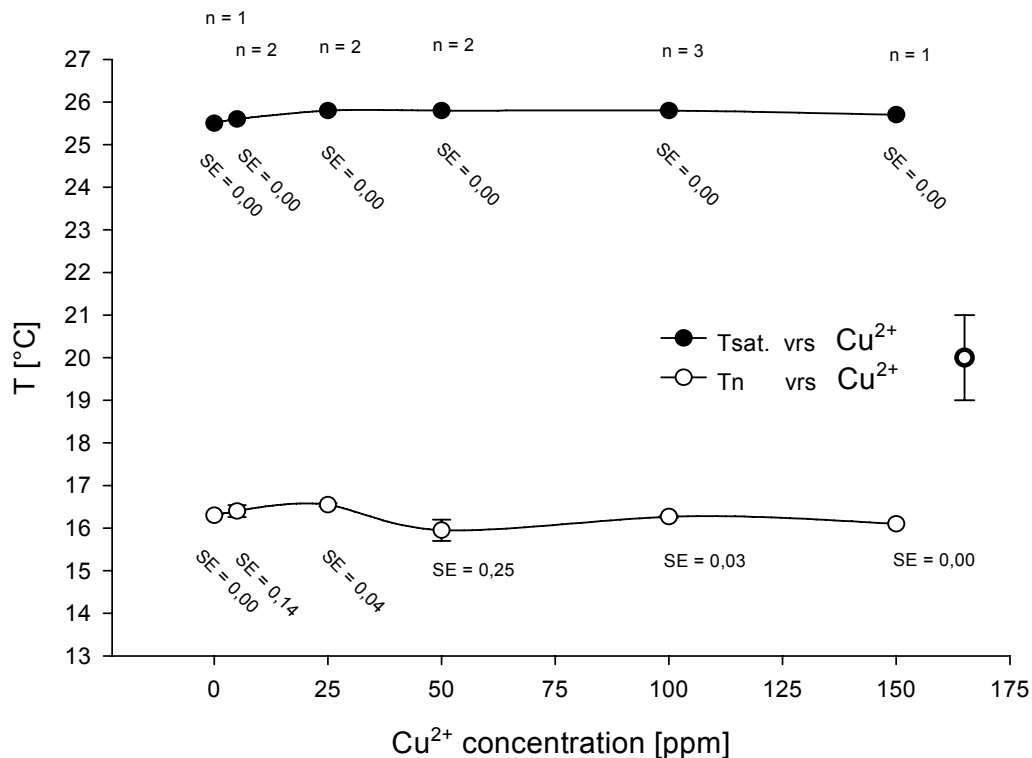
Figure 4-20: Effect of Cu^{2+} ions on the saturation and nucleation temperature of K_2SO_4 – water solution

4.1.3.2 The effect of $BaCl_2$ on the MSZ width of K_2SO_4

The MSZ width of K_2SO_4 was changed due to the $BaCl_2$ addition (5 ppm ≤ $[Ba^{2+}]$ ≤ 250 ppm) as shown in figure 4-21. The maximum enlargement of MSZ width of K_2SO_4 happened at $[Ba^{2+}]$ = 50 ppm. After this limit of additive addition, the MSZ width of K_2SO_4 is decreasing smoothly.

It can be seen in figure 4-22 that the addition of Ba^{2+} ions to the K_2SO_4 solution is effecting both saturation and nucleation temperatures to a small degree. The combination of these two effects a relatively high effects on the MSZ width of K_2SO_4. Additionally, it can be seen that the standard deviation values are rather low for nucleation temperature and saturation temperature, respectively. This leads to low values of the standard deviation for the MSZ width of K_2SO_4 solution as to be seen in figure 4-22.

The other important effect caused by Ba^{2+} ion addition is the change of the pH the of K_2SO_4 solution. In figure 4-21 a polynomial decreasing in pH value can be seen. It is due to Ba^{2+} addition in the concentration range of 5-75 ppm.
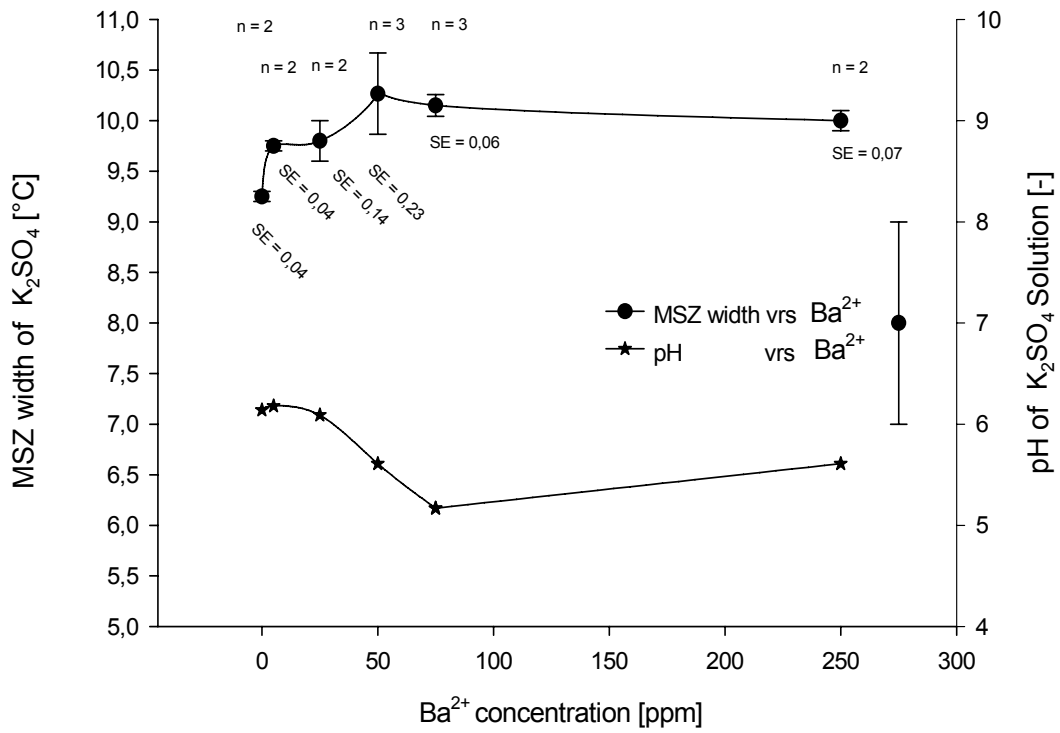
Figure 4-21: Effect of Ba^{2+} ions on the MSZ width and pH of K$_2$SO$_4$ – water solution
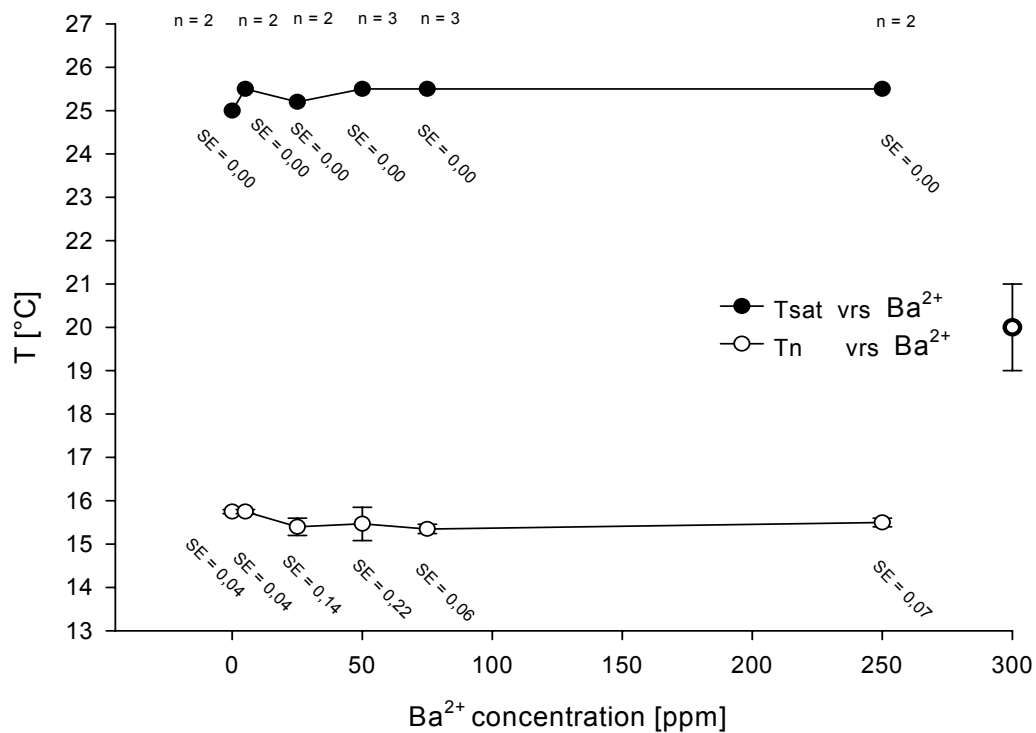
Figure 4-22: Effect of Ba^{2+} ions on the saturation and nucleation temperature of K$_2$SO$_4$ – water solution

4.1.3.3 The effect of Li_2SO_4 on the MSZ width of K_2SO_4

Figure 4-23 shows the MSZ width of K_2SO_4 solution as a function of Li^+ ion addition (5 ppm $\leq$ $[Li^+]$ $\leq$ 250 ppm). By an addition of 50 ppm of Li^+ ions to the solution, a maximum enlargement was found. This maximum value of MSZ width of K_2SO_4 solution is not as high as in the pure solution. Furthermore, adding more Li^+ ion than 50 ppm leads to deceasing MSZ width.

There is no change in pH of the K_2SO_4 solution, as to be seen in figure 4-23, due to the Li_2SO_4 addition.

Figure 4-24 shows both changes in saturation and nucleation temperature as a function of Li^+ ion addition in range 5 ppm $\leq$ $[Li^+]$ $\leq$ 250 ppm. One may see that the changes in the saturation and nucleation temperature are quite similar. Also it is shown by figure 4-24 that the standard deviation values are very small. This can also be found for the standard deviation value of MSZ width of K_2SO_4 solution as to be seen in figure 4-23.
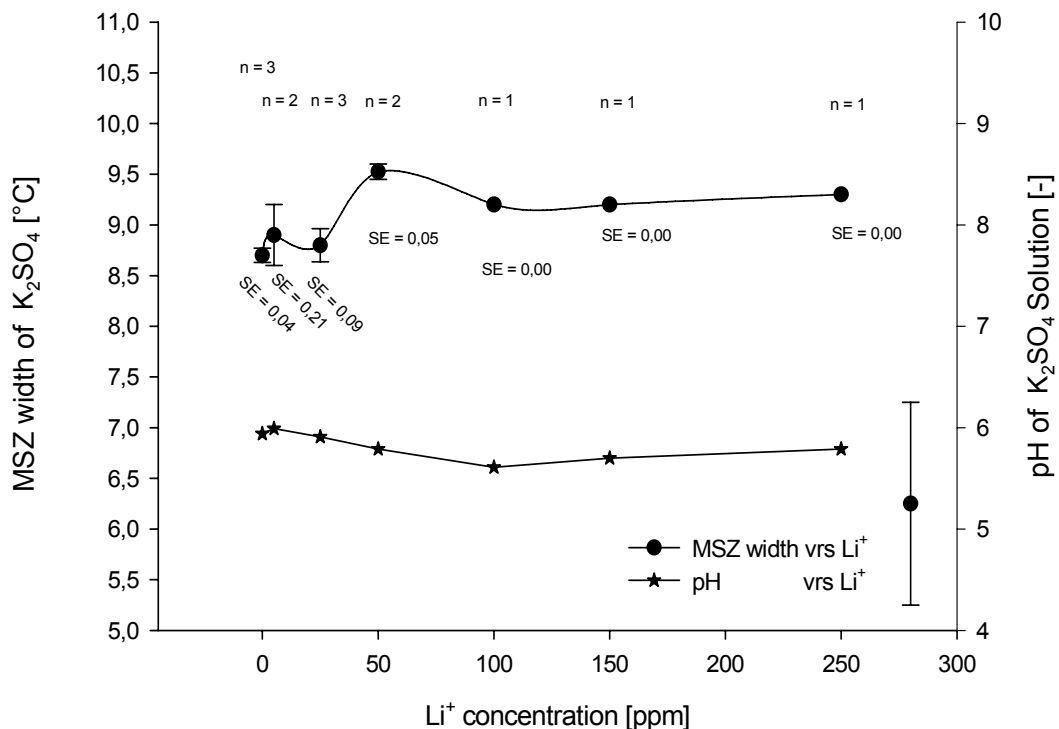
Figure 4-23: Effect of Li^+ ions on the MSZ width and pH of K_2SO_4 – water solution
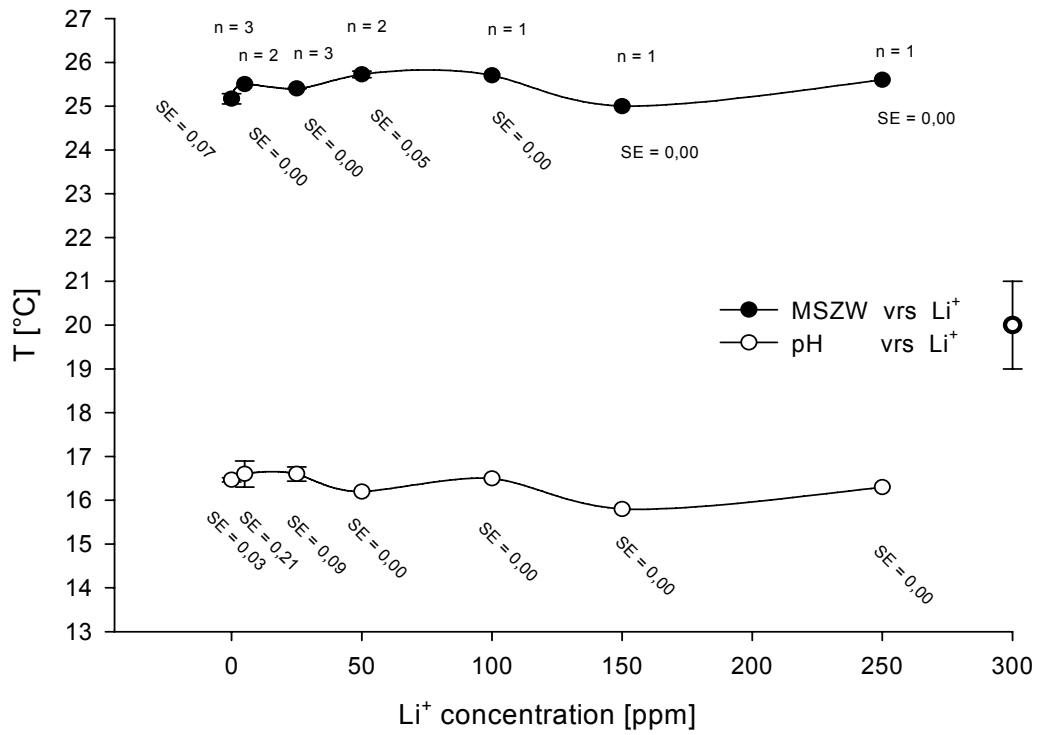
Figure 4-24: Effect of Li^+ ions on the saturation and nucleation temperature of K_2SO_4 – water solution

4.2   Determination the induction time of CaCO$_3$ in artificial seawater

The induction time of CaCO$_3$ precipitation can be determined by measuring the change in the pH of seawater solution starting from the moment of NaHCO$_3$ addition until the CaCO$_3$ precipitation has happened as shown in figure 4-25. The initial pH value of seawater at 30 °C has been decreased from 8 to 7.46 due to 0.3 g of NaHCO$_3$ addition to the ASW. Then a gradual increasing in the pH value was recorded till the precipitation of CaCO$_3$ occurred as shown in area 1 in figure 4-25. In this figure area 2 represents the period of precipitation from the start (5.67 h, pH=7.97) until the end of the process (10.23 h, pH=7.61).
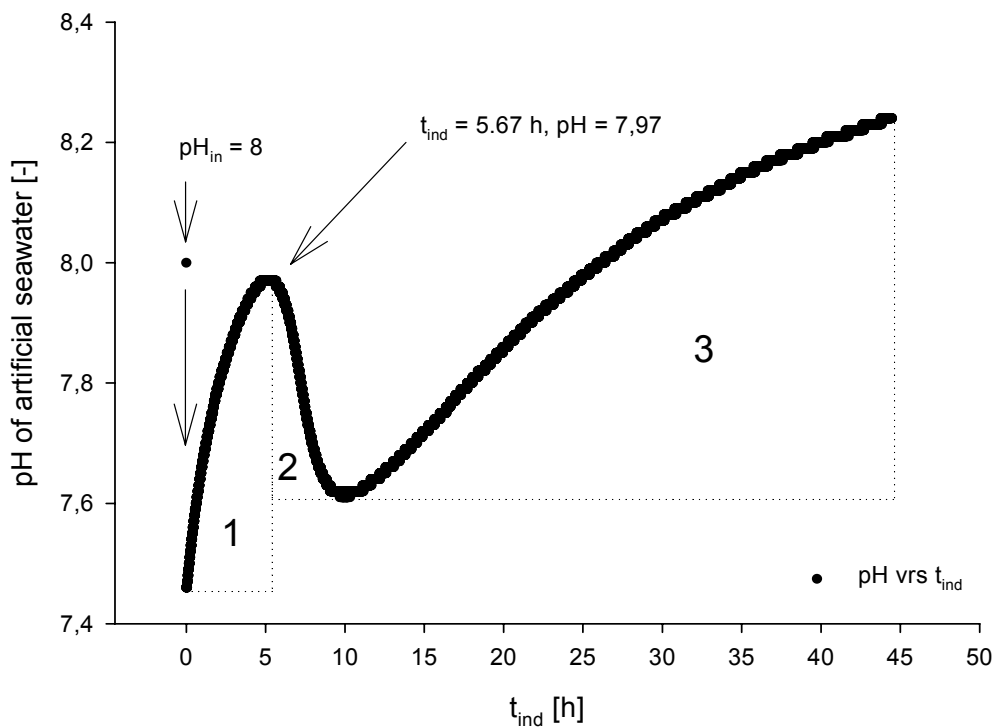
Figure 4-25: Determination the induction time of CaCO$_3$ precipitation in 125 mL ASW, 35 g/kg salinity, T=30 °C, NaHCO$_3$=0.3 g, stirrer speed=250 rpm

Figures 4-26 to 4-29 are showing a clear image of the relation between the time required for CaCO$_3$ precipitation and the amount of NaHCO$_3$ added in artificial seawater at different levels of temperatures and salinities.

4.2.1 **Induction time at 35 g/kg salinity**

4.2.1.1 Effect of NaHCO$_3$ addition on the induction time of CaCO$_3$

Polynomial inverse relation can be shown in figure 4-26 between the induction time of CaCO$_3$ in ASW and the mass of NaHCO$_3$ addition for a temperature level of 30, 40, 50 and 70 °C. The induction time for CaCO$_3$ is increased with decreasing temperature for the same amount of NaHCO$_3$. But this increase becomes smaller with increasing temperature whenever the amount of NaHCO$_3$ addition is exceeding about 1 g. On the other hand, vertical tangents can be drawn for each induction time – mass of NaHCO$_3$ curve in the limit of induction time measurement below 24 h. Each tangent can be used to determine the minimum addition of NaHCO$_3$ to precipitate CaCO$_3$ for each operational temperature. Consequently, 0.129 g, 0.072 g, 0.072 g and 0.036 g are representing the minimum mass of NaHCO$_3$ that can be added at 30, 40, 50 and 70 °C, respectively, in order to precipitate CaCO$_3$ in the limit of induction time measurements below 24 h.
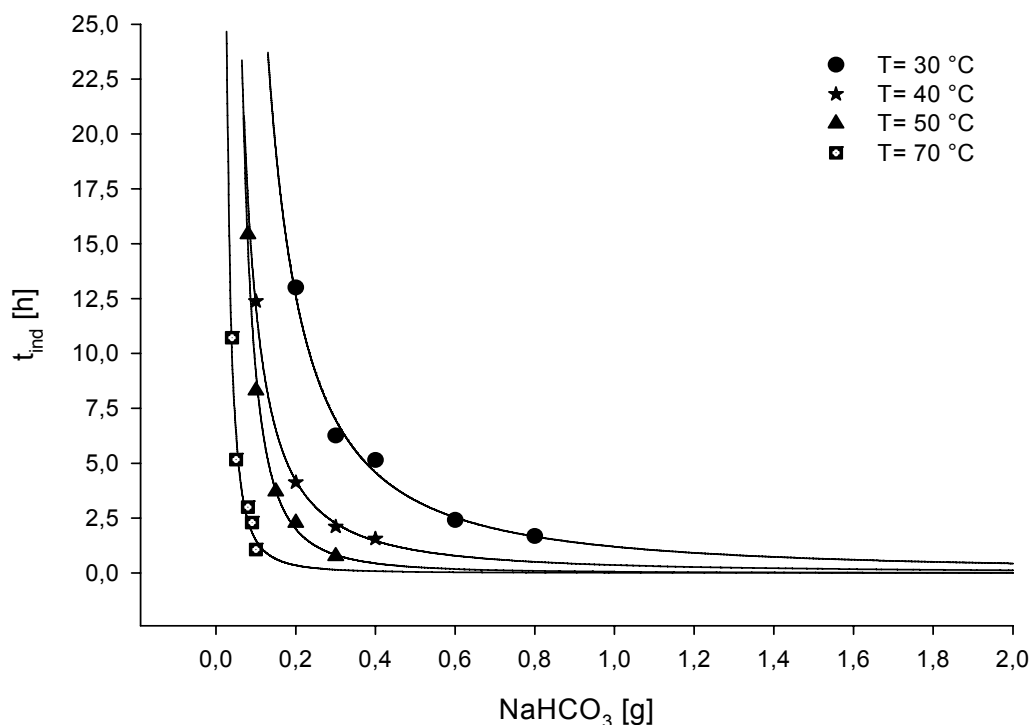
Figure 4-26: The effect of NaHCO$_3$ addition on the induction time of CaCO$_3$ in 125 mL artificial seawater, 250 rpm, 35 g/kg salinity

4.2.1.2 Induction time of CaCO₃ as a function of supersaturation and temperature (30, 40, 50 and 70 °C)

The experimental results are showing a linear relation between the induction time log(t_ind) for CaCO₃ in artificial seawater and supersaturation level log(S) for 30, 40, 50 and 70 °C as illustrated in the figure 4-27. These results are showing a good agreement with the following equation (see section 2.5):

$$\log(t_{ind}) = \frac{B}{T^3.\log^2(S)} + A \tag{4-1}$$

It can be seen that the slopes of those lines are increasing with rising temperature. Also one can observe that the decrease of CaCO₃ supersaturation leads to an increase in the induction time for the temperatures 30 and 40 °C. A small change in the supersaturation level leads to a big change in the induction time for the temperatures 50 and 70 °C.

A statistical evaluation is presented in figure 4-27 as vertical bars for the induction time measurements and horizontal bars for the supersaturation measurements. These bars are referred to the standard deviation of the average of each point.
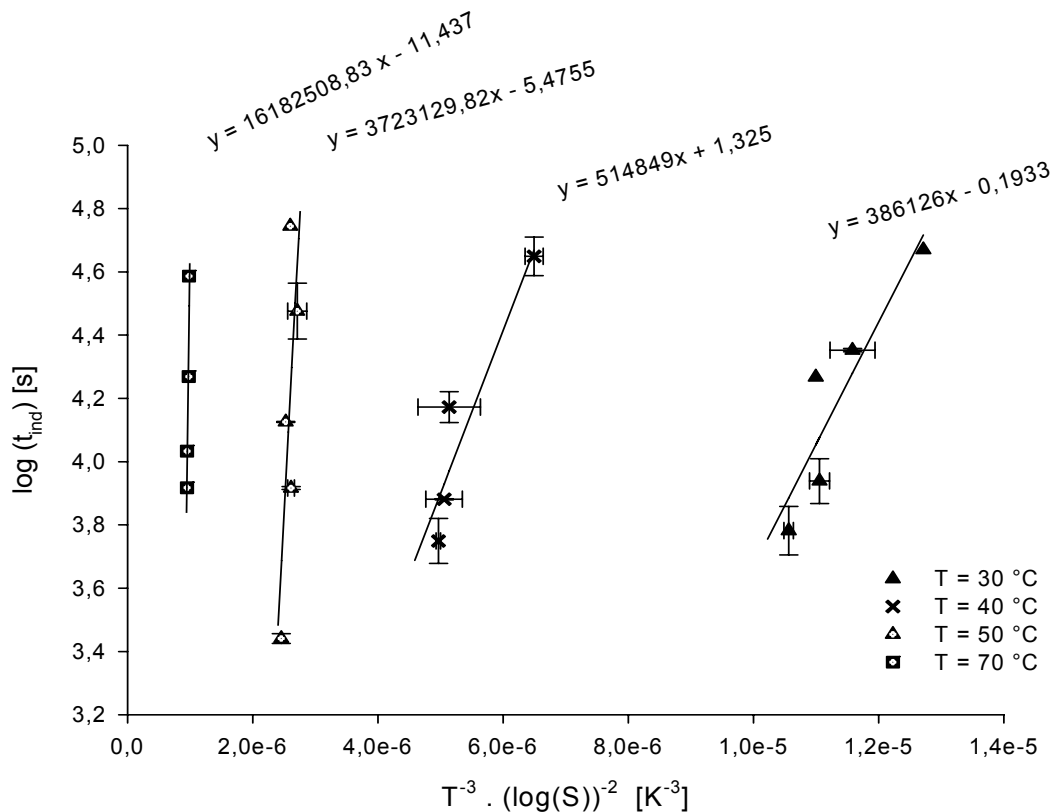
Figure 4-27: Induction time as a function of supersaturation for temperatures 30, 40, 50 and 70 °C, where $y = \log(t_{ind})$ and $x = T^{-3}.(\log(S))^{-2}$

4.2.2 Induction time at 55 g/kg salinity

4.2.2.1 Effect of NaHCO$_3$ addition on the induction time of CaCO$_3$

Figure 4-28 shows similar effects on the induction of CaCO$_3$ due to NaHCO$_3$ addition as shown in figure 4-26. The difference between the two measurements is that the induction time of CaCO$_3$ is here in 55 g/kg artificial seawater and before was 35 g/kg. Furthermore, the order of magnitude of increase of induction time with decreasing level of operational temperature is become smaller when the amount of NaHCO$_3$ addition is exceeding about 2 g.

For case of 55 g/kg seawater salinity, 0.22 g, 0.086 g and 0.0319 g is the minimum mass of NaHCO$_3$ given that can be added at 30, 50 and 70 °C, respectively, in order to precipitate CaCO$_3$ in the limit of induction time measurement in less than 24 h.
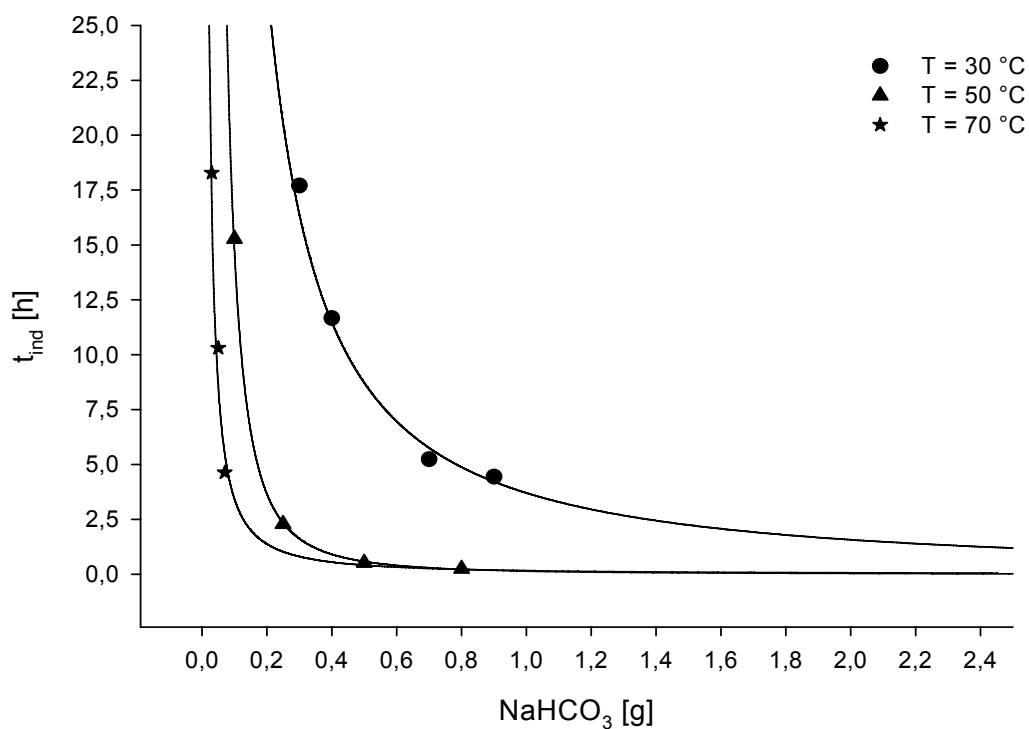
Figure 4-28: The effect of NaHCO$_3$ addition on the induction time of CaCO$_3$ precipitation in artificial seawater, 250 rpm, 55 g/kg salinity

4.2.2.2 Induction time of CaCO$_3$ as a function of supersaturation and temperature (30, 50 and 70 °C)

The results of the induction time measurements as a function of the level of supersaturation are shown in figure 4-29. The induction time is related linearly to the level of supersaturation for 30 °C and 50 °C. Also here the slope of the induction time is increasing with increasing the temperature as illustrated by the following equations:

$$\log(t_{ind}) = \frac{531051}{T^3 . \log^2(S)} - 1.0276 \qquad \text{at T=30 °C} \qquad (4\text{-}2)$$

$$\log(t_{ind}) = \frac{7 \cdot 10^6}{T^3 . \log^2(S)} - 3.1158 \qquad \text{at T=70 °C} \qquad (4\text{-}3)$$
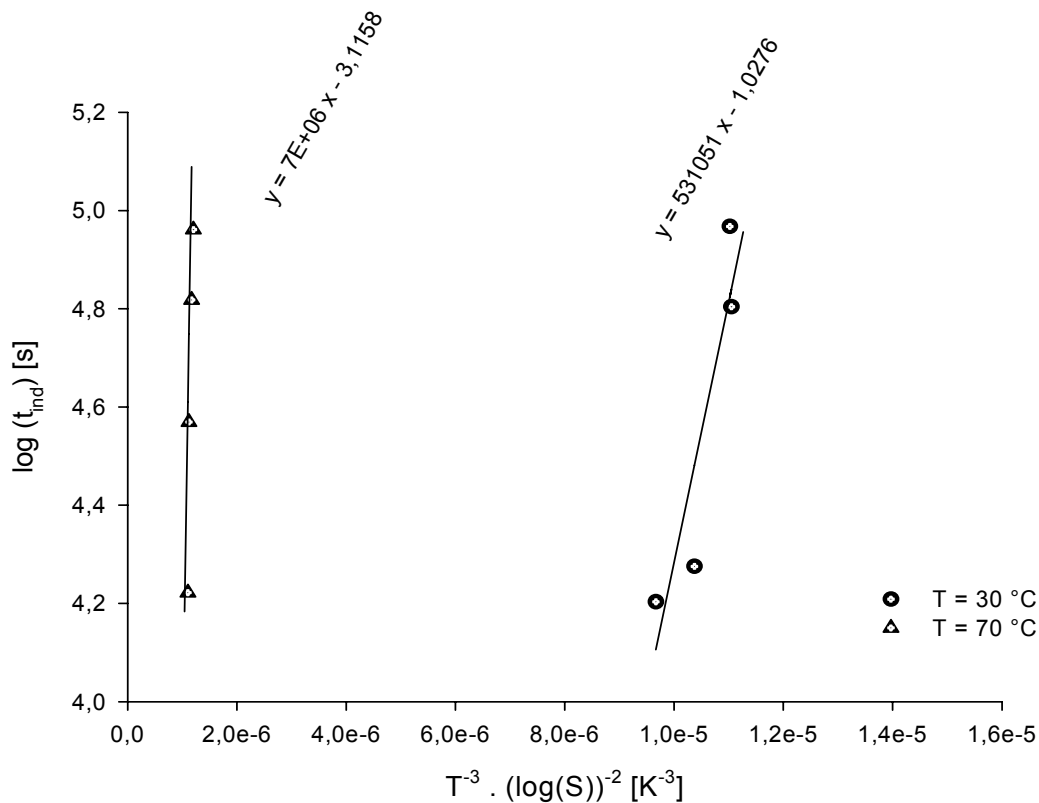
Figure 4-29: Induction time as a function of supersaturation for temperatures 30 and 70 °C, where $y = \log(t_{ind})$ and $x = T^{-3}.(\log(S))^{-2}$

4.3 Reduction of CaCO₃ by *seeding*; without chemical addition

The result of measuring the reduction of Ca^{2+} ion concentration in artificial seawater by using the atomic absorption spectroscopy is presented in figure 4-30. As to be seen the change in Ca^{2+} ion concentration due the use of fluidizing calcite seeds with time is extremely small. The temperature of 35 g/kg artificial seawater that was in contact with those seeds was 90 °C.
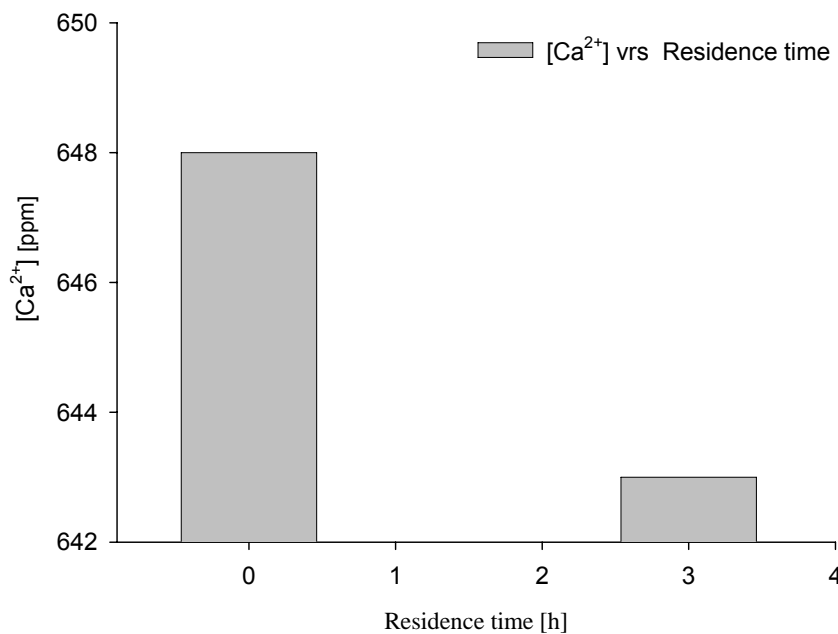
Figure 4-30: Calcium ion reduction by using a fluidized bed crystallizer, T=90 °C, mass of calcite seeds=5 g, seed size=1 mm, 35 g/kg salinity of artificial seawater

4.4 Reduction of CaCO₃ by a *hot finger*; without chemical addition

Instead of using calcite seeds, a hot finger coated with calcite was used as a media for the CaCO₃ growth process. Figure 4-31 shows the change in $[Ca^{2+} + Mg^{2+}]$ ion concentration in ASW with time. There is no change in Ca^{2+} ion concentration for the values with a residence time of 1, 2, 3 and 4 h. But there is a very small change in the Ca^{2+} concentration when the residence time was very long, 720 h, as shown in figure 4-31.

Furthermore, the change in the pH of seawater was small over the time of those measurements as to be seen in figure 4-31.
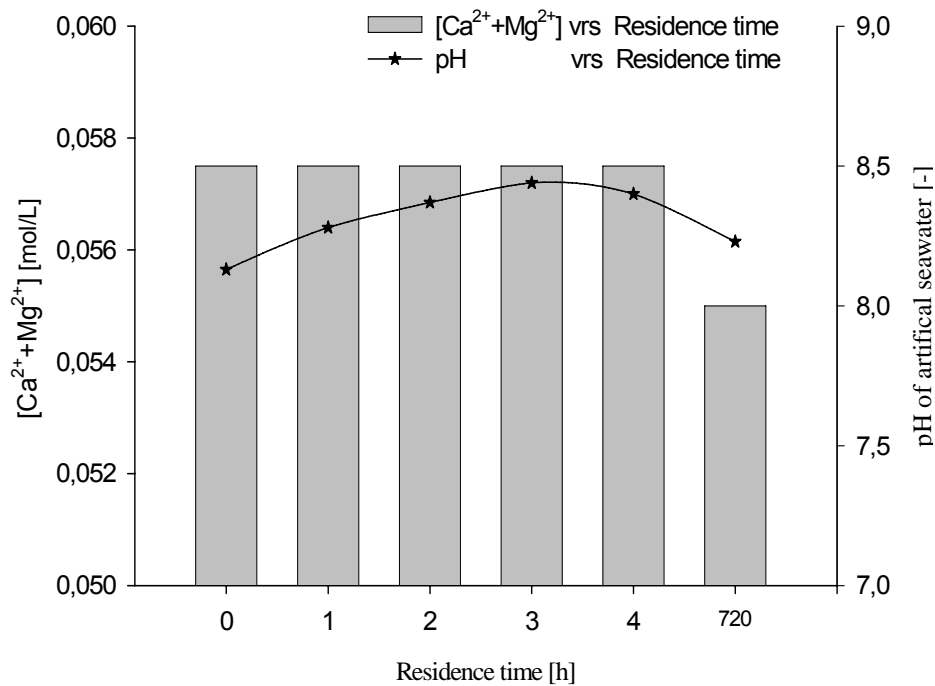
Figure 4-31: Calcium ion reduction by using a fluidized bed crystallizer, T_{ASW}=30 °C, $T_{hotfinger}$=90 °C , 35 g/kg salinity of artificial seawater

4.5   Reduction of $CaCO_3$ by *precipitation*; supersaturation modified by $NaHCO_3$

4.5.1 Reduction of calcium ion versus $NaHCO_3$ addition

The reduction of calcium ions in artificial seawater is essential to reduce the potentional of scale formation. Figure 4-32 shows the experimental and calculated results of $CaCO_3$ precipitation in the bulk of artificial seawater. A mathematical fit was used to find an equation (4-4) for the experimental data:

$$[Ca^{2+}+ Mg^{2+}] = 0.1109 - 0.0149\ M + 2.1422e\text{-}3\ M^2 - 4.9973e\text{-}5\ M^3 \qquad (4\text{-}4)$$

The determination of the total amount of Ca^{2+} and Mg^{2+} ions in ASW is referred to the amount of $CaCO_3$ precipitation. A very fast precipitation process in the bulk of ASW by ultrasonic irradiation is not possible without increasing the supersaturation of $CaCO_3$ in ASW! The trend of the $[Ca^{2+}+ Mg^{2+}]$ decrease due to $NaHCO_3$ addition as shown in figure 4-32 is an indication of increasing the amount of $CaCO_3$ precipitated. The slop of the decreasing curve goes to zero since the addition of $NaHCO_3$ is exceeding the limit of 2.5 g which is corresponding to the value of S=345.74, as may

be seen in figure 4-33. In this figure the degree of supersaturation of $CaCO_3$ has been calculated before and after the addition of $NaHCO_3$ to the artificial seawater.
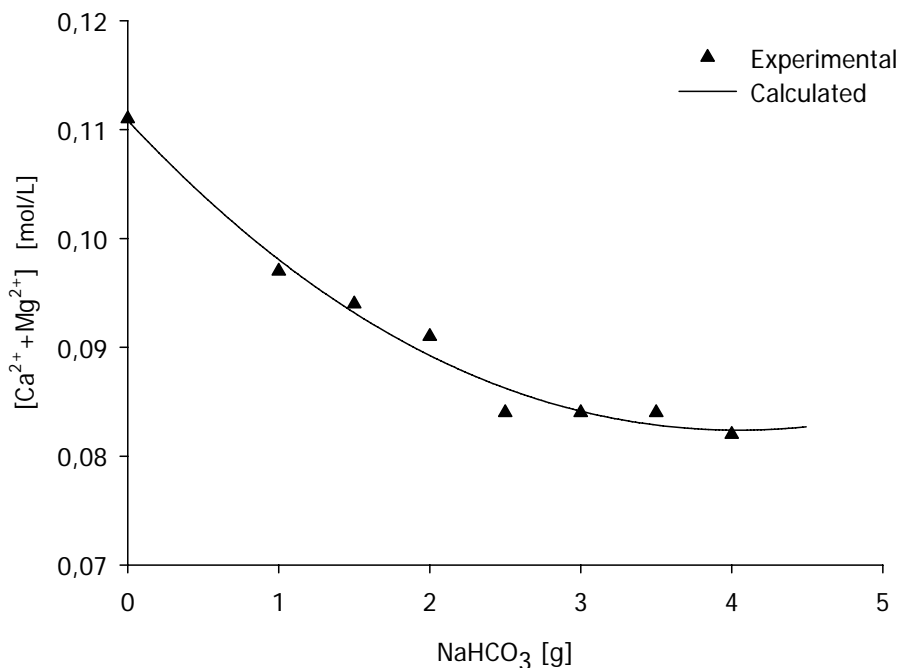
Figure 4-32: Calcium ion reduction due to the power of ultrasound and the modification of the degree of supersaturation. Ultrasonic power = 100 W, T=50 °C, V_{ASW}= 125 mL, t= 2 min, horn depth =2 cm and salinity=59 g/kg
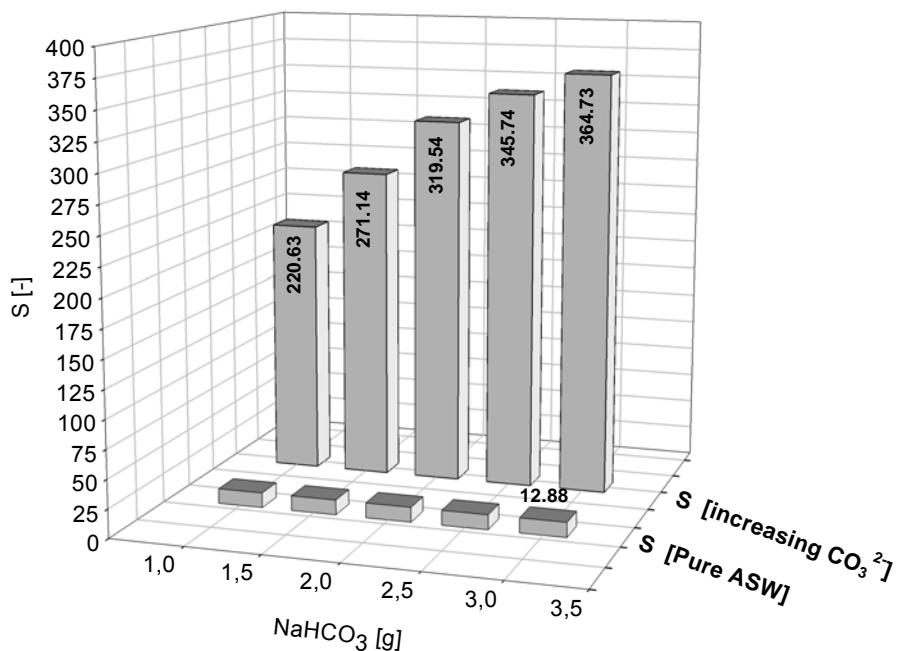
Figure 4-33: Degree of supersaturation (S) as a function of mass of $NaHCO_3$. Ultrasonic power = 100 W, T=50 °C, V_{ASW}= 125 mL, t= 2 min, horn depth =2 cm and salinity=59 g/kg

The degree of supersaturation was increased beyond the limit of meta-stability which is sufficient for precipitation of $CaCO_3$. However, the values of S are around 345.74 where the maximum amount of S is obtained due to 2.5 g of $NaHCO_3$ addition (see figure 4-32).

On the other hand, figure 4-34 shows the results of the X-ray diffraction analysis for the solid product of $CaCO_3$ which is precipitated out of the artificial seawater as described previously.
This pattern has been compared with the profile of pure $CaCO_3$. It indicates that the state of matching between the two patterns in terms of the 2-theta-scale shows a significant matching. But the intensity of the peaks is not similar.
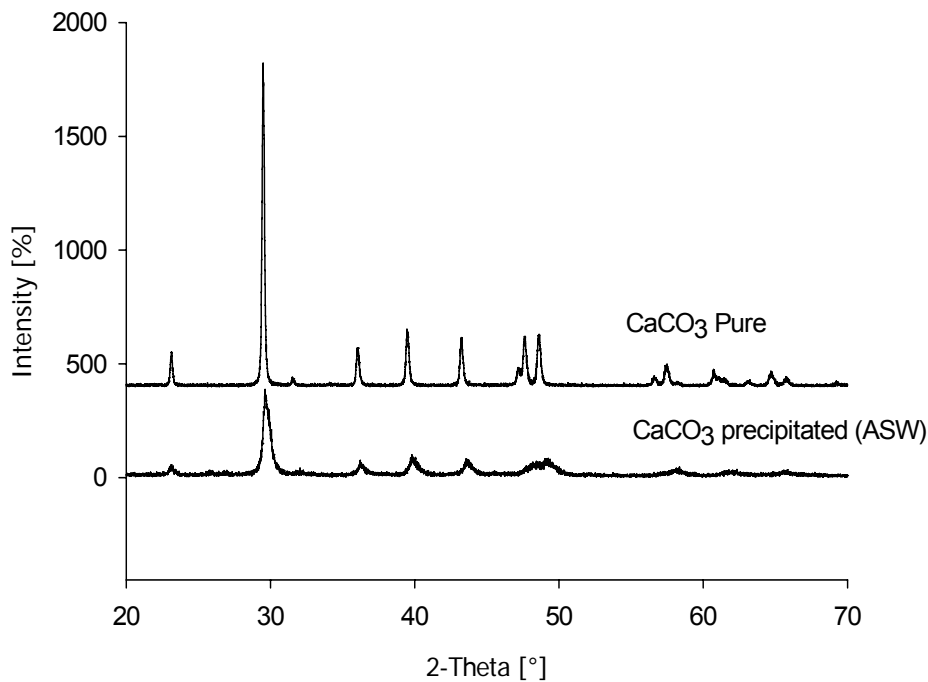
Figure 4-34: XRD patterns of $CaCO_3$ precipitated from artificial seawater (ASW) compared with pure $CaCO_3$

4.5.2 Reduction of calcium ion versus operational temperature

The effect of an increasing temperature on the calcium ion reduction can be seen clearly in figure 4-35. It is a large difference in Ca^{2+} ion reduction to be seen between the temperatures value of 50 and 90 °C. On the other hand, figure 4-36 shows the values of the degree of supersaturation which are corresponding to each temperature value.

56
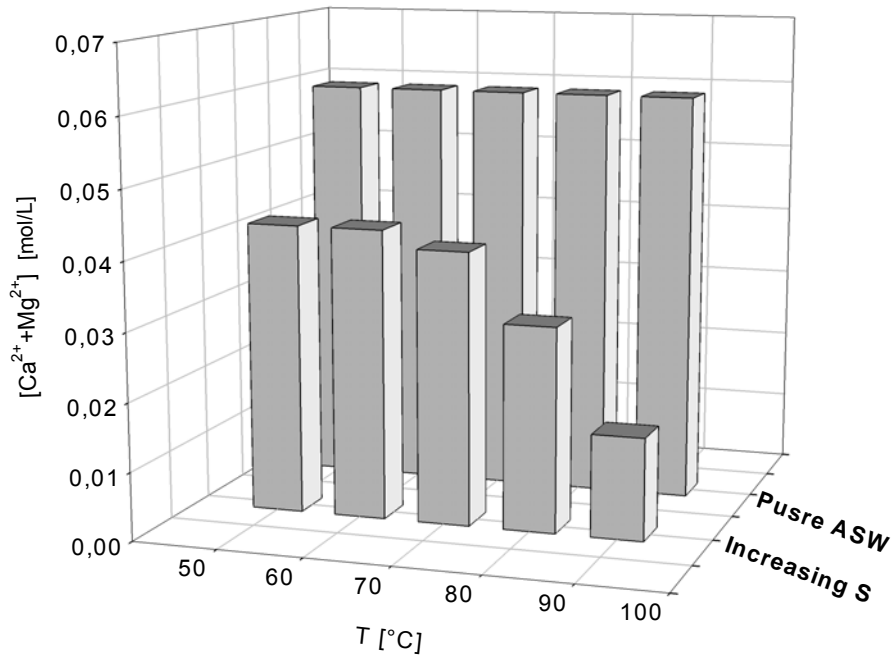
Figure 4-35: Calcium ion reduction versus operational temperature changing by using the power of ultrasound and the modification of the degree of supersaturation. Ultrasonic power = 100 W, V_{ASW}= 125 mL, t= 2 min, horn depth =2 cm and salinity=59 g/kg
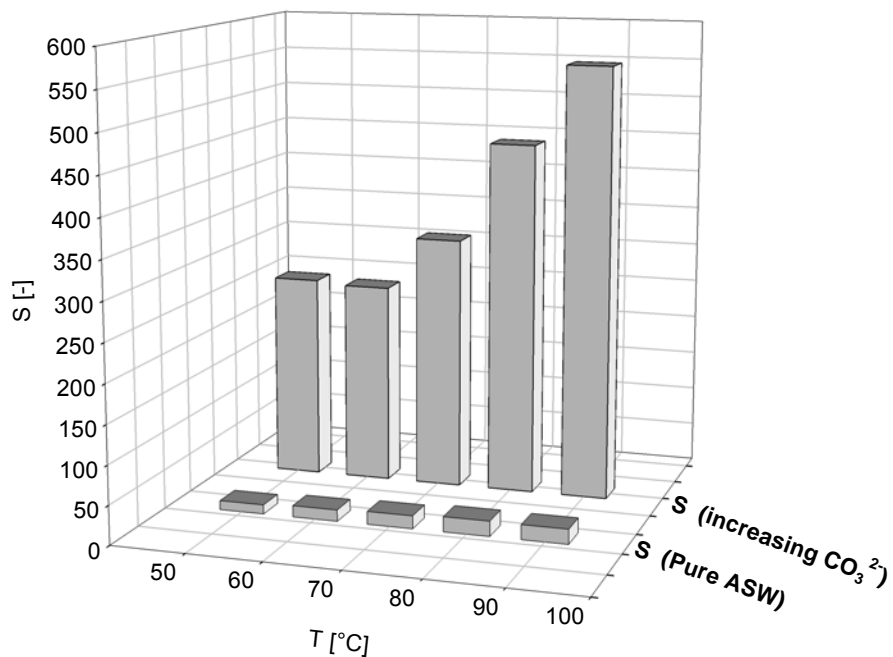
Figure 4-36: Degree of supersaturation (S) as a function of temperature. Ultrasonic power = 100 W, V_{ASW}= 125 mL, t= 2 min, horn depth =2 cm and salinity=59 g/kg

4.5.3 Reduction of calcium ion versus operational time, power of ultrasound and salinity

In this work, it has not been examined the induction time and how ultrasound can effect it. Since it is already known that the power of ultrasound reduces the induction time [LYC02].

The increase in time of ultrasonic power input is not making a large change in the reduction of calcium ions as may be seen from figure 4-37. The slop of the curve is only slightly negative with increasing time.
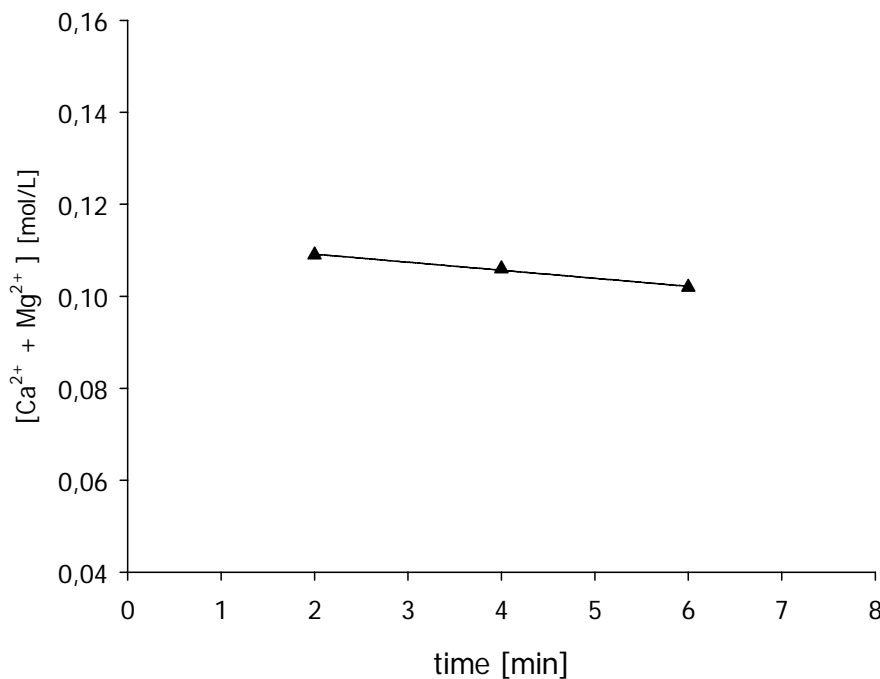
Figure 4-37: Calcium ion reduction versus operational time. Ultrasonic power = 100 W, V_{ASW}= 125 mL, horn depth =2 cm, T=50 °C and salinity=59 g/kg

Another operational condition has been studied, the effect of power input by ultrasound on the reduction process. Figure 4-38 shows an expected result of the power of ultrasound that is not affecting the rate of total Mg^{2+} and Ca^{2+} ion reduction. Furthermore, it can be seen from figure 4-38 that the yield of calcium ions as a function of salinity 35, 59 and 80 g/kg due to 2.5 g $NaHCO_3$ addition is increasing with increasing salinity of the seawater.
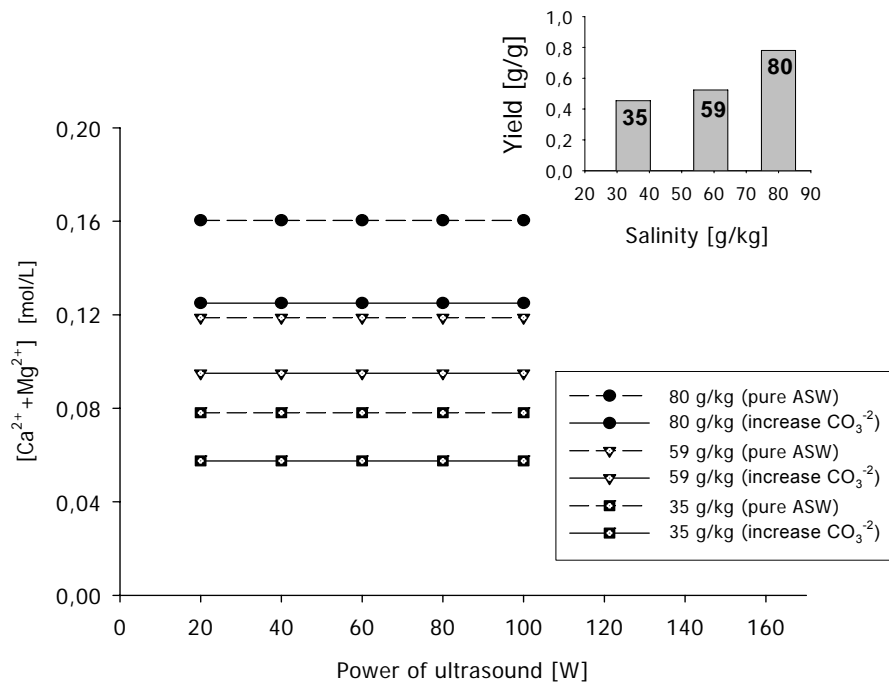
Figure 4-38: Calcium ion reduction versus salinity and power of ultrasound, V_{ASW}= 125 mL, T=50 °C, t= 2 min, horn depth =2 cm

5. Discussion

5.1 The effect of additives on the MSZ width

Nucleation of inorganic compounds in their pure and impure aqueous solutions is the case of this study for this section (see section 2.4).

5.1.1 ZnSO₄-H₂O solution

The figures 4-1 to 4-10 show different effects of suppression, enhancement and also non of both effects on the metastable zone width of $ZnSO_4$.

5.1.1.1 Effect of Al₂(SO₄)₃

Only the decrease in the width of MSZ (nucleation is increased) can be explained by means of the hydration enthalpy. The highest difference between the values of hydration enthalpies of Al^{3+} and Zn^{2+} ions, as shown in table 5-1, might be the reason of releasing the Zn^{2+} ions from ion-dipole bonds to be free in solution and bind with SO_4^{2-} as ionic bonds as a result decreasing in free energy of formation that is required to form a nucleus of $ZnSO_4$.

Table 5-1: Hydration enthalpies of individual ions of $Al_2(SO_4)_3$-$ZnSO_4$-H_2O at 25 °C [Mar87]

Cation	$\Delta_{hyd} H^o [kJ/mol]$	n	Anion	$\Delta_{hyd} H^o [kJ/mol]$	n
Al^{3+}	-4715	20.4	SO_4^{2-}	-1035	3.1
Zn^{2+}	-2070	9.6	OH^-	-520	2.7
H^+	-1103	12.0			

On the other hand the same concept using the hydration enthalpy to explain the increase in MSZ width (nucleation is decreased) for pure $ZnSO_4$ due to Al^{3+} addition is not possible. There are other important kinds of interaction forces, e.g. ion-ion that should also be taken into account. This interaction force can be estimated according to the equation 2-1 as can be seen in table 5-2.

Table 5-2: The electrostatic force of ion-ion interaction occurred in $Al_2(SO_4)_3$-$ZnSO_4$-H_2O

ion-ion	z_1	z_2	r_1 [nm]	r_2 [nm]	F [N]
Al-OH	3+	1-	0.053	0.133	3.20702E-09
Al-SO₄	3+	2-	0.053	0.230	2.77067E-09
Zn-OH	2+	1-	0.075	0.133	1.70966E-09
Zn-SO₄	2+	2-	0.075	0.230	1.59025E-09
H-OH	1+	1-	0.030	0.133	1.39197E-09
H-SO4	1+	2-	0.030	0.230	1.09418E-09

Hence the interaction force between Al^{3+}-OH^- is larger than Zn^{2+}-OH^-, which leads to an increase in H^+ ions that interact with SO_4^{2-}. The ability of Zn^{2+} ion to bind itself with the sulphate ions will be reduced. This might be the reason of the increase in the MSZ width due to very small addition of $Al_2(SO_4)_3$ **(nucleation is reduced).**

5.1.1.2 Effect of FeSO$_4$

The Fe^{2+} ion shows, figure 4-3, no effect on the MSZ width of $ZnSO_4$ due to the similar value of hydration enthalpy and the similar number of water molecules in hydration shell (see table 5-3) for both Fe^{2+} and Zn^{2+} ion.

Table 5-3: Hydration enthalpies of individual ions of $FeSO_4$-$ZnSO_4$-H_2O at 25 °C [Mar87]

Cation	$\Delta_{hyd}H^o[kJ/mol]$	n	Anion	$\Delta_{hyd}H^o[kJ/mol]$	n
Fe^{2+}	-1972	9.2	SO_4^{2-}	-1035	3.1
Zn^{2+}	-2070	9.6	OH^-	-520	2.7
H^+	-1103	12.0			

Additionally, both ions have the same strength of ion-ion force where the radius distance between Fe^{2+}-SO_4^{2-} and Zn^{2+}-SO_4^{2-} is similar. Furthermore, both have the same product charge as can be seen in table 5-4. As a result the structure of $ZnSO_4$ dose not changes due to addition of small amounts of $FeSO_4$.

Table 5-4: The electrostatic force of ion-ion interaction occurred in $FeSO_4$-$ZnSO_4$-H_2O

ion-ion	z_1	z_2	r_1 [nm]	r_2 [nm]	F [N]
Zn-OH	2+	1-	0.075	0.133	1.70966E-09
Fe-OH	2+	1-	0.078	0.133	1.66139E-09
Zn-SO$_4$	2+	2-	0.075	0.230	1.59025E-09
Fe-SO$_4$	2+	2-	0.078	0.230	1.55942E-09
H-OH	1+	1-	0.030	0.133	1.39197E-09
H-SO4	1+	2-	0.030	0.230	1.09418E-09

5.1.1.3 Effect of BaCl$_2$

Figure 4-5 shows the same response to $Al_2(SO_4)_3$ addition to the $ZnSO_4$ solution but with the low effect on the MSZ width of $ZnSO_4$. This is due to $\Delta H_{Ba^{2+}}$ is lower than $\Delta H_{Al^{3+}}$ as shown in table 5-5 and 5-1. Where value of $\Delta H_{SO_4^{2-}} < \Delta H_{Ba^{2+}} < \Delta H_{Zn^{2+}}$. The releasing of ions from the ion-dipole due to decreasing temperature of the solution is sequenced starting from the low value of hydration enthalpy to the highest one. In other words, SO_4^{2-} ions will be released from ion-dipole

bond, then Ba^{2+} ions and at the end Zn^{2+} ions to be free in the solution. Releasing the ion from ion-dipole depends on how much heat exchange between the system and the surrounding takes place, indeed this corresponds to the level of the temperature of the solution. That is the case of the addition of the Ba^{2+} ion, it needs extra heat to be removed from the system compared to pure case i.e., the nucleation temperature has to be shifted from 23.85 °C to 23.10 °C. This means, however, the use of the hydration enthalpy concept is applicable to explain the decrease but not the increase in the nucleation temperature of ZnSO$_4$!

Table 5-5: Hydration enthalpies of individual ions of BaCl$_2$-ZnSO$_4$-H2O at 25 °C [Mar87]

Cation	$\Delta_{hyd} H^o [kJ/mol]$	n	Anion	$\Delta_{hyd} H^o [kJ/mol]$	n
Ba^{2+}	-1332	5.3	SO$_4^{2-}$	-1035	3.1
Zn^{2+}	-2070	9.6	OH$^-$	-520	2.7
H$^+$	-1103	12.0	Cl$^-$	-367	2.0

Furthermore, the Zn^{2+}-SO$_4^{2-}$ ions force interaction is larger than the interaction forces between the cations and anions in the BaCl$_2$–ZnSO$_4$–water solution as shown in table 5-6. In this table, the difference between the value of electrostatic forces of Zn^{2+}- SO$_4^{2-}$ and Ba^{2+}- SO$_4^{2-}$ is high (i.e., Zn^{2+} ion is the dominator). Thus, it is not suitable to use the concept of ion-ion interaction force to explain the change in nucleation temperature which is extremely small.

Table 5-6: The electrostatic force of ion-ion interaction occurred in BaCl$_2$-ZnSO$_4$-H$_2$O

ion-ion	z_1	z_2	r_1 [nm]	r_2 [nm]	F [N]
Zn-OH	2+	1-	0.075	0.133	1.70966E-09
Zn-SO$_4$	2+	2-	0.075	0.230	1.59025E-09
H-OH	1+	1-	0.030	0.133	1.39197E-09
Zn-Cl	2+	1-	0.075	0.181	1.12864E-09
Ba-SO$_4$	2+	2-	0.136	0.230	1.10434E-09
H-SO4	1+	2-	0.030	0.230	1.09418E-09
Ba-OH	2+	1-	0.136	0.133	1.02219E-09
H-Cl	1+	1-	0.030	0.181	8.30694E-10
Ba-Cl	2+	1-	0.136	0.181	7.36067E-10

5.1.1.4 Effect of Li$_2$SO$_4$

In figure 4-8, the nucleation temperature has been shifted from 24.38 °C to 25.27 °C. This effect is not because of the lower value of $\Delta H_{Li^+} < \Delta H_{SO_4^{2-}} < \Delta H_{Zn^{2+}}$ as shown in the table 5-7, but it is because the Li$^+$ ion can be trapped by a higher number of water molecules (n) than SO$_4^{2-}$. i.e. the reduction of the water molecules that can interact

with SO_4^{2-} in the solution. This means SO_4^{2-} ions can be released from ion-dipole bonds to be free in solution with less amount of cooling.

Table 5-7: Hydration enthalpies of individual ions of Li_2SO_4-$ZnSO_4$-H_2O at 25 °C [Mar87]

Cation	$\Delta_{hyd} H^o [kJ/mol]$	n	Anion	$\Delta_{hyd} H^o [kJ/mol]$	n
Li^+	-531	5.2	SO_4^{2-}	-1035	3.1
Zn^{2+}	-2070	9.6	OH^-	-520	2.7
H^+	-1103	12.0			

On the other hand, the Li^+ ion has a low ion-ion strength force compared with Zn^{2+} as shown in table 5-8. As a result, the Zn^{2+}-SO_4^{2-} ions interaction is dominating the process of $ZnSO_4$ nucleation.

Table 5-8: The electrostatic force of ion-ion interaction occurred in Li_2SO_4-$ZnSO_4$-H_2O

ion-ion	z_1	z_2	r_1 [nm]	r_2 [nm]	F [N]
Zn-OH	2+	1-	0.075	0.113	2.09276E-09
H-OH	1+	1-	0.030	0.113	1.80856E-09
Zn-SO$_4$	2+	2-	0.075	0.230	1.59025E-09
Li-OH	1+	1-	0.069	0.113	1.11651E-09
H-SO4	1+	2-	0.030	0.230	1.09418E-09
Li-SO$_4$	1+	2-	0.069	0.230	8.27358E-10

5.1.1.5   Effect of K_2SO_4

In figure 4-10 the small change of the nucleation of $ZnSO_4$-H_2O due to the K^+ ion addition is not explainable in terms of the $\Delta H_{K^{1+}}$ value compared to the hydration value of the zinc ion as shown in table 5-9.

Table 5-9: Hydration enthalpies of individual ions of K_2SO_4-$ZnSO_4$-H_2O at 25 °C [Mar87]

Cation	$\Delta_{hyd} H^o [kJ/mol]$	n	Anion	$\Delta_{hyd} H^o [kJ/mol]$	n
K^+	-334	2.6	SO_4^{2-}	-1035	3.1
Zn^{2+}	-2070	9.6	OH^-	-520	2.7
H^+	-1103	12.0			

The interaction forces between the K^+ ion and the anions in the K_2SO_4–$ZnSO_4$–H_2O solution are very small, see table 5-10, when it is compared to the Zn^{2+} ion. Since the K^+ ion has a larger radius and lower charge than the Zn^{2+} ion. Thus, using the concept of ion-ion interaction is not applicable.

Table 5-10: The electrostatic force of ion-ion interaction occurred in Li_2SO_4-$ZnSO_4$-H_2O

ion-ion	z_1	z_2	r_1 [nm]	r_2 [nm]	F [N]
Zn-OH	2+	1-	0.075	0.113	2.09276E-27
Zn-SO$_4$	2+	2-	0.075	0.230	1.59025E-27
H-OH	1+	1-	0.030	0.113	1.80856E-27
H-SO4	1+	2-	0.030	0.230	1.09418E-27
K-OH	1+	1-	0.138	0.113	5.87027E-28
K-SO$_4$	1+	2-	0.138	0.230	5.46185E-28

5.1.2 LiCl-H$_2$O solution

The figures 4-11 to 4-18 show different effects of suppression, enhancement and also non of both effects on the metastable zone width of LiCl.

5.1.2.1 Effect of AlCl$_3$

There is no change in the nucleation temperature of LiCl due to addition of Al^{3+} ion in the range concentration 5-75 ppm to the solution. This result was not anticipated, be cause of the high value of enthalpy of hydration of Al^{3+} ion, see table 5-11. The structure of the solution in terms of ion-dipole interaction should be changed. Therefore, the concept using the hydration enthalpy is not applicable!

Table 5-11: Hydration enthalpies of individual ions of $AlCl_3$- LiCl-H_2O at 25 °C [Mar87]

Cation	$\Delta_{hyd}H^o[kJ/mol]$	n	Anion	$\Delta_{hyd}H^o[kJ/mol]$	n
Al^{3+}	-4715	20.4	Cl^-	-367	2.0
Li^+	-531	5.2	OH^-	-520	2.7
H^+	-1103	12.0			

Furthermore, the concept of electrostatic force interaction between the ions due to Al^{3+} addition to LiCl is not applicable, too, as can be seen in table 5-12.

Table 5-12: The electrostatic force of ion-ion interaction occurred in $AlCl_3$- LiCl -H_2O

ion-ion	z_1	z_2	r_1 [nm]	r_2 [nm]	F [N]
Al-OH	3+	1-	0.053	0.133	3.20702E-09
Al-Cl	3+	1-	0.053	0.181	2.02626E-09
H-OH	1+	1-	0.030	0.133	1.39197E-09
Li-OH	1+	1-	0.069	0.133	9.06365E-10
H-Cl	1+	1-	0.030	0.181	8.30694E-10
Li-Cl	1+	1-	0.069	0.181	5.91733E-10

5.1.2.2   Effect of FeCl$_2$

The nucleation temperature of LiCl is raised from about 10.5 to 12 °C in the concentration range of Fe^{2+} ions between 10 to 150 ppm as shown in figure 4-14. The highest difference between the value of hydration enthalpy of Fe^{2+} and Li$^+$ ions, and the numbers (n) of water molecules in the hydration shell of Fe^{2+}-dipole which is more than the Li$^+$-dipole, see table 5-13. This lead to release the Li$^+$ ions from ion-dipole to be free in the solution and can bind with the Cl$^-$ as ionic bonds and as a result reduce the free energy of formation that is required to form a nucleus of LiCl.

Table 5-13: Hydration enthalpies of individual ions of FeCl$_2$- LiCl-H$_2$O at 25 °C [Mar87]

Cation	$\Delta_{hyd} H^o [kJ/mol]$	n	Anion	$\Delta_{hyd} H^o [kJ/mol]$	n
Fe^{2+}	-1972	9.2	Cl$^-$	-367	2.0
Li$^+$	-531	5.2	OH$^-$	-520	2.7
H$^+$	-1103	12.0			

Table 5-14 shows the interaction electrostatic force when Fe^{2+} is added to the solution of LiCl. Those values are unusable for the interpretation of the effect of Fe^{2+} by means of ion-ion interaction concept.

Table 5-14: The electrostatic force of ion-ion interaction occurred in FeCl$_2$- LiCl-H$_2$O

ion-ion	z$_1$	z$_2$	r$_1$ [nm]	r$_2$ [nm]	F [N]
Fe-OH	2+	1-	0.078	0.133	1.66139E-09
H-OH	1+	1-	0.030	0.133	1.39197E-09
Fe-Cl	2+	1-	0.078	0.181	1.10265E-09
Li-OH	1+	1-	0.069	0.133	9.06365E-10
H-Cl	1+	1-	0.030	0.181	8.30694E-10
Li-Cl	1+	1-	0.069	0.181	5.91733E-10

5.1.2.3   Effect of MgCl$_2$

The interpretation of the Mg^{2+} ion effect on the nucleation temperature of LiCl-H$_2$O solutions as shown in figure 4-16 can be explained in the same way as explaining the effect of the Al^{3+} ion addition as shown in section of 5.1.1.1. The value of the hydration enthalpy of the Mg^{2+} ion that is needed for the interpretation is presented in table 5-15. In addition, the electrostatic forces of ion-ion interaction in MgCl$_2$- LiCl-H$_2$O values are shown in table 5-16.

Table 5-15: Hydration enthalpies of individual ions of $MgCl_2$- $LiCl$-H_2O at 25 °C [Mar87]

Cation	$\Delta_{hyd}H^o[kJ/mol]$	n	Anion	$\Delta_{hyd}H^o[kJ/mol]$	n
Mg^{2+}	-1949	10.0	Cl^-	-367	2.0
Li^+	-531	5.2	OH^-	-520	2.7
H^+	-1103	12.0			

Table 5-16: The electrostatic force of ion-ion interaction occurred in $MgCl_2$- $LiCl$-H_2O

ion-ion	z_1	z_2	r_1 [nm]	r_2 [nm]	F [N]
Mg-OH	2+	1-	0.072	0.133	1.76006E-09
H-OH	1+	1-	0.030	0.133	1.39197E-09
Mg-Cl	2+	1-	0.072	0.181	1.15557E-09
Li-OH	1+	1-	0.069	0.133	9.06365E-10
H-Cl	1+	1-	0.030	0.181	8.30694E-10
Li-Cl	1+	1-	0.069	0.181	5.91733E-10

5.1.2.4 Effect of $BaCl_2$

In table 5-17, Ba^{2+} ion has the highest value of enthalpy of hydration, this led to release the Li^+ ions from ion-dipole bonds to be free in solution and bind with Cl^- as ionic bonds as a result is the decrease in the free energy for the formation that is required for nucleation. Hence, the nucleation temperature of $LiCl$-H_2O is increased as shown in figure 4-18.

Table 5-17: Hydration enthalpies of individual ions of $BaCl_2$- $LiCl$-H_2O at 25 °C [Mar87]

Cation	$\Delta_{hyd}H^o[kJ/mol]$	n	Anion	$\Delta_{hyd}H^o[kJ/mol]$	n
Ba^{2+}	-1332	5.3	Cl^-	-367	2.0
Li^+	-531	5.2	OH^-	-520	2.7
H^+	-1103	12.0			

The electrostatic force (F) values, see table 5-18, of Ba^{2+}-Cl^- ions and Li^+-Cl^- ions to some degree are similar. Hence, the electrostatic force is not playing a role in explaining the effect of $BaCl_2$ on the nucleation temperature of $LiCl$-H_2O.

Table 5-18: The electrostatic force of ion-ion interaction occurred in $BaCl_2$- $LiCl$-H_2O

ion-ion	z_1	z_2	r_1 [nm]	r_2 [nm]	F [N]
H-OH	1+	1-	0.030	0.133	1.39197E-09
H-Cl	1+	1-	0.030	0.181	1.39197E-09
Ba-OH	2+	1-	0.136	0.133	1.02219E-09
Li-OH	1+	1-	0.069	0.133	9.06365E-10
Ba-Cl	2+	1-	0.136	0.181	7.36067E-10
Li-Cl	1+	1-	0.069	0.181	5.91733E-10

5.1.3 **K₂SO₄-H₂O solution**

The figures 4-19 to 4-24 show different effects of suppression, enhancement and also non of both effects on the metastable zone width of K_2SO_4.

5.1.3.1   **Effect of CuSO₄**

Addition of Cu^{2+} ions to K_2SO_4-H_2O solution has decreased the nucleation by a small degree, this very small change can not be explained by means of the value of enthalpy of hydration of Cu^{2+} ion, which has the highest value as shown in table 5-17. Figure 4-20 shows different result than what was expected to increase the nucleation temperature of K_2SO_4 solution due to Cu^{2+} ion addition!

Table 5-17: Hydration enthalpies of individual ions of $CuSO_4$- K_2SO_4-H_2O at 25 °C [Mar87]

Cation	$\Delta_{hyd} H^o [kJ/mol]$	**n**	**Anion**	$\Delta_{hyd} H^o [kJ/mol]$	**n**
Cu^{2+}	-2123	9.9	SO_4^{2-}	-1035	3.1
K^+	-334	2.6	OH^-	-520	2.7
H^+	-1103	12.0			

The electrostatic force interaction of K^+-SO_4^{2-} has the lowest value as seen in table 5-18. This might be the reason of the small degree in decrease of the nucleation temperature of K_2SO_4. Where the energy of formation is increased to release more K^+ ion form K-dipole to interact with SO_4^{2-} ions that are strongly interacting with the Cu^{2+} ions due to high value of the electrostatic force of Cu-SO_4.

Table 5-18: The electrostatic force of ion-ion interaction occurred in $CuSO_4$- K_2SO_4-H_2O

ion-ion	z_1	z_2	r_1 [nm]	r_2 [nm]	F [N]
H-OH	1+	1-	0.030	0.133	1.80856E-09
Cu-OH	2+	1-	0.096	0.133	1.69334E-09
Cu-SO_4	2+	2-	0.096	0.230	1.39197E-09
H-SO4	1+	2-	0.030	0.230	1.09418E-09
K-OH	1+	1-	0.138	0.133	5.87027E-10
K-SO_4	1+	2-	0.138	0.230	5.46185E-10

5.1.3.2   **Effect of BaCl₂**

The effect of Ba^{2+} ion on the nucleation temperature of K_2SO_4-H_2O solution has a similar interpretation as shown in section 5.1.3.1. Taking, however, into account the value of the hydration enthalpy of the Ba^{2+} ion and the electrostatic force of interaction of Ba^{2+}-SO_4^{2-} and K^+-SO_4^{2-} the interpretation are as shown in tables 5-19 and 5-20.

Table 5-19: Hydration enthalpies of individual ions of $BaCl_2$- K_2SO_4-H_2O at 25 °C [Mar87]

Cation	$\Delta_{hyd}H^o[kJ/mol]$	n	Anion	$\Delta_{hyd}H^o[kJ/mol]$	n
Ba^{2+}	-1332	5.3	SO_4^{2-}	-1035	3.1
K^+	-334	2.6	OH^-	-520	2.7
H^+	-1103	12.0	Cl^-	-367	2.0

Table 5-20: The electrostatic force of ion-ion interaction occurred in $BaCl_2$- K_2SO_4-H_2O

ion-ion	z_1	z_2	r_1 [nm]	r_2 [nm]	F [N]
H-OH	1+	1-	0.030	0.133	1.39197E-09
Ba-SO$_4$	2+	2-	0.136	0.230	1.10434E-09
H-SO4	1+	2-	0.030	0.230	1.09418E-09
Ba-OH	2+	1-	0.136	0.133	1.02219E-09
H-Cl	1+	1-	0.030	0.181	8.30694E-10
Ba-Cl	2+	1-	0.136	0.181	7.36067E-10
K-SO$_4$	1+	2-	0.138	0.230	5.46185E-10
K-OH	1+	1-	0.138	0.133	5.03579E-10
K-Cl	1+	1-	0.138	0.181	3.63433E-10

5.1.3.3   Effect of Li_2SO_4

The small difference between the values of hydration enthalpies of Li^+ and K^+ ions, as shown in table 5-21, might be the reason of no significant changed of the nucleation temperature of K_2SO_4-H_2O due to Li^+ addition as shown in figure 4-22.

Table 5-21: Hydration enthalpies of individual ions of Li_2SO_4- K_2SO_4-H_2O at 25 °C [Mar87]

Cation	$\Delta_{hyd}H^o[kJ/mol]$	n	Anion	$\Delta_{hyd}H^o[kJ/mol]$	n
Li^+	-531	5.2	SO_4^{2-}	-1035	3.1
K^+	-334	2.6	OH^-	-520	2.7
H^+	-1103	12.0			

On the other hand, the very small decrease in nucleation temperature might be due to the electrostatic force interaction between Li^+ and SO_4^{2-} ions which is larger than in the case of K^+ and SO_4^{2-} ions, see table 5-22.

Table 5-22: The electrostatic force of ion-ion interaction occurred in Li_2SO_4- K_2SO_4-H_2O

ion-ion	z_1	z_2	r_1 [nm]	r_2 [nm]	F [N]
H-OH	1+	1-	0.030	0.133	1.80856E-09
Li-OH	1+	1-	0.069	0.133	1.11651E-09
H-SO4	1+	2-	0.030	0.230	1.09418E-09
Li-SO$_4$	1+	2-	0.069	0.230	8.27358E-10
K-OH	1+	1-	0.138	0.133	5.87027E-10
K-SO$_4$	1+	2-	0.138	0.230	5.46185E-10

The previous results showed that the concept of the hydration enthalpy values (ion-dipole force) and ion-ion forces interaction can be used to explain the effect of some additives on the width of the metastable zone. But it dose not explain some of the other cases. It is suggested to examine the concept of intermolecular forces interaction with more and different cases of additives to clarify the still not explainable cases.

5.2   The induction time of CaCO₃ in artificial seawater

The change in pH of seawater solution is an indication of the chemical change in carbonate system of seawater solution (see section 2.7-1). Thus, this led to choose the pH measurement as method to determine the induction time of CaCO₃ nucleation in artificial seawater, e.g. [RUS92]. The HCO_3^- ion in ASW has been increased by NaHCO₃ addition as mentioned before (see section 2.12-2). In figure 4-25, the pH of 35 g/kg artificial seawater has been changed rapidly from 8 to 7.46 once the NaHCO₃ was added. This change in pH solution can be interpreted according to the following reversible reactions [Gla01]:

Reaction mechanism I (acidic mechanism):

$$\textbf{Step 1:} \qquad CO_2 + H_2O \overset{Slow}{\Leftrightarrow} HCO_3^- + H^+ \qquad\qquad (5\text{-}1)$$

$$\textbf{Step 2:} \qquad HCO_3^- \overset{Instant}{\Leftrightarrow} CO_3^{2-} + H^+ \qquad\qquad (5\text{-}2)$$

Reaction mechanism II (alkaline mechanism):

$$\textbf{Step 1:} \qquad CO_2 + OH^- \overset{Slow}{\Leftrightarrow} HCO_3^- \qquad\qquad (5\text{-}3)$$

$$\textbf{Step 2:} \qquad HCO_3^- + OH^- \overset{Instant}{\Leftrightarrow} CO_3^{2-} + H_2O \qquad\qquad (5\text{-}4)$$
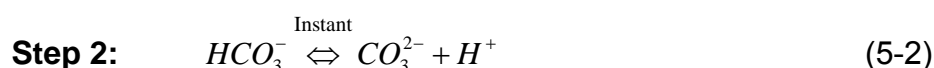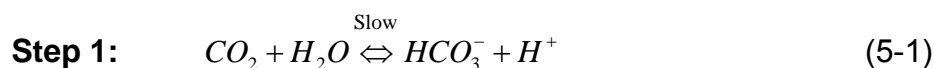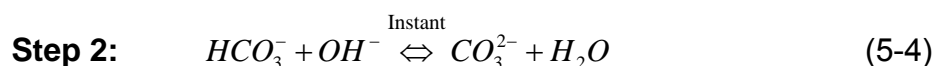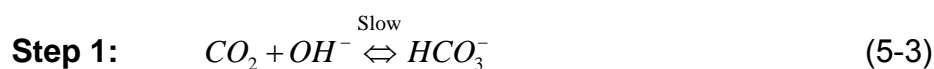
As can be seen in reaction 5-2, the increasing in the concentration of HCO_3^- ion leads to shift the reversible reaction to the right direction instantly **(Le Chatelier's Principle)**. As a result, the pH of seawater was decreased rapidly and CO_3^{2-} ions were increased at the same time which led to increase the supersaturation of CaCO₃ in artificial seawater. Subsequently, the pH value of ASW was slowly increasing with time (see area 1 in figure 4-25) due to raising the hydroxyl ion according to the

backward reaction in equation 5-3. The time of raising the concentration of the hydroxyl ions in ASW is affected by the high concentration of HCO_3^- ions, CO_2 concentration in ASW and the slow rate constant of the reaction. This raise in the hydroxyl ions will continue until the precipitation of $CaCO_3$ occurs.

Later on, another region can be seen in figure 4-25. Area 2 is representing the start of $CaCO_3$ precipitation and growth. The pH value in this area has been decreased slowly due to the consumption of CO_3^{2-} ions which are required for the $CaCO_3$ growth. This slow consumption leads to shift the reversible reaction in equation 5-2 to the right direction. Hence, the H^+ ions are increased during the up take process of CO_3^{2-} ions for a slow growth of $CaCO_3$ due to the low level of supersaturation as a result of the $CaCO_3$ precipitation. The growth of $CaCO_3$ will continue until the level of supersaturated of $CaCO_3$ will be very small and not enough for further growth. This is due to the reduction in Ca^{2+} ions which are considered the limiting reactant only after the $NaHCO_3$ addition to artificial seawater and $CaCO_3$ precipitation occurred.

The last region in figure 4-25 is the area 3 which represents the no growth process of $CaCO_3$. In this area, it can be observed that the pH is increased. This is due to the occurrence of the backward reaction 5-3.

There are no data available that can be shown of a similar study of determination of the induction time of $CaCO_3$ precipitation in artificial seawater as a result of $NaHCO_3$ addition. ***It is very important in estimating the applicability of using the ultrasonic technique as precipitation accelerator***. However, the $NaHCO_3$ has been used before for softening of seawater [HAY77] and for $CaCO_3$ precipitation [DRI04]. In addition, Na_2CO_3 has been used for the removal of calcium sulfate impurities from evaporated seawater [GUR05]. Furthermore, Pytkowicz [PYT65] has determined the induction time for inorganic precipitation of $CaCO_3$ over a wide range of supersaturation in natural seawater and in artificial seawater free of magnesium ions. Supersaturation was increased by adding a <u>solution</u> of Na_2CO_3. The induction time of $CaCO_3$ was found to be very short in magnesium-free artificial seawater comparable with normal artificial seawater. In addition, Rushdi *et al.* [RUS92] has investigated the effect of $[Mg^{2+}]$ to $[Ca^{2+}]$ mole ratio on the induction time and mineralogy of $CaCO_3$ precipitation while Na_2CO_3 was added.

In the other words, both $NaHCO_3$ and Na_2CO_3 compounds can be used to precipitate $CaCO_3$ out of the seawater. But which compound of those can be logically used in terms of the chemical reaction nature of each HCO_3^- ion and CO_3^{2-} ion as shown in equations 5-1 and 5-4, respectively? The answer can be characterized according to the type of reaction. An extra amount of CO_3^{2-} ions in seawater can lead to deplete water molecules in seawater which occurs not in the case of $NaHCO_3$ addition.

Hence, the addition of NaHCO₃ will be more logical compared to Na₂CO₃ addition by means of product yield of pure water. Furthermore, commercially sodium carbonate is coasted more than sodium bicarbonate (e.g. see [MER08]).

5.2.1 Effect the mass addition of NaHCO₃ at 35 and 55 g/kg salinity $(Sa.)$

The mass of NaHCO₃ addition and operational temperature, together can strongly effect the induction time of CaCO₃ precipitation. Those two parameters can be found in the following equations [ALR04]:

$$[CO_3^{2-}] = \frac{K_2^{SW} \cdot [HCO_3^-]}{[H^+]} \tag{5-5}$$

$$K_2^{SW} = \text{EXP}\left(\begin{array}{l} -0.84226 - \dfrac{3741.1288}{T} - 1.437139 \cdot \ln(T) + \left(-0.128417 - \dfrac{24.41239}{T} \right) \cdot Sa.^{0.5} + \\ 0.1195308 \cdot Sa. - 0.0091284 \cdot Sa.^{1.5} \end{array} \right) \tag{5-6}$$

$$K_{sp,calcite}^{SW} = 10^{\wedge}\left(\begin{array}{l} -171.945 - 0.077993T + \dfrac{2903.293}{T} + 71.595 \text{Log}(T) + \\ \left(-0.77712 + 0.0028426T + \dfrac{178.34}{T} \right) Sa.^{0.5} - 0.07711 \cdot Sa + 0.0041249 \cdot Sa.^{1.5} \end{array} \right) \tag{5-7}$$

$$t_{ind} \, \alpha \, \left(\frac{1}{S} = \frac{K_{sp}}{[Ca^{2+}][CO_3^{2-}]} \right) \tag{5-8}$$

The induction time is changing inversely with the concentration of CO_3^{2-} ions as shown in equation 5-8. Since the CO_3^{2-} ions are changing reversible with temperature and salinity of the seawater as can be seen in figure 5-1 which represents equation 5-6. When equation 5-6 is substituted in equation 5-5, the induction time will decrease with increasing temperature for the same level of NaHCO₃ addition as shown in figures 4-26 and 4-28.

At the same time of the elevating of the CO_3^{2-} ion concentration due to an increasing temperature, the solubility product of calcite $K_{sp,calcite}^{SW}$ is decreasing (see figure 5-2).
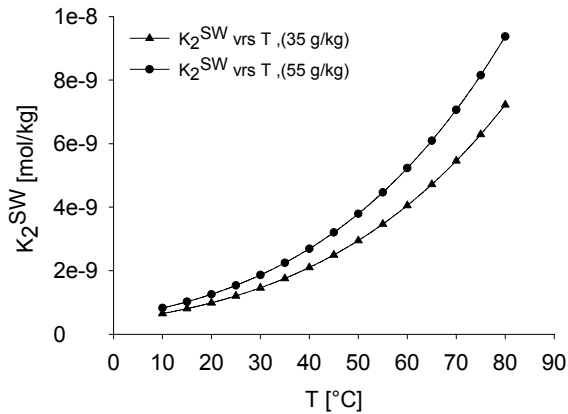
Figure 5-1: Second dissociation constant of reaction (5-2) versus temperature at 35 and 55 g/kg salinities
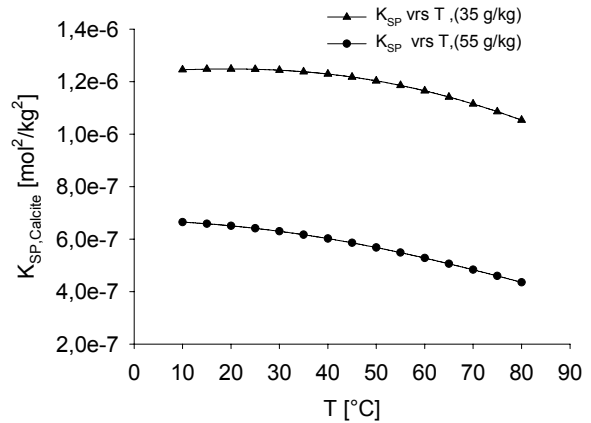
Figure 5-2: Solubility product of calcite in seawater versus temperature at 35 and 55 g/kg salinities according to equation (5-7)

This is an additional effect on the decrease of the induction time of the precipitation of $CaCO_3$. But the order of magnitude in change of K_2^{SW} is higher than the change of $K_{sp,calcite}^{SW}$. This means the change in the temperature is more effective on K_2^{SW} than $K_{sp,calcite}^{SW}$. On the other hand, the change in the temperature becomes ineffective concerning the induction time compared to the effect of the mass of $NaHCO_3$ when the addition exceeds 1 g and 2 g for 35 and 55 g/kg salinity, respectively, as predicted in figures 4-26 and 4-28. This can be explained by equation 5-5, where the increase in both the temperature and the HCO_3^- concentration can increase the concentration of CO_3^{2-} ions. However, the effect of increasing the $K_2^{SW} = f(T, Salinity)$ is not as high as the increase in the concentration of HCO_3^- within the temperature range of 30-70 °C. The limits of K_2^{SW} can be seen in figure 5-1 as maximum and minimum limit of K_2^{SW} versus temperature.

The salinity of seawater refers to the content of salt concentrations ratio as it is known, a higher salinity contains a higher content of Ca^{2+} ions and CO_3^{2-} ions. The solubility product is slightly decreased with increasing the salinity of artificial seawater (see figure 5-2). Therefore, the induction time of $CaCO_3$ at higher salinity should be shorter for the same amount of $NaHCO_3$ addition.

This can be clearly verified according to the mathematical relation between the induction time and solubility product on one side, and the product of the concentrations of Ca^{2+} and CO_3^{2-} which represented the denominator of equation (5-8) on the other side. But figure 5-3 shows a different result. An increasing in the induction time due to an increase in the seawater salinity for the same amount of $NaHCO_3$ addition! Rushdi *et al.* [RUS92] was found that the induction time of $CaCO_3$

was increased with increasing the Mg^{2+} ion concentration in seawater. Consequently, the induction time of $CaCO_3$ in seawater increased at higher salinities (higher content of Mg^{2+} ions) for the same amount of $NaHCO_3$ addition as shown in figure 5-3.
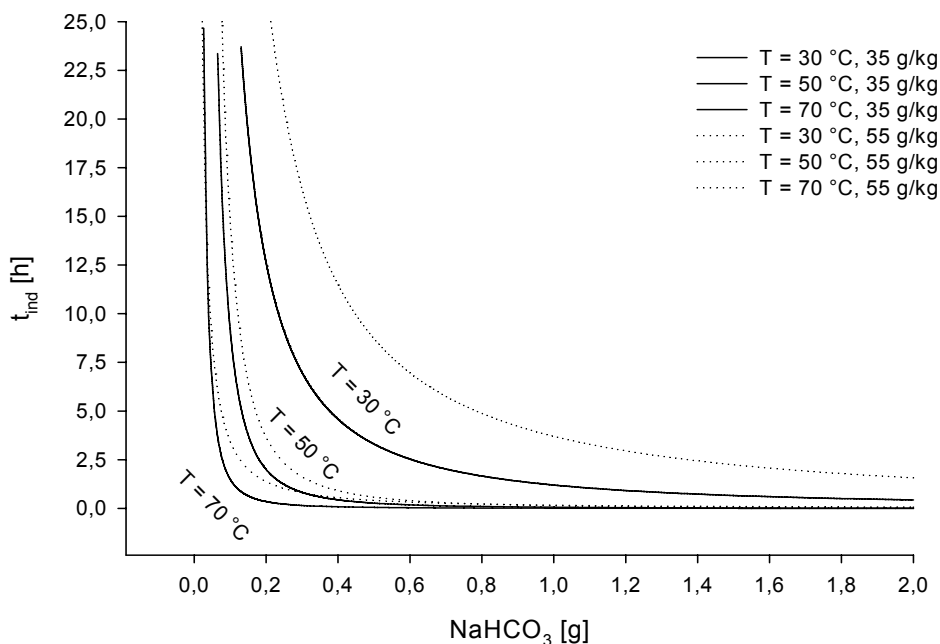
Figure 5-3: The effect of $NaHCO_3$ addition on the induction time of $CaCO_3$ precipitation in artificial seawater, 250 rpm, **35** and **55** g/kg salinity

5.2.2 Interfacial tension (surface energy) of CaCO₃ in ASW

One of the necessities to determine the induction time is to calculate the interfacial energy between the nuclei surface and the liquid solution. Interfacial tension is given by equation (2-12). Interfacial tension between the $CaCO_3$ and the liquid solution of seawater can be calculated from the slope of those lines as shown in the figures 4-27 and 4-29. The molar volume of $CaCO_3$ is 36.932 cm^3/mole for calcite and the correction factor $f(\Theta) = 0,01$. This value is valid when the nucleation is heterogeneous; this is indeed true, since foreign particles of $NaHCO_3$ were added to the metastable artificial seawater. The values of interfacial tension given in table 5-23 are increased with the temperature for the 35 and 55 g/kg salinity. Further the interfacial tension is decreased with increasing the salinity for the same level of nucleation temperature 70 °C.

Table 5-23: Estimated values of interfacial energy between the $CaCO_3$ and seawater

T [°C]	Salinity [g/kg]	σ [mJ/m^2]
30	35	26.97
40	35	29.68
50	35	57.40
70	35	93.67
30	55	29.99
70	55	70.84

Several values of interfacial energy of $CaCO_3$ can be found 7, 19.5, 205 and 280 mJ/m^2 in the literature [SOH82] for calcite nucleation (homogenous) in the pure and impure solutions. Unfortunately, for the case of $CaCO_3$ nucleation in seawater, there can be no data found in literature to compare the interfacial energy of $CaCO_3$ with these results.

5.3   Scale reduction of CaCO₃ in seawater desalination

5.3.1 Crystal growth

As mentioned in the section 2.6, the seawater under atmospheric pressure is metastable to CaCO₃, thereby, theoretically the driving force which is required for the overgrowth of CaCO₃ on the calcite in seawater is there! But is the growth rate high enough to achieve the aim of reducing the main scaling compound (CaCO₃) before the seawater enters e.g. the desalination plant in the available short time?

The answer is in the experimental results as shown in figures 4-30 and 4-31. Wherein those figures the reduction in Ca^{2+} ions is extremely low over a long residence time! The degree of supersaturation of CaCO₃ (S) in artificial seawater is not high enough to achieve the fast crystal growth (see table 2-6) as proven by the results. Additionally, the magnesium ions in seawater are suppressing the rate of nucleation and growth rate of CaCO₃ [PYT65], [RED76]. The proposed method to reduce Ca^{2+} ions is therefore not suited to achieve the reduction process as necessary.

5.3.2 Precipitation

When the precipitation of any compound occurred in its solution, the supersaturation is damping very fast. CaCO₃ precipitation can only occur when CO_3^{2-} ions are increased per unit volume of seawater. This can be done by chemical addition or reducing the amount of solvent.
The measured results of the induction time as shown in figures 4-26 and 4-28 is essential in employing the power of ultrasound to accelerate the precipitation process of CaCO₃. Thus, the time of precipitation will be controlled. Since shorting the time of precipitation is essential to increase the yield of the overall process.

A set of experiments were carried out. Focusing on the most important operational variables studying the Ca^{2+} ion reduction as a function of:

- Optimal amount of HCO_3^- ion addition
- Operational temperature
- Operational time of ultrasound
- Power of ultrasound and seawater salinity

5.3.2.1 Calcium ion reduction as a function of NaHCO₃ mass and temperature

In figure 4-32, the effective limit of $NaHCO_3$ mass addition has been found to be equal to 2.5 g which leads to a maximum reduction of Ca^{2+} ions. An addition of more leads to a smaller increase in the degree of supersaturation (see figure 4-33). This might be due to the reduction in the dissociation amount of bicarbonate to carbonate ions if a certain point at defined operational conditions is passed. Hence, the optimum value of $NaHCO_3$ which can be added to achieve the maximum reduction of calcium ions is adding 2.5 g of $NaHCO_3$ as shown in figure 4-32. The maximum percentage of Ca^{2+} ion reduction is equal **24.32 % by mol.**

This reduction can be increased to reach **75 % by mol** when the operation temperature is increased to 90 °C as can be seen in figure 4-35. Thus, the temperature can play an effective role on the amount of $CaCO_3$ precipitated. This behaviour is due to an increase in the dissociation rate of bicarbonate to carbonate ions with increasing the temperature. The numerical value of the numerator in the equation 2-20 has increased with remaining denominator without a significant change. Since the solubility product of $CaCO_3$ as shown previously in figure 5-2 is not changing very much when the temperature has increased.

The methods used to measure the Ca^{2+} ion concentrations in artificial seawater are showing different results in percentages of the reduction of Ca^{2+} ions. Figure 5-4 shows the concentration of Ca^{2+} ions measured by <u>atomic absorption spectroscopy</u> (AAS).

By AAS a reduction of Ca^{2+} ions are equal to **94.25 % by mol**. Comparing this value with that one obtained using the complex metric titration method to determine the total amount of magnesium and calcium ions in ASW, a significant difference can be recognized between those values. Hence, the accuracy of the methods used to determine the Ca^{2+} ion is playing an essential role in evaluation the efficiency of Ca^{2+} ion reduction.
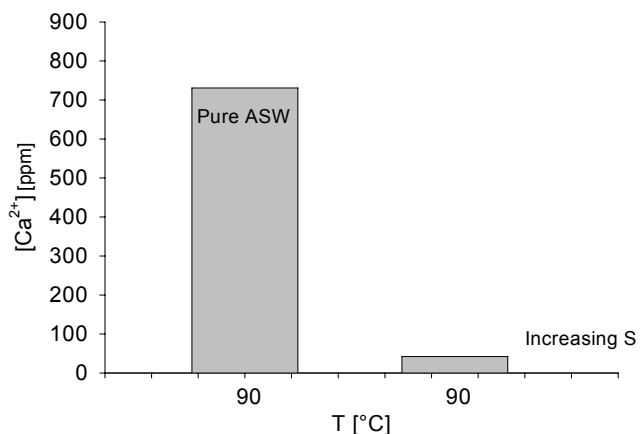
Figure 5-4: Calcium ion (measured by AAS) reduction versus 90 °C, with and without modification of the degree of supersaturation (S). Ultrasonic power= 100 W, V_{ASW}= 125 mL, t= 2 min, horn depth= 2 cm and salinity= 59 g/kg

Figure 4-34 shows the X-ray diffraction results of the precipitated solid material. It is shown that the intensity of the pattern peaks are not similar, this can be explained in terms of the differences between the two cases of $CaCO_3$ crystallization conditions. One of the reasons is the precipitation of $CaCO_3$ in the multi-components system, in our case is the precipitation in the seawater. It is known that the magnesium ion has an influence on the $CaCO_3$ crystal growth and morphology. This can be related to a substitution of magnesium ions instead calcium ions in the $CaCO_3$ crystal lattice [RED76, SAB93]. Moreover, it was reported that the peak intensity of limestone soaked by saline solution was changed. Due to the effect of saline solution on the limestone particles surface [CHA98]. In our case, the intensity of the diffraction of $CaCO_3$ has shown a lower value than the pure substance. Another possibility to explain the change in the diffracted intensity is in the change of the degree of crystallinity of $CaCO_3$ which can be influenced by the power of ultrasound. In this work, the most important result of the X-ray is to investigate the general type of the solid that is produced by precipitation.

5.3.2.2 Operational time of ultrasound, power of ultrasound and salinity change

Increasing the active time of ultrasonic irradiation is not an effective factor on the Ca^{2+} ion reduction. The little change found in the total amount of magnesium and calcium ions in ASW after an increase of radiation time are shown in figure 4-37. This change can be explained by the prolonged time of created locally high temperature and pressure. Hence the time of reaction will be increased. As a result the rate of $CaCO_3$ precipitation is slightly increased as has been reported by Nishida [NIS04].

On the other hand, it has been found that the results (see figure 4-38) achieved are similar insensitive to total power input of ultrasound concerning the precipitation rate of $CaCO_3$ in pure aqueous solution [NIS04].

5.3.3 An environmentally friendly and economically solution to reduce scaling

As shown in section 2.9 the problems caused by scale formation in seawater desalination and encrustation reduction can be solved (see section 2.10). For a comparison, table 5-24 shows the most conventional methods and the suggested method to reduce scale formation in seawater desalination.

Table 5-24: The most conventional methods used to reduce scales in seawater desalination

Method	Need extra equipment	efficiency	Disadvantages
◆ Acid cleaning	yes	very effective	◆ High risk of corrosion and hazard ◆ High costs
◆ Additives	no	very effective	◆ Unfriendly to environment ◆ High cost
◆ Ion exchange	yes	very effective	◆ Expansive process of chemical regeneration
◆ Minerals removal (suggested method)	yes	very effective (needs to be proved in industrial praxis)	◆ Needs probably extra equipment to reduce the CO_2 emission (future assessment) ◆ Extra costs are required

<u>The profit of using the suggested method is</u>:

- ◆ Production and marketing $CaCO_3$ that is produced from seawater.
- ◆ Reducing of the potential of scales formation in seawater desalination.
- ◆ No corrosion risk.
- ◆ No toxic additives are used.
- ◆ Environmental friendly.

<u>Further studies for an evaluation have to be done as follows</u>:

- ◆ The optimum amount of $NaHCO_3$ addition has to be found over a wide range of temperatures to determine the maximum reduction of Ca^{2+} ions.
- ◆ The minimum operation time, the minimum power input of the ultrasound and the total amount of CO_2 release (CO_2 emission problem) has to be found.
- ◆ A study of the crystal size distribution, shape, morphology and purity of the crystalline products of $CaCO_3$ with a comparison to the standard quality has to be done.
- ◆ A study comparing the $CaCO_3$ product yield to the maximum reduction of Ca^{2+} ions is needed.
- ◆ All above experiments should be carried out in artificial seawater alongside to the **real seawater** in order to take the biological effect into account.

Here, it is very necessary to show in a simple way how much $CaCO_3$ can be produced from seawater? Assuming a 100% of calcium ions to be converted to $CaCO_3$. This calculation can be done according to the following equations:

$$\because \quad Ca^{2+} + CO_3^{2-} \rightarrow CaCO_3 \tag{5-9}$$

$$\therefore \ [Ca^{2+}] = [CO_3^{2-}] = [CaCO_3] \quad mole/kg \tag{5-10}$$

$$\because \ [Ca^{2+}] = 2.934 \cdot 10^{-4} * Salinity \quad mol/kg_{seawater} \ [ALR04] \tag{5-11}$$

$$\therefore \ [CaCO_3] = 2.934 \cdot 10^{-4} * Salinity \quad mol/kg_{seawater} \tag{5-12}$$

$$\therefore \ [CaCO_3] = 0.029366 * Salinity \quad g/kg_{seawater} \tag{5-13}$$

Equation 2-13 is represented by figure 5-5 which shows the mass of $CaCO_3$ that can be produced at different levels of salinity, when the assumption is made of a 100 % conversion of calcium to $CaCO_3$ after the addition of $NaHCO_3$ to seawater. It can be seen how the production mass of $CaCO_3$ is **extreme small** can be proved to the mass of seawater used. Moreover, to have a clear impression on the total mount of $CaCO_3$ that can be produced according to the data found in literature of the typical production

Figure 5-5: CaCO3 mass production against salinity of seawater, 100% conversion assumed

rate of fresh water. A desalination plant capacity of fresh water production is 25.000 ton/day [GRA04]. The typical mass ratio of fresh water out let to the intake feed of seawater is equal 1:3 [GLA01]. Consequently, the inlet feed of seawater is 75.000 ton/day. Thus, by applying equation 5-13 for 35 and 59 g/kg salinity, it gives 77.09 and 129.95 ton/day of $CaCO_3$, respectively.

After all, designing and manufacturing a new process might be suggested to produce $CaCO_3$ from seawater and reduce the scale formation. This suggestion might only be valid when a complete economic evaluation study will be carried out. The out come depends mainly upon investment costs of employing the suggested method which should be equal (or less than) to the total costs caused due to the impact of scale formation in seawater desalination plant **plus** the profit of marketing the $CaCO_3$ produced from seawater. I.e. keeping the price of fresh water at the same market level and solving the problem of encrustation in seawater industry in friendly way to environment.

6. <u>Conclusion</u>

Interpreting the effect of impurities using the concept of intermolecular interactions by means of ion-ion and ion-dipole forces in solution due to changes of its content by additives is in some cases possible as summarized in table 6-1.

Table 6-1: Summarized the success of the suggested method in interpreting the effect of additives on nucleation temperature

Solution	additive	Interpretation	
		ion-dipole	ion-ion
ZnSO$_4$ – H$_2$O	Al^{3+}	+	+
	Fe^{2+}	+	+
	Ba^{2+} and Cl$^-$	+	–
	Li$^+$	–	–
	K$^+$	–	–
LiCl – H$_2$O	Al^{3+}	–	–
	Fe^{2+}	+	+
	Mg^{2+}	+	+
	Ba^{2+} and Cl$^-$	+	–
K$_2$SO$_4$ –H$_2$O	Cu^{2+}	–	+
	Ba^{2+} and Cl$^-$	–	+
	Li$^+$	+	+

<u>Note:</u> (+) successful, (-) unsuccessful

The suggested rule of taking the hydration enthalpy values as main factor can be used in explaining the effect of some additives but not without using the strength of ion-ion force for some other cases of additives. This might be due to not taking into account the dipole-dipole attraction forces (Van der Waals forces). The suggested concept is already helpful in some cases where additives influence the width of the MSZ. Unfortunately not all cases could be treated satisfactory up to now. Further experiments and theoretical improvements (e.g. introducing dipole-dipole interactions) are required. *Even so, the partially success which is shown in this study that the change in the structure of the solution due to presence the impurities is the key of interpretation of their effect.*
Additionally, it should be mentioned that the maximum change in the MSZ width that was recorded in literature, can not be generalized. Because the experimental results found here showed no appropriate effect and but to postulate also a minimum change in the MSZ width due to adding a very small amount of additives is possible.

On the other hand, the possibility of reducing the amount of the calcium ions in artificial seawater is shown in this work by adopting two concepts. Reduction by crystal growth and precipitation of $CaCO_3$ in seawater.

The crystal growth principle can not be applied to serve to reduce scale formation in seawater desalinisation due to the experimental results which proved no significant reduction in the calcium ions in artificial seawater.

On the other side, precipitation of $CaCO_3$ in artificial seawater is promising to solve the scaling problem in seawater desalinisation. This process as such can not be carried out without modifying the degree of supersaturation of $CaCO_3$ in the artificial seawater for all salinities. The degree of supersaturation was increased by addition $NaHCO_3$. The induction time of $CaCO_3$ precipitation in artificial seawater has been reduced with increasing the mass of $NaHCO_3$ for a certain limit of addition. An increase in the temperature of precipitation is decreasing significantly the induction time.

The reduction process that is achieved by the precipitation process of $CaCO_3$ can be accelerated by the power of ultrasound. The optimum degree of supersaturation which can achieve the maximum reduction of calcium ions is equal to 345.74 at 50 °C and 2 min operation time. The required value to be obtained for the maximum reduction of calcium ions of different kinds of salinities and volumes of seawater are related to the above mentioned conditions. The operational conditions of mass of $NaHCO_3$ addition, temperature, time of ultrasound, power of ultrasound and seawater salinity were studied. There were no changes on the $[Ca^{2+} + Mg^{2+}]$ ion reduction due to the change of the power of ultrasound. The most important conditions that should be optimised are temperature, time and mass of addition for $NaHCO_3$. The highest value of temperature and time are related to the optimum amount of $NaHCO_3$ addition that can achieve the maximum reduction of calcium ions.

The optimisation process can be carried out by taking the costs of the pre-treatment of the process plus the benefit of producing $CaCO_3$ and environmental effects as essential factors, which are, however, so far not in consideration in this stage of the study. Then again, the result of this optimisation process should be compared with other methods described in literature to estimate the applicability of the method presented here as an alternative solution for scale prevention in seawater desalination.

7. <u>**Summary**</u>

The most important influences on the width of the metastable zone are the kind and concentration of the impurities existing in the solution. The presence of impurities in solution leads to different disturbances on the yield of a product. Only an experimental determination for the effects of impurities exists in the relevant literature without any interpretation of the existing results. Most explanations of crystal growth under additive effects start at the solid phase but do not take into account the change in the structure of the solution when additives are added to a solution.

Here it was investigated if the properties of intermolecular interactions cations and anions each for additive, solvent and salt in solution are the key to an interpretation of influences of additives on the metastable zone width of inorganic compounds.

The polythermal method was used to measure the effect of the additives, e.g. Al^{3+}, Fe^{2+}, Ba^{2+}, Li^+ and K^+ on the MSZ width of $ZnSO_4$, Al^{3+}, Fe^{2+}, Mg^{2+} and Ba^{2+} on the MSZ width of LiCl and Cu^{2+}, Ba^{2+}, Li^+ on the MSZ width of K_2SO_4. These additive ions were selected according to a suggested rule, which takes the amount of hydration enthalpy values into account. The results show that the additives affect the MSZ width not always as expected. Also it is explained that the effect of some additives on the MSZ width can be given in terms of hydration enthalpy values and ion-ion interaction forces. This approach is, however, still not sufficient to interpret the effect of all additives.

Also this study shows the possibility to reduce scale formation e.g. in seawater desalination. The principal idea of the concept is a reduction of the amount of calcium ions, which are causing the main scaling problem in seawater desalination such as $CaCO_3$ and $CaSO_4$ scales. This reduction of calcium ions can be carried out before the feed of the seawater enters the desalination unit. It can be defined as precipitation and separation unit. In this unit, it is suggested to use the power of ultrasound to accelerate the precipitation of calcium carbonate after modifying the degree of supersaturation in seawater. By adding a stoichiometric amount of an inorganic compound that is the source of carbonates ions. Normally the CO_3^{2-} ions are the limiting reactant in seawater, which is not enough to reach the required degree of supersaturation for a precipitation. Thus $NaHCO_3$ was added to increase the degree of $CaCO_3$ supersaturation in artificial seawater. The induction time of $CaCO_3$ precipitation was investigated after modifying the degree of supersaturation. As a result the interfacial tension of $CaCO_3$ in artificial seawater was determined at different level of temperature and salinity without applying the power of ultrasound.

On the other hand, the power of ultrasound was used to accelerate the $CaCO_3$ precipitation as essential to accelerate the process of calcium ion reduction in seawater.

The experimental work is focused on several operational variables studying the calcium ion reduction as a function of:

1. Optimum amount of HCO_3^- ions addition

2. Operational temperature

3. Operational time of ultrasound

4. Power of ultrasound and seawater salinity

The maximum necessary addition of HCO_3^- ions in seawater was determined to reach a maximum decrease in calcium ions. As a result of this reduction the conditions to control the scale formation will be achieved. Additionally, it was found that the closer the process to optimal operation conditions of temperature and time is the more increased is the efficiency of reduction. In addition, there has been no change recorded in calcium ion reduction due to the change of power input of power of ultrasound. This work can be considered a first step to evaluate the combined chemical-mechanical methods as anti-scaling operations in seawater desalination. Environment and economic aspects would benefit if the present results could be transferred to industry.

8. <u>**Nomenclature**</u>

F	Electrostatic force between ions	N
z_i	Valence of ion	-
e	Elementary charge	C
r	Distance between ions	nm
ΔG	Overall excess free energy	J
ΔGs	Surface excess free energy	J
ΔG_V	Volume excess free energy	J
ΔG_{crit}	Minimum value of free energy required for nucleation	J
ΔG_v	Free energy change of the transformation	J/m^3
r_c	Critical size of nucleus	m
T	Temperature	°C
R	Gas constant	J/mol K
m_i	Concentration of component (i)	mol/L
$\bar{G}_i^o(T)$	Partial molar Gibbs free energy	J
$\Delta G_{f_i}^o$	Gibbs free energy of formation of component (i) at standard condition	kJ/mol
K_{sp}	Solubility product constant	mol^2/L^2
t_{ind}	Induction time of precipitation	s
N_A	Avogadro's number	mol^{-1}
V_m	Molar volume	cm^3/mol
$[CO_3^{2-}]$	Molality of carbonate ion in seawater	mol/kg
$[Ca^{2+}]$	Molality of calcium ion in seawater	mol/kg
S	Degree of supersaturation of CaCO$_3$ in seawater	-
K_{so}	solubility product constant of CaCO$_3$ in seawater	mol^2/kg^2
$K_{sp,calcite}^{SW}$	solubility product constant of CaCO$_3$ in seawater	mol^2/kg^2
$[Ca^{2+}+Mg^{2+}]$	Total concentration of Ca^{2+} and Mg^{2+} ion in seawater	mol/L
M	Mass of NaHCO3	g
V_{ASW}	Volume of artificial seawater	mL
t	Time of ultrasonic irradiation	min
$\Delta_{hyd}H^o$	Enthalpy of hydration of ion	kJ/mol
n	Number of water molecules in hydration shell	-
Sa.	Salinity	g/kg H$_2$O
K_2^{SW}	Second dissociation constant of carbonic acid in seawater	mol/kg$_{solution}$

Greek letters

ε	Dielectric constant of the solvent	$C^2/N.m^2$
ε_r	Relative dielectric constant	-
ε_o	Vacuum permittivity	$C^2/N.m^2$
γ	Interfacial tension	mJ/m^2
σ	Interfacial tension	mJ/m^2
$\mu_i(T)$	chemical potential at certain temperature and pressure	J
$\mu_i^o(T)$	chemical potential at standard condition	J
γ_i	Activity coefficient of component (i)	-
$\gamma_\pm^v$	Total activity coefficient	-

Abbreviations

MSZ	Metastable zone
ASW	Artificial seawater
AAS	Atomic absorption spectroscopy
rpm	Revolution per minute
M_{CaCO_3}	Mass of $CaCO_3$

9. <u>References</u>

[ALB93]   Al-Bakeri, F.; El Hares, H. "Optimization of sponge ball cleaning system operation and design in MSF plants" Desalination 92 (1993) 1-3, 353-375.

[ALR04]   Al-Rawajfeh, A. "Modelling and simulation of CO_2 release in Multiple-effect distillers for seawater desalination" PhD thesis, Martin Luther University Halle-Wittenberg, Shaker Verlag, Aachen, 2004.

[ACC08]   Accepta, Advanced environmental technologies, http://www.accepta.com/industry_water_treatment/reverse_osmosis_scal e_inhibitors.asp, 25/03/08.

[BUR88]   Burgess, J. "Ions in solution: basic principles of chemical interactions" Ellis Horwood Limited, Chichester; 1988.

[BUT82]   Butler, J.N. "Carbon dioxide equilibria and their applications": Addison-Wesley, Canada; 1982.

[CHA70]   Chave, K.E.; Suess, E. "Calcium carbonate saturation in seawater: effect of dissolved organic matter1" Limnology and Oceanography 15 (1970) 4, 633-637.

[CHA98]   Chang L.; Zhu S.; Xie K.; Bao W. "Effect of impurities on desulphurization properties of limestone during coal gasification" Journal of Environmental Sciences 10 (1998).

[CTS08]   Chemistry the science in context, chapter 13 "Dissolution of ammonium nitrate"   http://www.wwnorton.com/college/chemistry/   gilbert2/chemtours /chemtour.asp#13, 01/08/2008.

[DAN67]   Dana, K.; Iver, D.; Donald, C.; Ricardo, P. "Preparation of artificial seawater" Limnology and Oceanography 12 (1967) 1, 176-179.

[DAV74]   Davey, R.J.; Mullin, J.W. "Growth of the {100} faces of ammonium dihydrogen phosphate crystals in the presence of ionic species" Journal of Crystal Growth 26 (1974) 45-51.

[DAV95]   David, R.L. "Handbook of chemistry and physics" CRC Press, Boca Raton; 1995.

[DOG85]   Dogonadze, R.R.; Kálmán, E. "The chemical physics of solvation". 3 Vol., Elsevier, Amsterdam; 1985-88.

[DRI04]   Drioli; E.; Curcio, E.; Criscuoli, A.; Di Profio, G. "Integrated system for recovery of $CaCO_3$, NaCl and $MgSO_4 \cdot 7H_2O$ from nanofiltration retentate" Journal of Membrane Science 239 (2004) 27-38.

[ELF04]   Elfil, H.; Roques, H. "Prediction of the limit of metastable zone in the $CaCO_3$-CO_2-H_2O System" AIChE Journal 50 (2004) 8, 1908-1916.

[HAN03]   Hanbury, W.T.; Hodgkiess, T.; Al-Omari, K. "Aspects of acid-cleaning operation in MSF plants" Desalination 158 (2003) 1, 1-1.

[HAR08]   Hari, J. K. "Introduction to desalination technologies" http://texaswater.tamu.edu/conservation.desalination.html, 25/03/08.

[HAS67]   Hasson, D.; Avriel, M.; Resnick, W.; Rozenman, T.; Windreich, S. "Mechanism of calcium carbonate scale deposition on heat-transfer surfaces" Industrial and Engineering Chemistry Fundamentals 7 (1967) 1, 59-65.

[HAS85]   Hasson, D.; Bramson, D. "Effectiveness of magnetic water treatment in suppressing calcium carbonate scale deposition" Industrial & Engineering Chemistry Process Design and Development 24 (1985) 3, 588-92.

[HAS98]   Hasson, D.; Semiat, R.; Bramson, D.; Busch, M.; Limoni-Relis, B. "Suppression of CaCO3 scale deposition by anti-scalants" Desalination 118 (1998) 1-3, 285-296.

[HAY77]   Hayakawa, K.; Nishimoto, T. "Treatment for distilled water" patent No. JP 52144145, 1977.

[HEN98]   Hendriksen, B.A.; Grant, D.J.W.; Meenan, P.; Green, D.A. "Crystallisation of paracetamol (acetaminophen) in the presence of structurally related substances" Journal of Crystal Growth 183 (1998) 4, 629-640.

[Gla01]   Glade, H. "Transport und reaktion von kohlendioxid in entspannungsverdampfern zur meerwasserentsalzung" PhD Thesis, University of Bremen, 2001, VDI Fortschritt-Berichte, Series 3, No. 699 VDI Verlag, Düsseldorf, 2001.

[GLA01]   Glade, H.; Ulrich, J. "Scaling in seawater desalination - Is molecular modeling the tool to overcome the problem?" Eds: H. Glade, J. Ulrich; Shaker Verlag, Aachen, 2001.

[GIN93]   Ginde, R.M.; Myerson, S. "Effect of impurities on cluster growth and nucleation". Journal of Crystal Growth 126 (1993) 216-222.

[GOM96]   Gomez-Morales, J.; Torrent-Burgues, J.; Lopez-Macipe, A.; Rodriguez-Clemente, R. "Precipitation of calcium carbonate from solutions with varying Ca^{2+}/carbonate ratios" Journal of Crystal Growth 166 (1996) 1-4, 1020-1026.

[GUO06]   Guo, Z.; Jones, A.G.; Li, N. "Interpretation of the ultrasonic effect on induction time during $BaSO_4$ homogeneous nucleation by a cluster coagulation model" Journal of Colloid and Interface Science 297 (2006) 190-198.

[GUR05]   Gurumoorthy, K. "Calcium impurity removal from evaporated sea salt by precipitation with soluble carbonate" patent No. IN 2003CH00832, 2005.

[GRA04]   Grassi, G.; Nilsson, L.; Passalacqua, F. "New promising heat market for biofuels (innovative seawater desalination)" 2nd World Conference on Biomass for Energy, Industry and Climate Protection, 10-14 May 2004, Rome, Italy.

[KOU84]   Koutsoukos, P.G.; Kontoyannis, C.G. "Precipitation of calcium carbonate in aqueous solutions" Journal of the Chemical Society, Faraday Transactions (80) (1984) 1, 1181-1192.

[KRU92]   Kruse, M. "Zur Modellierung der Wachstumskinetik in der Lösungskristallisation" Ph.D. Thesis, University of Bremen, Bremen 1992, VDI-Verlag, Düsseldorf 1993.

[KUB95]   Kubota, N.; Fukazawa, J.; Yashiro, H.; Mullin J.W. "Impurities effect of chromium (III) on the growth and dissolution rates of potassium sulfate crystals" Journal Of Crystal Growth 149 (1995) 113-119.

[KUB97]   Kubota, N.; Yokota, M.; Mullin, J.W. "Supersaturation dependence of crystal growth in solutions in the presence of impurities" Journal of Crystal Growth 182 (1997) 86-94.

[LOB89]   Lobo, V.M.M. "Handbook of electrolyte solutions" Elsevier, Amsterdam; 1989.

[LYC02]   Lyczko, N.; Espitalier, F.; Louisnard, O., Schwartzentruber, J. "Effect of ultrasound on the induction time and the metastable zone widths of potassium sulphate" Chemical Engineering Journal 86 (2002) 233-241.

[MAR87]   Marcus, Y. "The thermodynamic of solvation of ions part 2 – the enthalpy of hydration at 298.15 K" Journal of the Chemical Society, Faraday Transactions 83 (1987) 1, 339-349.

[Mar87]   Marcus, Y., The thermodynamics of solvation of ions part 2 – the enthalpy of hydration at 298.15 K. Journal of chemistry society faraday transactions83(1) (1987) 339-349.

[MER98]   Mersmann, A.; Bartosch, K. "How to predict the metastable zone width" Journal of Crystal Growth 183 (1998) 240-250.

[MER08]   http://www.merck-chemicals.com/, 10/07/2008.

[MIL00]   Millero, F.J. "The carbonate system in seawater in Chemical Processes in Marine Environments" eds., A. Gianguzza, E. Pellizzetti and S. Sammartano, Springer-Verlag, Berlin 2000, Chapter 1, 9-41.

[MUC83]   Mucci, A. "The solubility of calcite and aragonite in seawater at various salinities, temperatures, and one atmosphere total pressure" American journal of science 283 (1983) 9, 780-799.

[MUL93]   Mullin, J.W. "Crystallization" Butterworth-Heinemann, Oxford; 1993.

[MUR84]   Murrell, J.N.; Jenkins A.D. "Properties of liquids and solutions". John Willey and Sons, Chichester; 1984.

[NIS04]   Nishida, I. "Precipitation of calcium carbonate by ultrasonic irradiation" Ultrasonic Sonochemistry 11 (2004) 6, 423-428.

[NYV85]   Nyvlt, J.; Söhnel, O.; Matuchova, M.; Broul, M. "The kinetics of industrial crystallization" Academia Praha, Prague; 1985.

[NYV98]   Nyvlt, J.; Hostomska, V. "Influence of the pH-Value on the Metastable Zone Width of Potassium Sulphate" Crystal Research and Technology 33 (1998) 5, 767-775.

[OMA99]   Omar, W.; Strege, Ch.; Ulrich, J. "Determination of the metastable zone of real solutions by means of ultrasonic for online control of crystallization processes" Chemische Technik 51 (1999) 5, 286-290.

[ONO68]   Ono, S.; Yamaguchi, G.; Yanagida, H.; Shimizu, T. "Effects of impurities on hydrothermal reactions of alumina" Yogyo Kyokaishi 76 (1968) 207-18.

[PYT65]   Pytkowicz, R. "Rates of inorganic calcium carbonate nucleation" Journal of Geology 73 (1965) 1, 196-9.

[RED71]   Reddy, M.M.; Nancollas, G.H. "The crystallization of calcium carbonate I. isotopic exchange and kinetics" Journal of Colloid and Interface Science 36 (1971) 2,166 – 171.

[RED76]   Reddy, M. M.; Nancollas, G. H. "The crystallization of calcium carbonate IV. the effect of magnesium, strontium and sulfate ions" Journal of Crystal Growth 35 (1976) 33-38.

[RUS92]   Rushdi, A. I.; Pytkowicz, R. M.; Suess, E.; Chen, C. T. " The effects of magnesium-to-calcium ratios in artificial seawater, at different ionic products, upon the induction time, and the mineralogy of calcium carbonate: a laboratory study" Geologische Rundschau 81 (1992) 2, 571-578.

[SAB93]   Sabbides, T. G.; Koutsoukos, P. G. "The crystallization of calcium carbonate in artificial seawater; role of the substrate" Journal of Crystal Growth 133 (1993) 13-22.

[SAN04]   Sangwal, K.; Mielniczek-Brzoska, E. "Effect of impurities on metastable zone width for the growth of ammonium oxalate monohydrate crystals from aqueous solutions" Journal of Crystal Growth 267 (2004) 662-675.

[SAN07]   Sangwal, K. "Additives and crystallization processes from fundamentals to applications" John Willey and Sons, Ltd, Chichester; 2007.

[SAY01]   Sayan, P.; Ulrich, J. "Effect of various impurities on the metastable zone width of boric acid" Crystal Research and Technology 36 (2001) 4-5, 411-417.

[SOH82]   Söhnel, O.; Mullin, J.W. "Precipitation of calcium carbonate" Journal of Crystal Growth 60 (1982) 239-250.

[SOH92]   Söhnel, O.; Garside, J. "Precipitation basic principles and industrial applications" Butterworth-Heinemann, Oxford; 1992.

[TAO06]   Tao C.; Anne N.; Mingdong Y. "Influence of Mg^{2+} on $CaCO_3$ formation-bulk precipitation and surface deposition" Chemical Engineering Science 61 (2006) 5318 – 5327.

[TIT02]   Titiz-Sargut, S.; Ulrich, J. "Influence of additives on the width of the metastable zone" Crystal Growth and Design 2 (2002) 5, 371-374.

[UOC08]   University of Canterbury, college of science "Determination of total calcium and magnesium ion concentration" www.outreach.canterbury. ac.nz/chemistry/calcium_magnesium.shtml, 01/01/2008.

[WAN07]   Wang, Y.; Wang, L.L.; Liu, M.Y. "Antifouling and enhancing pool boiling by tio2 coating surface in nanometer scale thickness" AIChE Journal 53 (2007) 12, 3062-3076.

[ZEM86]   Zemaitis, J.F.; Clark, D.M.; Rafal, M.; Scrivner, N.C. "Handbook of Aqueous Electrolyte Thermodynamics: Theory & Application" Willey, New York; 1986.